THE APPLICATION OF SPECKLE INTERFEROMETRY TO INFRA-RED ASTRONOMY

BY

RICHARD WADE B.Sc

A thesis submitted for the degree of Doctor of Philosophy of the University of London and for the Diploma of Imperial College.

Astronomy Group,
Blackett Laboratory,
Imperial College,
London, S.W.7.

March, 1979

The Application of Speckle Interferometry to Infra-red Astronomy.

Richard Wade

ABSTRACT

The main limitation to resolving power when using a single telescope of fixed aperture is the astronomical seeing. The causes of seeing are discussed and its value (at differing times and for differing wavelengths) is evaluated.A method for obtaining diffraction limited information while using the full aperture of a large telescope (Stellar Speckle Interferometry) is described.A technique is then outlined by which the method may be extended to the near infrared (1-5um).The implementation of this technique is discussed and some preliminary results are presented.

Contents

List of Figures

Acknowledgements

My thanks go to my supervisor Mike Selby and to Carlos Sanchez for many ideas suggestions and discussions.

I am also grateful to Bill and Jack of the Astronomy Group workshop at Imperial College and to Victor for friendship and help in all directions.

My deepest gratitude however goes to Elaine.

Introduction

The problem to which this thesis will be addressed is that of measuring the angular diameters of Infrared Objects.

Clearly in order to measure a sample of stellar radii at any wavelength interferometrically, an extended baseline of some sort must be used. The highest resolution so far achieved is at microwave frequencies (Cohen 1973 (0.1)) using a very long baseline and a heterodyne system to give a resolution of 1msec-arc. This technique has been extended to the middle infrared ($\sim 10\mu m$) by Johnson et al (0.2) using an infrared laser as local oscillator. At visible wavelengths the first attempt to measure stellar angular diameters using interferometric techniques was due to Michelson and Pease (0.3) in 1921 using a 20ft amplitude interferometer. In an attempt to further improve the available resolving power Pease later constructed a 50ft interferometer but the effect of atmospheric turbulance proved to be a major limitation and the instrument was only able to measure a handful of stars.

The Intensity Interferometer of Hanbury Brown (0.4,0.5) gets round the two main problems encountered by the Michelson Interferometer as its operation is not so critical on path length differences and is not affected by atmospheric turbulence. The Interferometer was built at Narabri, Australia and had two 6.5m diameter reflectors with a maximum separation of about 180m. Due to fundamental limitations of the method however, the magnitude limit obtained at visible wavelengths was only about +2 mag in 1 hour. The Narabri Interferometer was therefore only used to make a study of 32 stars before being dismantled.

Blackwell and Shallis (0.6) have pointed out that Intensity Interferometry is the only direct method of angular diameter measurement which has yielded any reasonable high accuracy. They suggest that indirect (photometric) methods are as accurate and can be applied to a greater range of objects.

Although the measurement of stellar radii at infrared wavelengths is in general beyond the resolution of a single telescope, there are a large number of interesting objects which may be resolved. These include such objects as dust shells around proto-stars and late spectral type stars, binary systems and the cores of some Seyfert galaxies.

Since these objects are not normally main sequence stars and we are not dealing with the measurement of a simple stellar radius,

the indirect method of Blackwell and Shallis is not applicable and in general a direct method of measurement must be used.A second point about these objects is that generally speaking the nature of the object is not well known and the high accuracy (better than 2%) discussed by Blackwell and Shallis,in connection with the measurement of main sequence objects,is not essential.

Two methods have so far been used at Infrared wavelength to obtain high resolution on a single telescope.McCarthy and Low (0.7) used a classical Michelson arrangement with a double aperture mask producing the interfering beams.The fringes are focused onto aFizeau mask and are oscillated across the mask to give an AC signal which can be used as a measure of the fringe visibility,Secondly the technique of Lunar Occultations has been used by Toombs et al (0.8) and by Ridgeway and Wells(0.9).This technique may prove to be a useful complement to other methods since although the positional applicability of the method is limited,the resolution available (of the order of milli arc-seconds in the near infrared) would only be matched by a two beam interferometer of about 50m baseline.

In Chapter 1 of this thesis the effect of atmospheric turbulance on the resolution of large telescopes will be discussed. In Chapter 2 Stellar Speckle Interferometry,a method for obtaining diffraction limited information while still using the full aperture, at visible wavelengths will be reviewed.The main body of the thesis will then be devoted to describing the implementation of a technique by which Speckle Interferometry may be used at infrared wavelengths.In the final chapter some preliminary results will be presented.

Chapter 1 The Theory of Astronomical Seeing

Introduction

In this first chapter I shall discuss the two main limitations to the angular resolving power obtainable using conventional telescopes.

The first, and most fundamental limit is due to diffraction. Consider the case where the telescope is used to observe two stars of angular separation $\Delta\theta$. Neglecting the effects of aberrations the image of each star will be an Airy diffraction pattern in the focal plane of the telescope. The distance between the centres of the two patterns may be incresed but this does not increase the resolving power as the sizes of the Airy patterns are also increased. We thus have a limit on the resolving power of the telescope. In order to apply a criterion by which any telescope system could be judged Rayleigh suggested that the angular resolution of a telescope should be defined as the angle between two stars when the maximum of the diffraction pattern of one falls exactly on the first dark ring of the other. So that for a circular aperture we have

$$\text{angular resolving power} = 1.22\lambda/D$$

where λ = wavelength of light

D = diameter of aperture

The second limitation on resolving power is due to the atmosphere being in a state of turbulent motion which affects the propagation of light through it.

Aristotle is said to have noticed the scintillation of the stars, but it was not until the construction of telescopes of diameter larger than about 10cm that it was realized that atmospheric turbulence and not diffraction would limit the available resolving power.

In 1730 Sir Isaac Newton wrote (1.1)." If the theory of making telescopes could at length be fully be brought into practice, yet there would be certain bounds beyond which telescopes could not perform. For the air through which we look upon the stars, is in perpetual tremour; as may be seen by the tremulous motions of the shadows cast from high towers, and by the twinkling of the fix'd stars. But these stars do not tremble when viewed through telescopes which have large apertures. For the rays of light which pass through diverse parts of the aperture, tremble each of them

apart and by means of their various and sometimes contrary tremors, fall at one and the same time upon different points in the bottom of the eye,and their trembling motions are too quick and confused to be perceived severally.And all these illuminated points constitute one broad lucid point,composed of many trembling points,confusedly and insensibly mixed with one another by very short and swift tremors,and thereby cause the star to appear broader than it is and without any trembling of the whole.The only remedy is a most serene and quiet air,such as may perhaps be found in the tops of the highest mountains above the grosser clouds".

In the next section I shall attempt to bring together the many ideas from the literature which go to form a description of the "perpetual tremor"or turbulent motion of the atmosphere and the effect on light waves transmitted through it.

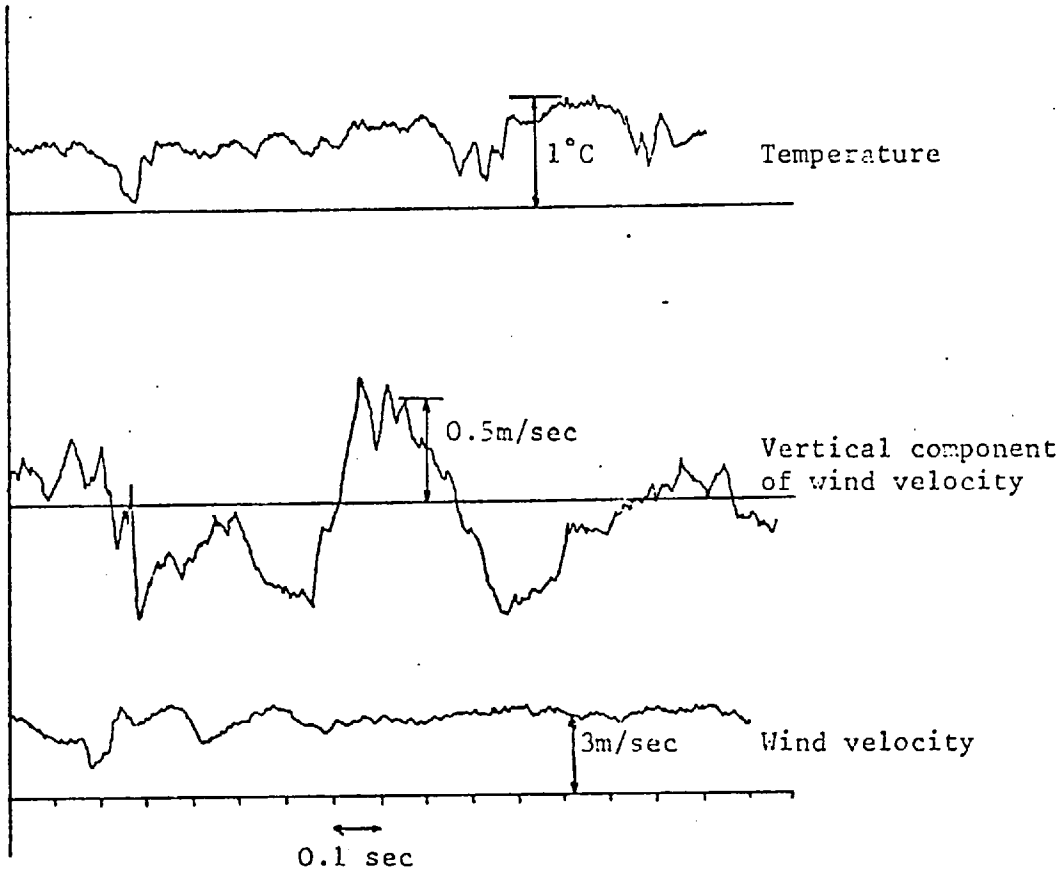

Fig. 1.1 Simultaneous record of temperature and wind velocity

The Theory of Atmospheric Turbulence

In studying the effect of turbulence in the atmosphere we are concerned with changes in the refractive index of the air between the source and the observer.Now the index of refraction of the atmosphere for electromagnetic waves is a function of the temperature,pressure and humidity of the air.We know however that the atmosphere is in a state of turbulant motion and hence the values of for example,the wind velocity and temperature at every point in space undergo irregular fluctuations;similarly the values of wind velocity and temperature taken at different spatial points at the same instant of time also differ from one another in a random fashion.Figure1.1 is a sample of the record of the instantaneous values of the wind velocity and temperature at one point,(due to Tatarski (1.2)).

It is natural that statistical methods are used to describe the laws characterising the structure of such fluctuating quantities and these are outlined briefly in Appendix 1.In the next section the structure of turbulant flow and its effect on the refractive index of the atmosphere will be discussed.

Turbulent Flow

The initial laminar flow of a viscous fluid may be characterised by its viscosity ν ,density ρ ,velocity V and length L of flow .

Consider now the situation where a velocity fluctuation v_ℓ arises in a region of sizeℓ.The characteristic time scale of the fluctuation is give by

$$\tau = \ell / v_\ell$$

and the kinetic energy of the fluctuation is $v_\ell^2/2$per unit mass.

So that the amount of energy per unit time going from the laminar flow to the fluctuation is of the order v_ℓ^3/ℓ

But for the viscous flow

$$F/A = \rho\nu dv/dy$$

where F = force required to maintain the motion
A = characteristic area
dv/dy = velocity gradient

Now for our velocity fluctuation the local velocity gradient is v_ℓ/ℓ so that the energy ε dissipated as heat per unit time per unit mass is given by

$$\varepsilon = \nu v_\ell^2/\ell^2$$

It is clear that for the fluctuation to be stable

$$v_\ell^3/\ell > \nu v_\ell^2/\ell^2$$

so that $$\ell v_\ell/\nu > 1 \qquad (1.2)$$

Now we refer to the LHS of equation1·2 as ,the Renolds Number Re_ℓ corresponding to the fluctuation of size ℓ.

The above arguments are only of order of magnitude accuracy and the criterion applied for a stable fluctuation of size ℓ is

$$R_{e_\ell} > R_{ecr}$$

where R_{ecr} is a constant whose value cannot be determined accurately. If the condition $v_\ell \ell/\nu > R_{ecr}$ is not met for a given flow then a laminar flow is stable.

If now we have a flow for which the Renolds number for the flow as a whole R_{eL} is far in excess of R_{ecr} then velocity fluctuations may be excited for which the inner Renolds number $R_{e\ell}$ is also in excess of R_{ecr} ,so that the first order fluctuations become unstable and transfer their energy to smaller scale,second order fluctuations.This process is repeated until the inner Renolds number for the highest order fluctuation (of velocity v_o and scale ℓ_o) is below R_{ecr}.The energy is then dissipated in the form of heat. The rate of dissipation of energy by these small fluctuations is given by

$$\varepsilon \simeq \nu v_o^2/\ell_o^2$$

now since fluctuations of lower order ie. for which $R_{e_\ell} > R_{ecr}$ receive their energy from larger fluctuations and subsequently pass this energy on down to smaller fluctuations,it can be seen that the rate of energy flow is $\simeq \varepsilon$ .Therefore for velocity fluctuations of all scales except the smallest

$$v_\ell^3/\ell \sim \varepsilon$$

so that

$$v_\ell \sim (\varepsilon\ell)^{1/3}$$

Now in order to describe the fluctuations in the velocity field we can use the structure function $D(r)$ (see Appendix 1). If we take a value of r which is large in comparison to the inner scale of turbulance ℓ_o but small in comparison to the outer scale of turbulence L, then $D(r)$ is mainly due to fluctuations of characteristic size r so that

$$D(r) \sim v_r^2$$

since

$$D(r) = \overline{(v_{r_1} - v_{r_2})^2}$$

where

$$\vec{r} = \vec{r}_1 - \vec{r}_2$$

but we know that

$$v_r \sim (\epsilon r)^{1/3}$$

and therefore $\underline{\underline{D(r) = C(\epsilon r)^{2/3}}}$ where C = constant

This is the "Two-thirds Power Low" first obtained by Kolmogorov (1.3)

Conservative Passive Additives

Characteristics of the atmosphere such as temperature and humidity can often be regarded as passive additives. A volume of air is characterised by a concentration θ of additive. If the value of θ does not change as the volume of air observed is moved then the additive is said to be conservative. The additive is passive if it does not affect the dynamics of the turbulance. This assumption cannot be strictly justified for temperature as temperature inhomogeneities introduce buoyancy forces.

Using similar arguments to those used in the discussion of the velocity field it can be shown (1.2) that the structure function of the additive

ie $$D_\theta(r) = \overline{(\theta(r_1) - \theta(r_2))^2} \qquad \ell_o << r << L_o$$

depends only on r, ϵ and N where ϵ has the same meaning as before and N is the amount of inhomogeneity which disappears per unit time due to molecular diffusion.

ie $$D_\theta(r) = F(N, \epsilon, r)$$

dimensional considerations lead to

$$D_\theta(r) = \frac{a^2 N r^{2/3}}{\varepsilon^{1/3}} \qquad \ell_o << r << L_o$$

where a is a numerical constant.

We can define the temperature structure constant such that

$$C_T^2 = a^2 N/\varepsilon^{1/3} \qquad C_T = \text{temperature structure constant}$$

In terms of which

$$D_T(r) = C_T^2 r^{2/3} \tag{1.4}$$

so that $D_T(r)$ is the temperature structure function.

Now since the refractive index n is of the form

$$n = 1 + (CP/T) \times 10^6$$

where C = constant

P = pressure

and since in a turbulent medium temperature fluctuations are much stronger than pressure fluctuations;which are very quickly dissipated, we can say that the refractive index fluctuations are mainly produced by temperature fluctuation and hence

$$D_n(r,h) = C_n^2(h)\, r^{2/3} \tag{1.5}$$

where $C_n^2(h)$ is the refractive index strucutre constant and is a function of height h.

Having now calculated the form of the refractive index structure function we are in a position to go on and calculate the wave structure function for electromagnetic waves propagating through the whole or part of the atmosphere,and hence obtain an expression for the modulation transfer function of the atmosphere.

Modulation Transfer Function of the Atmosphere

Consider a diffraction limited lens of focal length R and diameter D,and denote position in the plane tangent to the lens by the vector v.At a point x in the focal plane of the system we can represent the phase and amplitude of the image by u(x) (1.4)

where $$u(x) = A\int dv U(v) \exp\left(-i\frac{2\pi v x}{\lambda R}\right) \tag{1.6}$$

where U(v) represents the plane wave as collected by the lens and A is a constant.

Now the intensity of the image is $u(x).u^*(x)$ and the MTF (modulation transfer function) of the system is given by

$$\tau(f) = B \int dx u^*(x)u(x)\exp(2\pi ifx) \qquad (1.7)$$

on substitution of (1.6) into (1.7) we can obtain (see Fried (1.5))

$$\tau(f) = A^2B \int dv U^*(v-\lambda Rf)U(v) \qquad (1.8)$$

Now if $\phi(v)$ denotes the random phase variations and $\chi(v)$ the random variations of the log amplitude then we can say

$$U(v) = W(v)\exp(\chi(v) + i\phi(v))$$

where $W(v)$ is the aperture function. (1.8) can now be re-written as

$$\tau(f) = A^2B \int dv W(v-\lambda Rf)W(v)\exp((\chi(v) + \chi(v-\lambda Rf)) + i(\phi(v) - \phi(v-\lambda Rf))) \qquad (1.9)$$

now if we denote the average long exposure MTF by $\langle\tau(f)\rangle$ where $\langle\rangle$ denotes ensemble average then

$$\langle\tau(f)\rangle = A^2B \int dv W(v-\lambda Rf)W(v) \times \langle\exp(\chi(v) + \chi(v-\lambda Rf)) + i(\phi(v) - \phi(v-\lambda Rf))\rangle \qquad (1.10)$$

By defining the phase and log amplitude structure functions as

$$D_\phi(r) = \langle(\phi(v) - \phi(v'))^2\rangle$$

$$D_\chi(r) = \langle(\chi(v) - \chi(v'))^2\rangle$$

where $r = |v - v'|$

Fried (1.5) is able to show that the ensemble averaged exponential term in (1.10) is given by

$$\exp(-1/2\ D_\chi(\lambda Rf) - 1/2\ D_\phi(\lambda Rf))$$

now by defining the wave structure funciton as

$$D(r) = D_\chi(r) + D_\phi(r)$$

and substituting back into (1.10) we obtain

$$\langle\tau(f)\rangle = A^2B \int dv W(v-\lambda Rf)W(v)\exp(-1/2D(\lambda Rf)) \qquad (1.11)$$

we can now define the quantity $T_o(f)$ as

$$T_o(f) = A^2B \int dv W(v-\lambda Rf)W(v)$$

so that

$$\langle\tau(f)\rangle = T_o(f)\exp(-1/2D(\lambda f')) \quad \text{where} \quad f' = Rf \qquad (1.12)$$

and since $T_o(f)$ is the transfer function of the aperture then $\exp(-1/2D(\lambda f))$ can be interpreted as the long exposure transfer function ot the atmosphere.

The Form of the Wave Structure Function

In order to describe the effect of atmosphere turbulence on the MTF Fried (1.5) represents the wave structure function D(r) by

$$D(r) = Ar^{5/3} \qquad (1.13)$$

where Hufnagel and Stanley (1.6) and Tatarski (1.2) have shown that the constant A is given by

$$A = 2.91\ k^2 \sec\alpha \int_o^H C_N^2\, dh \qquad (1.14)$$

where $k = \frac{2\pi}{\lambda}$ α = zenith angle, and the integration is over the path length through the atmosphere. C_N^2 is the structure constant of N = (n-1) where n is refractive index.

It should be noted that r is now the magnitude of the vector between two points in the plane tangent to the collecting surface or lens, rather than the three dimensional vector used for the velocity, temperature and refractive index structure functions discussed previously.

The derivation of A depends on approximate solutions to the wave equation describing the propagation of electromagnetic waves. The most commonly used approximation is that of Rytov although Hufnagel and Stanley (1.6) question its validity and Fried (1.5) even questions its origin. However, the form of (1.14) seems to be generally accepted as correct.

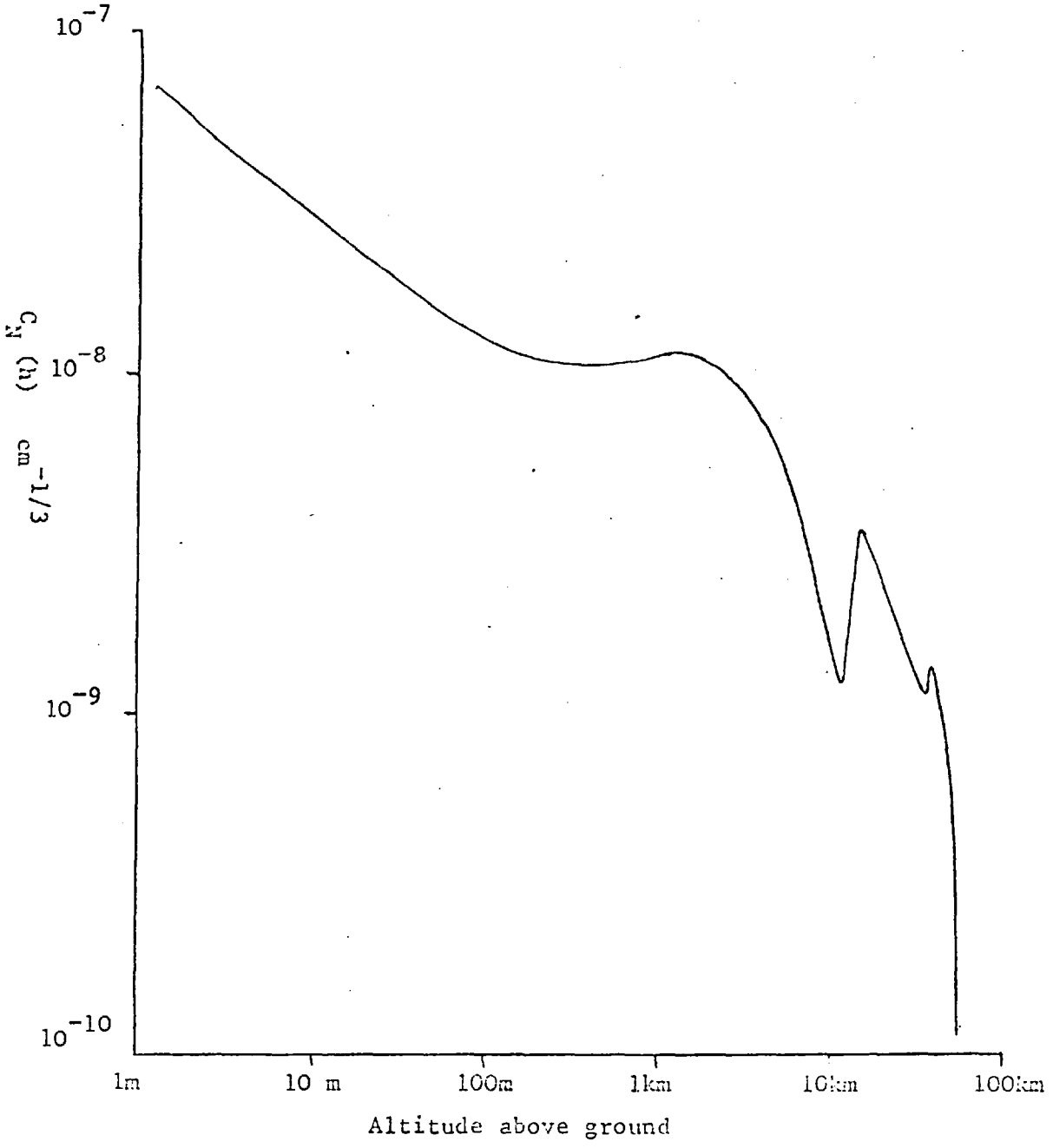

Fig.1.2 Refractive index structure constant vs. altitude

In order to characterise the atmospheric turbulence in terms of one quantity, Fried (1.5) defined the property r_o such that

$$r_o = (6.88/A)^{3/5} \qquad (1.15)$$

The significance of the factor 6.88 is to give r_o a physical interpretation which will become apparent later.

In terms of r_o then the wave structure function becomes

$$D(r) = 6.88(r/r_o)^{5/3}$$

and we can now say that the long exposure MTF of the atmosphere is given by

$$<\tau_A(f)> = \exp(-3.44(\lambda Rf/r_o)^{5/3}$$

or

$$<\tau_A(f')> = \exp(-3.44(\lambda f'/r_o)^{5/3} \qquad (1.16)$$

where f' = spatial frequency (cycles/radian)

The Evaluation of the Atmospheric MTF

We are now in a position to model the shape of the atmospheric MTF for a given value of r_o and it remains only to evaluate r_o. Recalling the definition of r_o we have

$$r_o = (6.88/A)^{3/5}$$

where $A = 2.91\ k^2 \sec\alpha \int_o^H C_N^2(h)\ dh$

in order to evaluate r_o then it is necessary to know, or be able to model the function $C_N^2(h)$.

The first attempt to model the refractive index structure constant was due to Hufnagel and Stanley (1.6). Using the averated results obtained by other workers for dissipation rate (1.7, 1.8) potential temperature gradient (1.9) and wind shear (1.10) they were able to obtain the function of figure 1.2. Using this function they were then able to obtain the value of the integral in the definition of A (equation 1.12) as

$$\int_o^\infty C_N^2\ dh = 6\times10^{-11}\ cm^{-1/3} = 1.29 \times 10^{-11}\ m^{-1/3}$$

Hufnagel and Stanley then calculated the average transfer function and average function for zenith viewing through the whole atmosphere.

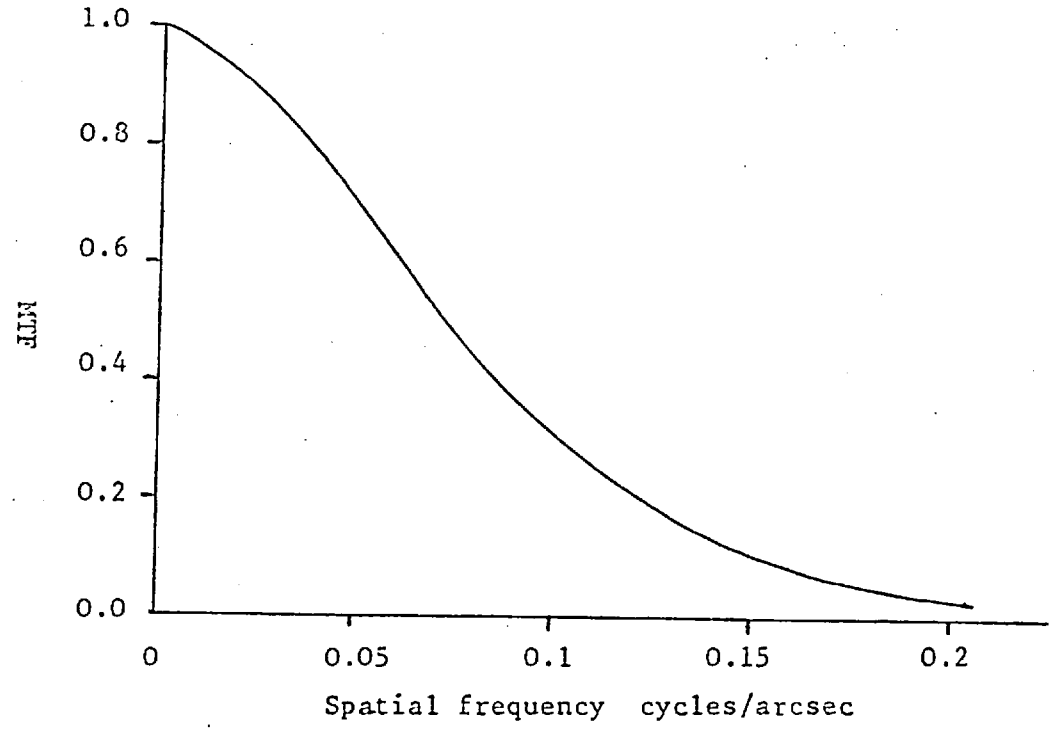

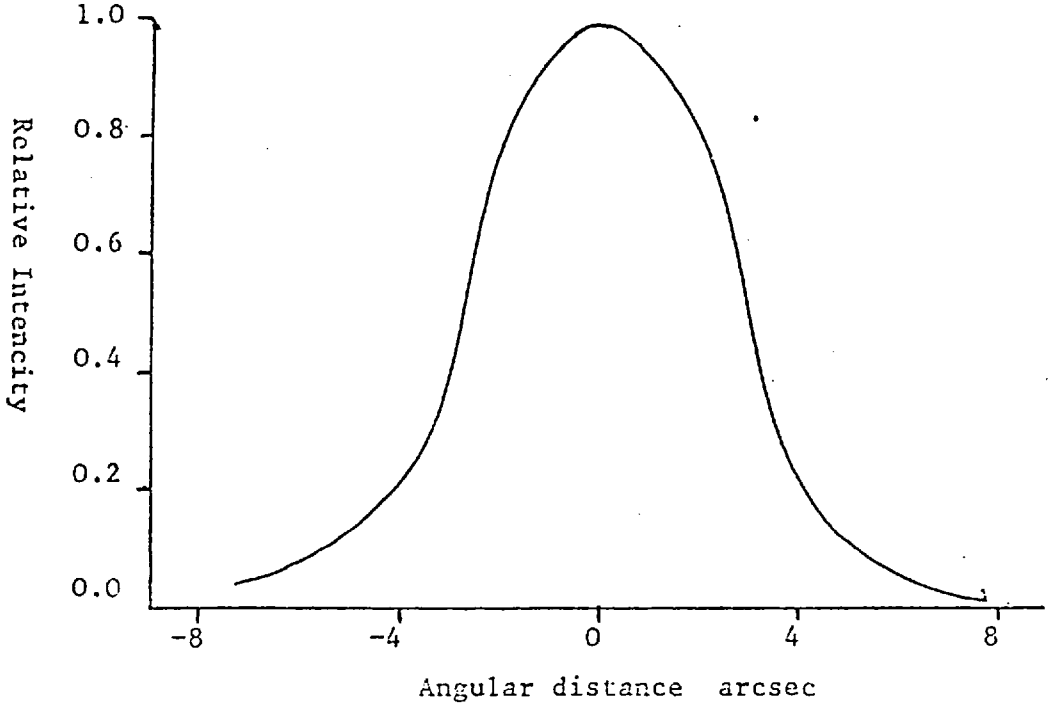

Fig. 1.3 Transfer function and intensity function for zenith viewing (Hufnagel and Stanley)

Their results are shown in figure1·3.They noted however that these results applied to daytime conditions for which Hosfeld (1.11) had said that the half width of typical stellar images were about twice that for nightime observations.Hufnagel realised therefore that the values in figure1·2 represented a degree of turbulence which was too high to be applicable to nightime observations. He therefore proposed the revised model of figure 1.4 (1.12,13) This model takes into account the different amounts of turbulence present on sunny days,clear nights,the dawn and dusk minima and conditions where disturbed boundary layers are present.

Brookner (1.13) has fitted the following empirical expression to the Hufnagel revised model :-

$$C_N^2(h) = C_{NO}^2 h^{-b} \exp(-h/h_o) + C_{NP} \delta(h-h_p)$$

where h_o is a scale height for the atmosphere, $\delta(h)$ is the delta function and C_{NP} represents the integral $C_N^2(h)$ under its peak which occurs at the tropopause altitude $h_p \simeq 12$ km.The values of b, h_o and C_{NO}^2 are given in table 1.

Table 1·1

	b	h_o m	C_{NO}^2 $m^{-1/3}$	C_{NP} $m^{-1/3}$
Sunny Day	5/6	320	3.6×10^{-13}	4.3×10^{-13}
Clear Night	1	320	1.6×10^{-13}	4.3×10^{-13}
Dawn/Dusk min	2/3	320	8.7×10^{-15}	4.3×10^{-13}

In order to evaluate the integral

$$\int_o^\infty C_N^2 \, dh$$

Brookner defines the quantity C_N^+ where

$$C_N^+ = \int_{h_a}^{h_b} C_N^2(h) \, dh$$

using h_a = 3m and h_b = 10km he then obtains the following values for C_N^+

Sunny Day - 2.4×10^{-12}

Clear Night - 5.8×10^{-13}

Dawn/dusk min - 1.7×10^{-13}

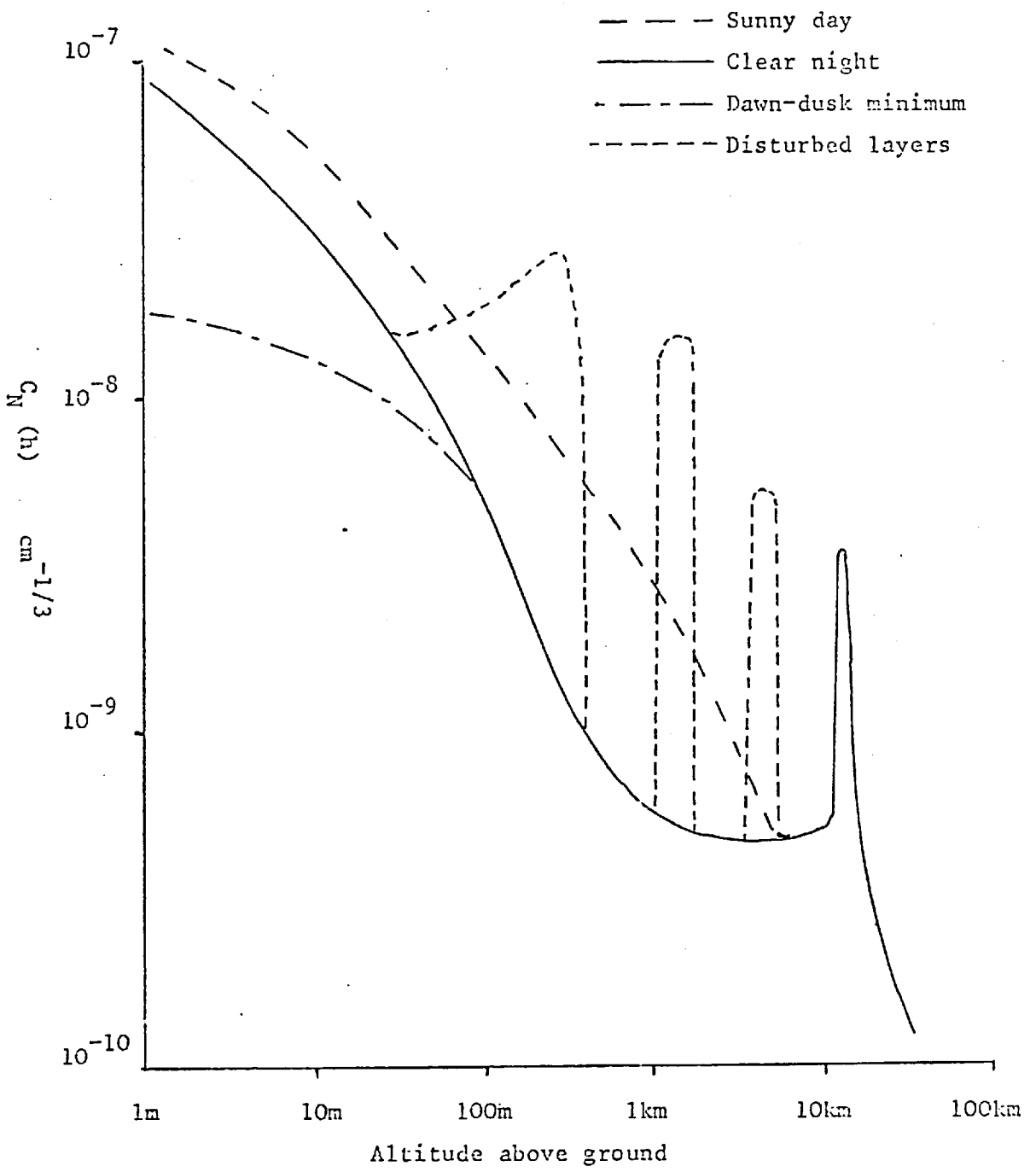

Fig. 1.4 Hufnagel's revised model

Now since most of the contribution to C_N^+ comes from the lower levels of the atmosphere it is sufficient to use these values of C_N^+ combined with the above value of C_{NP} to evaluate the integral

$$\int_o^\infty C_N^2(h)\, dh$$

we obtain therefore (recalling also the value for Hufnagel's first model) the values of table 1.2.

TABLE 1.2

	$\int_o^\infty C_N^2(h)dh$ $m^{-1/3}$	A	r_o m
Old Model	1.29×10^{-11}	5.93×10^{3}	1.7×10^{-2}
Sunny Day	2.83×10^{-12}	1.3×10^{3}	4.3×10^{-2}
Clear Night	1.01×10^{-12}	4.6×10^{2}	8.0×10^{-2}
Dawn/Dusk min	6.00×10^{-13}	2.6×10^{2}	1.13×10^{-1}

Also given in table 1.2 are the values of the constant A and r_o calculated from equations 1.12 and 1.11 respectively for a wavelength of 0.55 μm.

Comparison of theoretical values of r_o with measured values

Care should be taken in comparing the values of r_o in table 1.2 with the limited data available from observatory quality sites, since the models used for the evaluation of the integral $\int_o^\infty C_N^2(h)dh$ apply to clear, flat ground and not mountain tops.

Fried and Mevers (1.14 have made a study of the median value of r_o using results obtained by Hoag (1.15) at the U.S Naval Observatory at Flagstaff, Arizona and by Meinel at Kitt Peak National Observatory during the site test survey for the National Astronomical Observatory. Measurements were made by Hoag on 200 nights over a one year period. Fried treated the two sets of data separately and found r_o to be a log-normally distributed random variable. The median value for Hoog's data was 0.111m and for Meinel;s data 0.117m for $\lambda = 0.55\mu m$.

Based on this information and various theoretical considerations concerning r_o Fried and Mevers recommended that for nightime operation from a carefully selected site r_o should have a median

value

$$(r_o)\ \text{median} = 0.114\ (\lambda/5.5\times10^{-7})^{6/5}\ (\sec\alpha)^{-3/5}$$

It should be noted that in the original paper which appeared in 'Applied Optics' there is an unfortunate misprint which could lead to some confusing predictions.

Dainty and Scaddon (1.17) made measurements using a coherence interferometer at Mauna-Kea Observatory during June 1974, the values they derived for r_o together with their visual estimates of seeing for the observing period are given in table 1.3.

TABLE 1.3

Date	Seeing*	r_o cm
1974 June 21	Poor	5.6
22	Average	7.4
23	Good	16.2
24	Good	14.8
25	Average	9.1
26	Average	10.5
27	Average	13.1
28	Good	19.3
29	Good	17.6
30	Good	15.5

*Seeing
Poor image diameter > 3
Average image diameter ≈ 1.5–3
Good image diameter <1.5

As can be seen therefore the values of r_o obtained for observatory quality sites are larger than predicted for normal sites although a large spread in the values for r_o may still be encountered even at the best of sites.

The Significance of r_o

In order to realise the significance of the value of r_o we must first consider the limits on angular resolution which

the atmosphere imposes.

As mentioned previously,in order to define the resolution of an optical system we must set some arbitrary criterion by which we may judge its performance.For the purposes of this argument, following Korff (1.18) we may say that the resolution limit may be defined as the angle $\Delta\theta$ such that the transfer function of the system falls to 1/10 of its maximum value at a spatial frequency $f = 1/\Delta\theta$

Recalling then the transfer function of the atmosphere we have the condition

$$\exp(-3.44(\lambda/r_o\Delta\theta)^{5/3}) \simeq 0.1$$

so that

$$\Delta\theta \simeq 1.27\lambda/r_o$$

We may note however that the diffraction limited resolution of a telescope of aperture D was defined earlier as

$$\Delta\theta = 1.22\ \lambda/D$$

It can be said therefore that by this simple argument the significance of r_o is that the resolution availailable in the presence of atmospheric turbulance is approximately equal to the resolution which would be obtained by using a circular aperture of diameter r_o. In fact by defining the resolution in terms of spatial bandwidths Fried (1.5) showed that the resolution for the two cases were in fact exactly equal.

Another interesting property of r_o may be noted by refering back to fig 1.3.As can be seen the half intensity full width of the seeing disc profile is $\simeq 6''$ and the value of r_o for this model was calculated to be 0.017 m from which we may note that $\lambda/r_o = 6.1$ .It is in this respect that r_o is often talked of as a measure of the correlation scale of the atmospheric turbulance.

Short Exposure Seeing

So far in this discussion we have limited ourselves to the case of long exposures.This is in fact the case of relevance to most astronomical applications ,for example photographic integration and small aperture photometry.We shall now however turn briefly to the short exposure case.

The distortion of the wavefront from a star may be considered to be made up of two components,Firstly corrugations of

scale larger than the telescope pupil and secondly corrugations of comparable and smaller scale to the telescope pupil.

The large scale corrugations will be seen by the telescope as wavefront tilts and hence their effect will be to displace the image of the star in the focal plane of the telescope.The small scale corrugations on the other hand will have the effect of causing image blurs in the focal plane.

It can now be said therefore that if we take a short exposure image of the star,only the small scale corrugations will affect the image quality,whereas a long exposure image will also have the integrated effects of image motion.This argument also explains why a small telescope will exhibit a diffraction limited image which dances about in the focal plane,whereas a larger telescope gives a more stable but extended seeing disc.

In order to remove the effects of image tilt Fried (1.5) defined a random vector $\underline{a}$ which was related to $\phi(v)$ in such a manner that $\underline{a}.\underline{v}$ gave the best least-squares fit to $\phi(v)$. By subtracting this average tilt from the phase terms of equation 1·9 he was then able to show that in the case where $D \gg (H\lambda)^{\frac{1}{2}}$ (H = propagation length) , this is the case which is almost always applicable to atmospheric seeing effects in the visible , the short exposure transfer function of the telescope atmospheric system was given by

$$\langle T(f)\rangle_{SE} = T_o(f)\exp(-3.44(\lambda Rf/r_o)^{5/3}(1-(\lambda Rf/D)^{1/3})) \qquad (1.19)$$

Two points should be noted here.Firstly we have an extra term in the exponant which is dependant on the telescope diameter and which will tend to reduce the predicted seeing disc diameter.Secondly, we are no longer able to assign a unique transfer function to the atmosphere,as the nature of the seeing is now heavily dependant on the form of the aperture used.

The Infrared Seeing

In a previous section it was noted that for a given value of r_o the seeing size was given by the approximate relationship

$$\Delta\theta \simeq \lambda/r_o$$

No rigorous definition of $\Delta\theta$ was applied although the measure

used was the half intensity full width of the seeing profile. It may be more appropriate to use the equivalent width of the profile in the above relationship especially in view of the idea that r_o represents the width of the autocorrelation function of the atmospherically distorted wavefront. However, since the intensity profile of the seeing disc cannot be represented analytically it is not possible to define an equivalent width for the function which lends itself to measurement. We must therefore content ourselves with the half intensity full width of the profile as a measure of the seeing size.

In order to predict the size of the infrared seeing disc we wish to know the behaviour of r_o with wavelength. Recalling the definition of r_o given by Fried (1.5)

$$r_o = (6.88/A)^{3/5}$$

where $A = 2.91k^2 \sec \alpha \int_c^\infty C_N^2(h)dh$

so that $A \propto \lambda^{-2}$

and hence $r_o \propto \lambda^{6/5}$

so given that $\Delta\theta \simeq \lambda/r_o$

we have $\Delta\theta \propto \lambda^{-1/5}$

Figure1.5 shows a graph of seeing size against wavelength for average r_o at visible wavelength of .114m (1.14)

At this stage it is worth comparing the theoretical predictions for infrared seeing with two contrasting opinions on the subject which have appeared in the literature. Low and Rieke (1.19) make the following observation...
"No detailed studies of the infrared seeing have been carried out; however from experience at the telescope it appears that the seeing disc at 10μm is at least half as large as it is in the visible". From figure1.5 it can be seen that this observation is in reasonable agreement with the theoretical predictions.

In contrast, Andriesse and Wiersta (1.20) suggest that the infrared seeing is much better than this. They define a quantity A* for which the image sizes due to seeing and diffraction are equally large, this of course corresponds to r_o. They modelled the

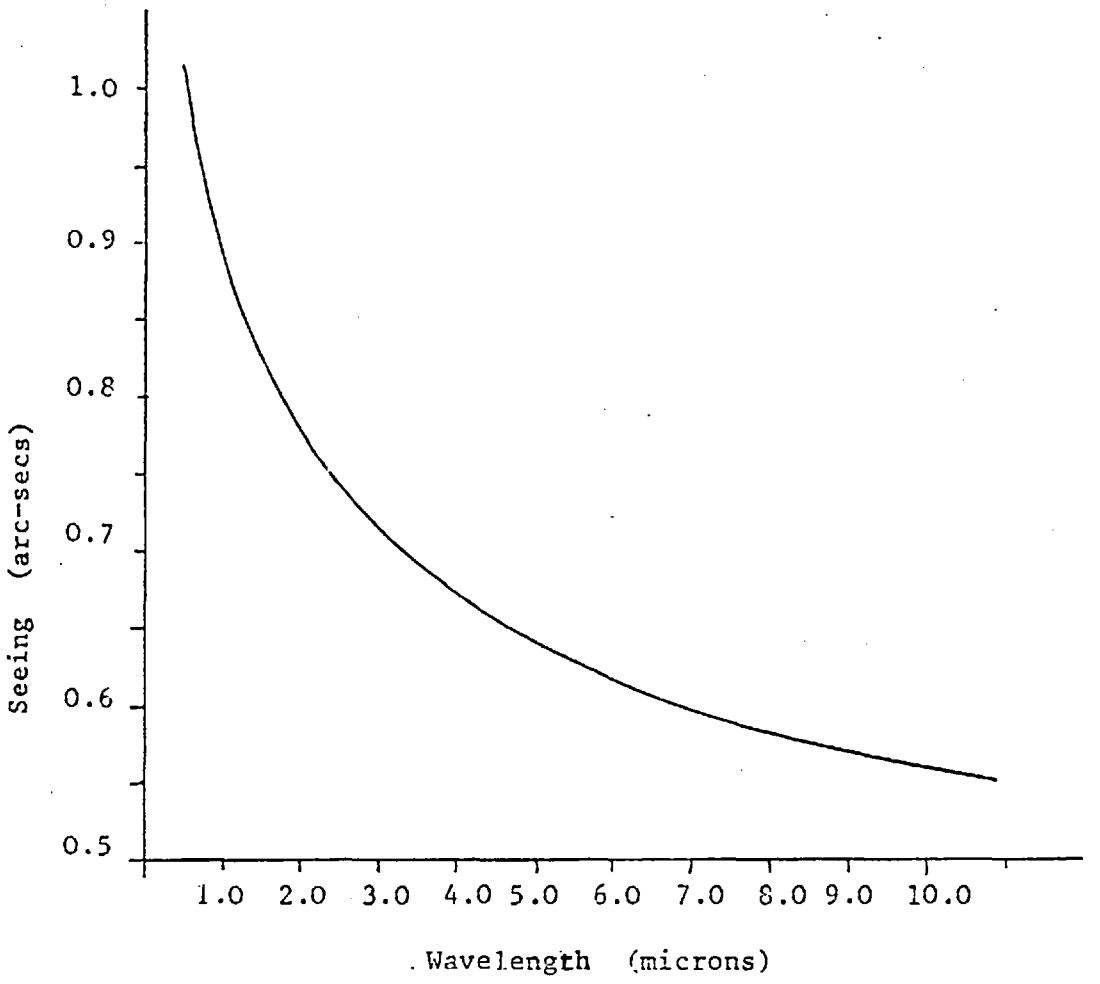

Fig. 1.5 Seeing vs. Wavelength (Visual seeing $1\hat{''}$)

effects of the atmosphere on the wavefront using a computer simulation.Based on this work they say "For = 1μm this aperture (A*) would be of the order of 1m at 'normal seeing'." However, this suggests that the seeing at 1μm would be equal to 0.2″ .This is clearly neither in agreement with the theoretical prediction or with the observation of Low and Rieke.

The observation of Low and Rieke that no detailed studies of infrared seeing have been carried out is still true and the behaviour of the infrared seeing disc is not well known.

Chapter 2 Stellar Speckle Interferometry

Introduction

The origin of the term ' speckle' can easily be appreciated by observing the grainy structure of the pattern formed when laser light is reflected from a rough surface.In fact speckle patterns are produced whenever partially coherent light encounters random phase delays across its wavefront.Since atmospheric turbulence imposes random phase perturbations on the wavefront of light coming from objects outside the earth's atmosphere,stellar images are also speckle patterns.However, since the phase perturbations imposed by the atmosphere change rapidly in time the speckle patterns tend to blur into a disc of diameter much larger than the diffraction pattern of the telescope.

In this chapter a technique will be discussed by which the information in the speckles may be retrieved and hence by which diffraction limited information may be obtained.

Visible Stellar Speckle Interferometry

Stellar speckle interferometry was originally suggested by Labeyrie (2.1) as a method for obtaining diffraction limited information in the presence of a turbulent atmosphere.The technique was first implemented by Gezari et al (2.2) and is now well established with several groups obtaining useful results (2.3-2.6)

Generally the technique at visible wavelengths involves recording a large number of short exposure images of the star through a narrow bandwidth filter.The instantaneous image intensity may be expressed as

$$I(x,y) = O(x,y) \otimes t(x,y) \qquad (1.1)$$

where $O(x,y)$ is the object intensity

$t(x,y)$ is the instantaneous point spread function of the atmosphere telescope system

$\otimes$ represents convolution

Each of the short exposure images contains high spatial frequency information about the object,the cut-off frequency being equal to the diffraction limit of the telescope pupil (2.7-2.9). If these images were simply co-added,a characteristic seeing disc of about 1-2$''$ would be obtained and the high spatial frequency information would be lost.Alternatively if their spatial frequency power spectra are co-added then diffraction limited information is retrieved for many telescopes and seeing conditions prevailing in the visible.

It is not possible to uniquely reconstruct an arbitrary object intensity function since the power spectrum contains no phase information,although methods have been suggested for its retrieval (2.10-2.11).For instance,if a suitable point source can be found in the same isoplanatic patch as the object of interest then it should be possible to reconstruct the object intensity function by suitable deconvolution techniques.However,short exposure studies of double stars (2.12) indicate that the speckle pattern for each star of the pair are only identical for stars closer than 2-3$''$.This then gives an idea of the limit of this technique.

In the spatial frequency domain the average power spectrum of the image intensity is given by

$$\langle |i(u,v)|^2 \rangle = |o(u,v)|^2 \cdot \langle |T(u,v)|^2 \rangle \qquad (2.2)$$

where i (u,v), o (u,v) and T (u,v) are the Fourier transforms of I (x,y),O(x,y) and t (x,y) respectively.$\langle |T(u,v)|^2 \rangle$ is then the transfer function of the speckle technique;in the next section I shall discuss its form and indicate that it is insensitive to aberrations provided the optical system is of sufficient quality to resolve the atmospherically induced seeing disc.

The Speckle Transfer Function

It can be shown (2.13) that apart from a constant factor, the transfer function T (u,v) for incoherent illumination is the auto-correlation of the pupil function of the system G (x,y) where distances x,y in the plane of the pupil are related to spatial frequency variables in the image plane by $x=\lambda fu, y=\lambda fv$,where f is the focal length of the system.

We have then

$$T(u,v) = \int\int_{-\infty}^{\infty} G(x_1,y_1)G^*(x_1+x,y_1+y)dx_1dy_1 \qquad (2.3)$$

Following Dainty (2.9),in the case where we are imaging through a random medium the pupil function may be split into a product ot two functions,one representing the effect of the random medium and one representing the pupil function of the imaging component

$$G(x,y) = A(x,y)Z(x,y) \qquad (2.4)$$

here A (x,y) is the pupil function of the imaging part of the system and Z (x,y) is the complex amplitude in the plane of the pupil due to a point source in the object plane.

Combining 2.3 and 2.4 gives

$$T(u,v) = \int\int_{-\infty}^{\infty} A(x_1,y_1)A^*(x_1+x,y_1+y)Z(x_1,x)Z^*(x_1+x,y_1+y)dx_1dy_1 \qquad (2.5)$$

The transfer function of the system for normal time-averaging may now be obtained by taking the ensemble average of T (u,v) so that

$$\langle T(u,v)\rangle = \int\int_{-\infty}^{\infty} A(x_1,y_1)A^*(x_1+x,y_1+y)\langle Z(x_1,y_1)Z^*(x_1+x,y_1+y)\rangle dx_1 dy_1 \tag{2.6}$$

The autocorrelation of Z (x,y) may be defined as

$$C_Z(x,y) = \langle Z(x_1,y_1)Z^*(x_1+x,y_1+y)\rangle \tag{2.7}$$

and is independent of (x,y) if the random process is stationary (see Appendix 1).

Now the transfer function of the optical system alone may be defined as

$$T_o(u,v) = \int\int_{-\infty}^{\infty} A(x_1,y_1)A^*(x_1+x,y_1+y)dx_1 dy_1 \tag{2.8}$$

and so from equations 2.6,7 and 2.8

$$\langle T(u,v)\rangle = T_o(u,v)C_Z(x,y) \tag{2.9}$$

Now since $C_Z(x,y)$ falls to zero faster than $T_o(u,v)$ (the telescope being able,in general to produce an image in the abscence of turbulance,which is smaller than the seeing disc,which is produced in the presence of turbulance) the resolution is limited by the seeing.

In speckle interferometry however we are interested in finding the average of the squared modulus of T (u,v) so that from equation 2.6 we have

$$\langle |T(u,v)|^2\rangle = \int\int\int\int_{-\infty}^{\infty} A(x_1,y_1)A^*(x_1+x,y_1+y)A^*(x_2,y_2)A(x_2+x,y_2+y) \times \langle Z(x_1,y_1)Z^*(x_1+x,y_1+y)Z^*(x_2,y_2)Z(x_2+x,y_2+y)\rangle dx_1 dy_1 dx_2 dy_2 \tag{2.10}$$

If the R.M.S phase fluctuations on the wavefront are larger than π then we can say that the phase of the wavefront should be random in the interval π to π and we can approximate Z (x,y) to a complex Gaussian random variable.These approximations turn out to be good for visible wavelengths but may get worse at longer wavelengths since the phase fluctuations will be smaller.

For a complex Gaussian process then it can be shown that (2.14)

$$\langle Z_1 Z_2^* Z_3^* Z_4\rangle = \langle Z_1 Z_2^*\rangle\langle Z_3^* Z_4\rangle + \langle Z_1 Z_3^*\rangle\langle Z_2^* Z_4\rangle$$

so that equation 2.10 can be rewritten as

$$\langle |T(u,v)|^2 \rangle = \int\int_{-\infty}^{\infty} A(x_1,y_1)A^*(x_2,y_2)A^*(x_1+x,y_1+y)A(x_2+x,y_2+y) \cdot (|C_Z((x_2-x_1)(y_2-y_1))|^2 + |C_Z(x,y)|^2) \cdot dx_1 dy_1 dx_2 dy_2 \tag{2.11}$$

and using equation 2.9 we have

$$\langle |T(u,v)|^2 \rangle = |\langle T(u,v) \rangle|^2 + \int\int_{\infty}^{\infty} |C_Z(x_2-x_1,y_2-y_1)|^2 \cdot A(x_1,y_1)A^*(x_2,y_2)A^*(x_1+x,y_1+y) \cdot A^*(x_2+x,y_2+y)\, dx_1 dx_2 dy_1 dy_2 \tag{2.12}$$

From Chapter 1 however we know that the atmospherically distorted wavefront has a characteristic scale r_o such that for $r \leqslant r_o$ $C_z(r) \simeq 1$ and for $r \gg r_o$ $C_z(r) \simeq 0$. If we then assume a situation where the telescope aberrations remain reasonably constant over any region of diameter r_o then we can rewrite 2.12 as

$$\langle |T(u,v)|^2 \rangle = |\langle T(u,v) \rangle|^2 + k \int\int_{\infty}^{\infty} A(x_1,y_1)A^*(x_1,y_1) \cdot A^*(x_1+x,y_1+y)A(x_1+x,y_1+y)\, dx_1 dy_1 \tag{2.13}$$

Now A (x,y) is the pupil function of the imaging part of the system so that if $r = (x^2 + y^2)^{1/2}$

$A(r) = \exp(i\beta(r))$ for $|r| < D/2$

$A(r) = 0$ for $|r| > D/2$

where β (r) is a function which represents the aberrations of the system. If then we form the function W (r) such that

$$W(r) = A(r)\, A^*(r)$$

then $W(r) = 1$ for $|r| < D/2$

$W(r) = 0$ for $|r| > D/2$

so that W(r) is just the aperture function of the optical system and is not affected by aberrations.

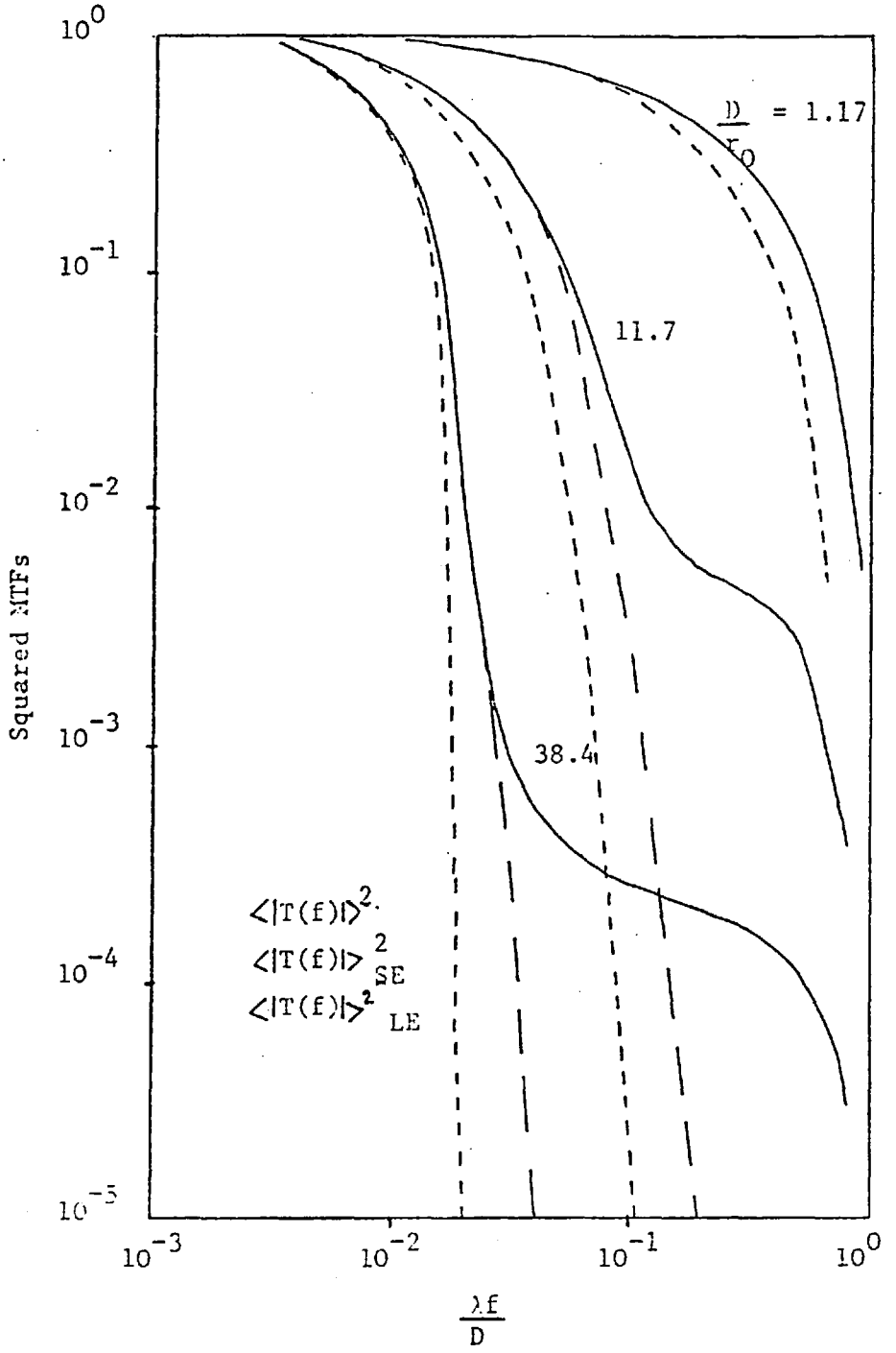

Fig. 2.1 $\langle|T(f)|^2\rangle$ vs. $\lambda f/D$ for D/r_o = 1.17, 11.7 and 38.4 corresponding to D~15cm, 1.5m and 5m for 0.9" seeing

The diffraction limited transfer function of the optical system can now be defined as

$$T_D(u,v) = \iint_{\infty}^{\infty} W(x_1,y_1)W^*(x_1+x,y_1+y)dx_1dy_1 \qquad (2.14)$$

and so from equation 2.13 and 2.14 we have

$$\langle |T(u,v)|^2 \rangle = |\langle T(u,v)\rangle|^2 + kT_D(u,v) \qquad (2.15)$$

The speckle transfer function is therefore made up of two components.The first is just the square of the time averaged transfer function and is due to the average distribution of intensity in the image.The second term is due to fluctuations of intensity caused by the speckles and carries diffraction limited information.Here k is a constant which takes into account the normalisation of the two functions.Dainty (2.8) suggests that the two functions should be normalised such that their volumes are equal.This is based on the idea that the variance of a speckle pattern equals the square of the mean intensity (2.15).Thus the constant k is given by the ratio of the volumes of the functions $|\langle T(u,v)\rangle|^2$ and $T_D(u,v)$ which gives

$$k \simeq r_o^2/D^2 \qquad (2.16)$$

(Dainty 2.16 has numerically integrated the two functions to find, the more exact result $k = 0.435r_o^2/D^2$)

It should be noted that the second term in equation 2.15 is only proportional to the diffraction limited transfer function when $r_o \ll D$,that is for poor seeing on large telescopes and will in general depend to some extent on the form of $C_z(x,y)$ and the aberrations of the telescope.To a first approximation the condition that the telescope must be free of aberration over scales of the order of r_o is equivelent to saying that the telescope is capable of resolving the seeing disc.A similar result has been obtained by Korff,Dryden and Miller (2.7).

The Log-Normal Model

Dainty's treatment of the problem of modelling the speckle transfer function was based,as mentioned earlier,on a model for

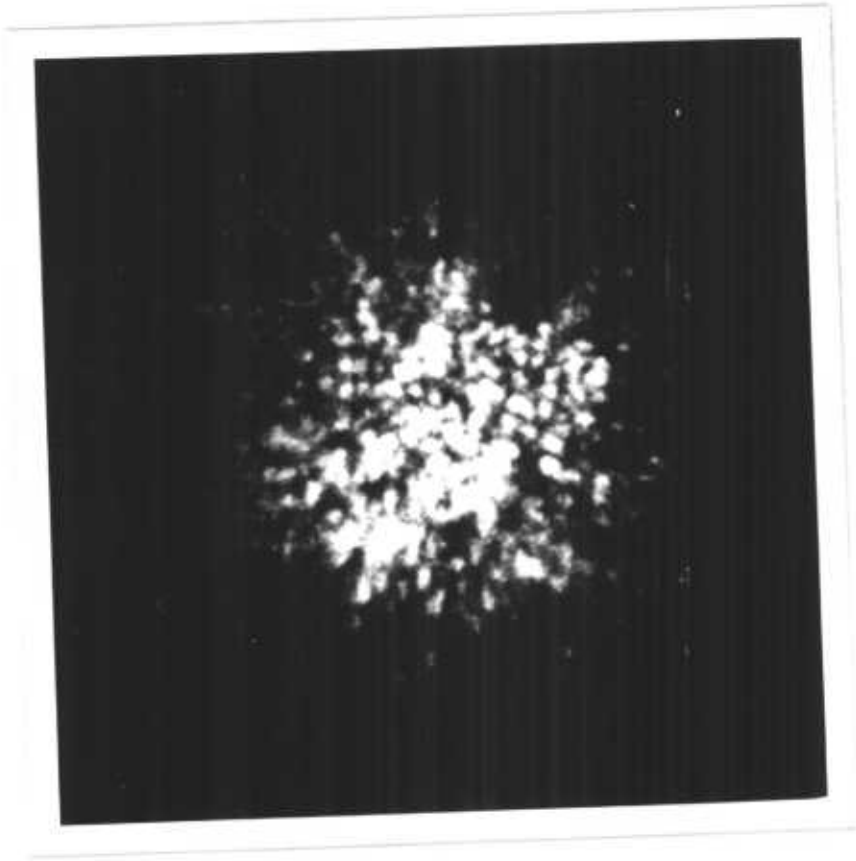

Fig. 2.2 Short exposure (0.008 sec) image of Vega recorded on the 2.5m INT

atmospheric turbulance in which both the phase and amplitude of the wavefront were zero mean Gaussian random variables.However,as shown is Chapter 1,the atmosphere is best described by a log-normal model where the phase and log amplitude are assumed to have Gaussian distributions.

Korff(2.17) has used this model in an analysis similar to that described in Chapter 1 for the evaluation of $< T(u,v) >$, but applied to the problem of finding $< |T(u,v)|^2 >$.Figure2.1 shows Korff's predicitons of $< |T(u,v)|^2 >$ for three values of r_o/D

The transfer function again consists of two terms,the first however is now equal to the square of the short exposure transfer function but the second still has a term which is roughly proportional to the diffraction limited transfer function of the telescope.

Implementation of Speckle Interferometry at Visible Wavelengths

As mentioned previously the technique of speckle interferometry at visible wavelengths involves recording a large number of short exposure images through a narrow bandwidth optical filter. One such speckle image (obtained by Richard Scaddan of Imperial College) is shown in figure 2.2.Here the diffraction limited speckles can clearly be seen within an overall envelope of about $1''-2''$

The apparatus used by Beddoes et al (2.5) is typical and is shown schematically in Figure 2.3.The telesope is focused onto a rotating shutter.The speed of rotation and the angle of the aperture of the shutter determines the exposure time.The results of Roddier and Roddier (2.18) suggest that for an aperture diameter of 2.5m and seeing of about $3''$,an exposure time of 10ms should be short enough to 'freeze'the speckle patterns.After passing through the shutter the light passes through a pair of non-deviating but dispersing prisms which are set to produce an equal and opposite dispersion to that imparted by the atmosphere.

In order now to calculate the width of the optical filter required we may note that the number of fringes across the seeing disc which would be produced by two correlation cells of scale r_o at opposite ends of a diameter in the aperture plane,

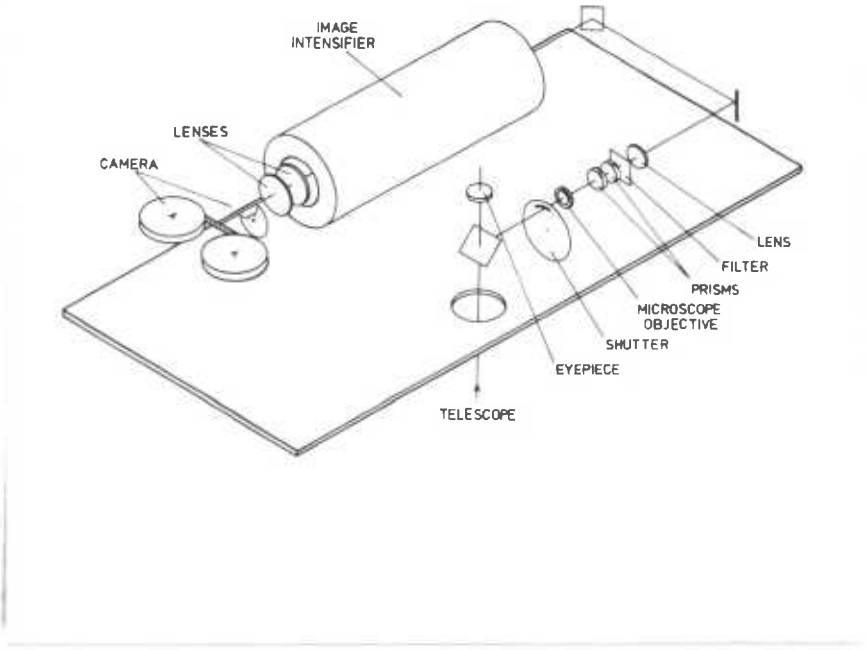

Fig. 2.3 Schematic diagram of a speckle interferometer

is of order D/r_o so that the path difference for the extreme fringes differs by $\lambda D/r_o$. Now the coherence length of the light is $\lambda^2/\Delta\lambda$ and hence for maximum visibility of speckles we require that

$$\Delta\lambda = \frac{\lambda r_o}{D} = \frac{\lambda^2}{D\Delta\theta_s} \qquad (2.17)$$

where $\Delta\theta_s$ is the seeing angle.

After passing through an optical filter of the appropriate bandwidth the light is reimaged onto the photocathode of an image intensifier with a gain in excess of 10^6. The phosphor screen at the output of the image intensifier is then reimaged onto the focal plane of a cine camera which is driven syncronously with the shutter to give framing rates of beween 1 and 30 frames per second.

In order to analyse the data each frame of the processed film is illuminated with coherent light from a laser which is then imaged by a lens onto a second piece of film where the squared modulus of the Fourier transform of the image is recorded. By this means the image power spectrum may be averaged over many frames.

It is also possible to reduce the data digitally by calculating the ensemble average space autocorrelation function of the instantaneneous intensity, which from equation 2.1 is given by

$$\begin{aligned} C(x,y) &= \langle I(x,y)*I(x,y)\rangle \\ &= (O(x,y)*O(x,y))\otimes(t(x,y)*t(x,y)) \end{aligned} \qquad (2.18)$$

where * represents the space autocorrelation. This method will probably become more popular since it lends itself to on line data analysis, especially when using diode arrays as detectors.

Results and Magnitude Limits for Visible Speckle

By considering the statistics of the formation and detection of speckles Dainty (2.19) showed that the signal to noise available from visible speckle interferometry is given by

$$Q = \frac{\langle n_{ph}\rangle}{M}\left(\frac{n_p}{\langle n_s\rangle}\right)^{1/2} \qquad (2.19)$$

where n_p is the total number of pictures, $\langle n_s\rangle$ is the average number of speckles per picture (speckle pairs for a binary object), $\langle n_{ph}\rangle$ is the average number of detected photons per picture and M is the number of resolution cells in the object (one for a single star,

two for a binary system,etc).Using realistic values in equation 2.19 Dainty estimates that the limiting magnitude for a binary should be +20 in three hours,however he does point out that +16 may be a more realistic limit.

The first measurements made using stellar speckle interferometry were due to Gezari et al.(2.2),they resolved 9 stars with diameters down to 0.016$''$.Using the 200inch they estimated that the practical resolution limit was 0.01 $''$ for stellar objects as faint as m_v = +9.

Most of the results from visible speckle relate to observations of binary systems.This is due to the fact that the fringe spacing (and hence binary separation) can be measured directly from the power transform,comparison with a point source transform not being necessary.

Blazit et al (2.3) reported observations of 60 objects including 3C273 (which remained point-like (< 0.02 $''$)) most of the resolved sources were binary systems.

McAlister (2.6) reported observations of 70 binary systems with separations in the range 0.037$''$ to 1.877$''$.Morgan (2.20) report observations of 30 binaries.

Clearly speckle interferometry has the advantage of greater sensitivity over both Michelson and Intensity Interferometry,although lacking the resolution of the latter.The advantage of speckle interferometry over the Lunar Occultation technique lies in its ability to be used for long integrations on any object visible at a given site.The number of objects available therefore to the method is very large and will increase as on-line digital processing becomes more common.

Chapter 3 Infrared Speckle Interferometry

Introduction

Unfortunately the methods described in Chapter 2 for visible speckle interferometry are not suitable for use at infrared wavelengths since sensitive image forming detectors are not available for wavelengths longer than about 1μm.Arrays of detector elements are available but would be prohibitively expensive for this application.

In the infrared therefore a single element detector is used and the image is spatially filtered to give speckle measurements in one direction.

The Infrared Speckle Method

A method of performing speckle interferometry in the near infrared has been described by Selby,Wade and Sanchez (3.1). In this method the time-averaged spatial frequency power spectrum of the instantaneous image I(x) (in one dimension) is sampled sequentially using a series of spatial frequency filters in the focal plane of the telescope.Transmission gratings with a range of grating constants from zero to the corresponding diffraction limit of the telescope are used as the individual filters,so that the method is equivalent to sampling a slice in one dimension through the centre of the two dimensional spatial frequency power spectum of the instantaneous image.

With any one filter in position the image is oscillated across the grating normal to the grating lines using a sawtooth motion so that the signal received by the detector is modulated at a quasi-constant frequency.The image is moved across the grating rather than the reverse case for two reasons.Firstly it is mechanically simpler to move the image and secondly the danger of modulating the infrared background radiation is removed if the image is moved.There is still unwanted background modulation but this occurs at the chop frequency,well away from the signal passband.A modulation frequency of 120Hz is used which is convenient for the detector system and at this rate the image remains 'frozen'during its motion over several periods of the grating.The sawtooth image motion is programmed with constant amplitude and differing frequencies so as to maintain a constant modulation frequency over the entire range of gratings used.With a given sawtooth amplitude the aperture size is carefully chosen so that the energy in the image remains well within the aperture.

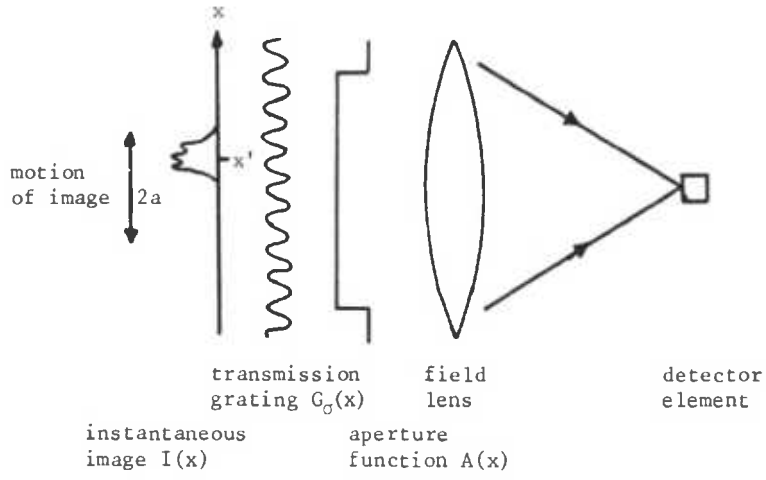

Fig. 3.1 One dimensional spatial frequency filter
I(x), G_σ(x) and A(x) all lie in the focal plane.

With reference to Figure3.1, the image I(x) is at an arbitrary position x′ and the detector signal may be expressed as

$$S_{\sigma'}(x) = \int I(x-x') \; (G_{\sigma'}(x)A(x)) \; dx' \qquad (3.1)$$

where the integration is over all values of x for which I(x) is non-zero. So that

$$S_{\sigma'}(x) = I(x) \otimes \left[G_{\sigma'}(x) \; . \; A(x) \right] \qquad (3.2)$$

where $\sigma' = 2\pi/\lambda'$ and $1/\lambda'$ is the grating constant.

The transfer function of the spatial frequency filter is given by

$$T_{\sigma'}(\sigma) = g_{\sigma'}(\sigma) \otimes a(\sigma) \qquad (3.3)$$

where $g_{\sigma'}(\sigma)$ and $a(\sigma)$ are the Fourier transforms of $G_{\sigma'}(x)$ and $A(x)$ respectively.

Assuming $G_{\sigma'}(x) = \cos(\sigma' x + \phi)$ ie. taking the fundamental only, with ϕ as an arbitrary phase factor, then

$$g_{\sigma'}(\sigma) = FT\left\{ \cos(\sigma' x + \phi) \right\} \qquad (3.4)$$

$$= 1/2 \int_{-\infty}^{+\infty} \left(\exp(i(\sigma' x + \phi)) + \exp(-i(\sigma' x + \phi)) \right) \exp -i\sigma x \; dx$$

This step can be justified by noting that in the power spectrums of the signal, the convolution of Equation3.2 is replaced by a multiplication, so that the harmonics of $G_{\sigma'}(x)$ just produce higher requencies plus a DC term which can be filtered out.

$$g_{\sigma'}(\sigma) = 1/2\left(\int_{-\infty}^{+\infty} \exp(i(\sigma' - \sigma)x + i\phi) dx + \int_{-\infty}^{+\infty} \exp(-i(\sigma' + \sigma)x - i\phi) dx \right)$$

$$= 1/2\left(\delta(\sigma = \sigma') \exp i\phi + \delta(\sigma = -\sigma') \exp -i\phi \right) \qquad (3.5)$$

The filter $T_{\sigma'}(\sigma)$ then is peaked at $\sigma = \pm\sigma'$ and has an equivalent bandwidth $\Delta\sigma = \pi/b$, where 2b is the width of the aperture function A(x) (this is a good approximation for $b >> \lambda$ ie $\Delta\sigma/\sigma' << 1$

Now

$$S_{\sigma'}(x) = FT\left\{ i(\sigma) \; . \; T_{\sigma'}(\sigma) \right\} \qquad (3.6)$$

where $i(\sigma) = i_a(\sigma) \exp(i\phi(\sigma))$ is the Fourier transform of I(x)

to a good approximation then we may write

$$S_{\sigma'}(x) = \Delta\sigma / 2\ i_a(\sigma')\ \left(\exp(i(\phi + \sigma' x + \Phi)) + \exp(-i(\phi + \sigma' x + \Phi)) \right)$$

$$= \underline{\underline{i_a(\sigma')\Delta\sigma \cos(\sigma' x' + \phi + \Phi(\sigma'))}} \qquad (3.8)$$

Assuming for the moment then that I(x) is constant in time it is evident that the mean power in the signal $S_{\sigma'}(x)$ is proportional to the spatial frequency power per unit bandwidth $i_a^2(\sigma')$ at $\sigma = \sigma'$ when averaged over an infinite range of x'.

Errors in the Measurement of the Spatial Frequency Power of the Image

Using a sawtooth motion of finite amplitude a measure of $< |S_{\sigma'}(X)|^2 >$ leads to a systematic error in the assessment of $i_a^2(\sigma')$, which depends on the sawtooth amplitude (a) and the phase factors ϕ, $\Phi(\sigma')$

During any half period of the sawtooth chop of the image I(x), the signal $S_{\sigma'}(x)$ may be expressed in time as

$$S_{\sigma'}(t) = i_a(\sigma')\Delta\sigma \cos(2\pi f_o t + \phi + \Phi(\sigma')) \qquad (3.9)$$

where f_o is the modulation frequency given by

$$f_o = 4af_c / \lambda'$$

and f_c is the sawtooth chop frequency. If I(x) remains stationary in time a periodic signal is produced which has a period $1/f_c$ and thus its power spectrum is a line spectrum with harmonic spacing f_c peaking at frequencies around f_o.

It is shown in Appendix 2 that the total power of the signal is then given by

$$P_{\sigma'} = i_a^2(\sigma')\Delta\sigma^2 \sum_{n=0}^{\infty} \left[\cos\Omega \sin\pi(n_c+n) - \sin\Omega(1-\cos\pi(n_c+n)) \right.$$
$$\left. + \cos\Omega \sin\pi(n_c-n) - \sin\Omega(1-\cos\pi(n_c-n)) \right]^2 \qquad (3.10)$$

where n is an integer which corresponds to the order of the harmonic so that

$$\omega = 2\pi n/T \qquad \text{and} \qquad n_c = 4a/\lambda'$$

Ω is the phase factor given by $\Omega = \phi + \Phi(\sigma')$

It can be shown that when $4a/\lambda' \to \infty$ the summation term approaches unity and as $4a/\lambda'$ decreases the deviation from unity increases.

Assuming the phase factor to be completely arbitrary and random over the total integration time used for one spatial frequency filter, M.J.Selby (3.2) has evaluated Equation 3.10 and has found the errors in the power measurement to be tolerable, but the use of coarser gratings would require an increase in chop amplitude with an accompanying increase in the size of the sky aperture A(x).

Limiting Speckle Magnitudes

In this section I shall attempt to calculate the limiting magnitude for a 1.5m telescope and also for larger telescopes.

As mentioned in Chapter 2, at visible wavelengths the limiting magnitude is ultimately restricted by the shot noise associated with the average number of photons per speckle.

In the infrared however (particularly at the longer wavelengths) the dominant limitation is the shot noise of the infrared backbackground.

I shall define the limiting infrared magnitude as that source which can be measured with an angular extension of $\Delta\theta_D = \lambda/D$, with a signal to noise ratio of one. $\Delta\theta_D$ is the diffraction limited resolution and here is considered to be the equivalent width of the sources intensity function.

With reference to Figure 3.2a, let $S^*(q)$ be the spatial frequency power spectrum of the extended source and $S(q)$ the corresponding spectrum of a point source.

$S^*(q)$ and $S(q)$ are sampled at $q=qm$ and then compared. Here q is the spatial frequency normatized to 1 at $\sigma = D/\lambda$.

Recalling Equation 15 of chapter 2 we have

$$\langle |T(u,v)|^2 \rangle = |\langle T(u,v) \rangle|^2 + kT_D(u,v)$$

so that for $qm > r_o/D$ we may write

$$S(q_m) = k\beta S_o D^4 T_D(q_m) \qquad (3.11)$$

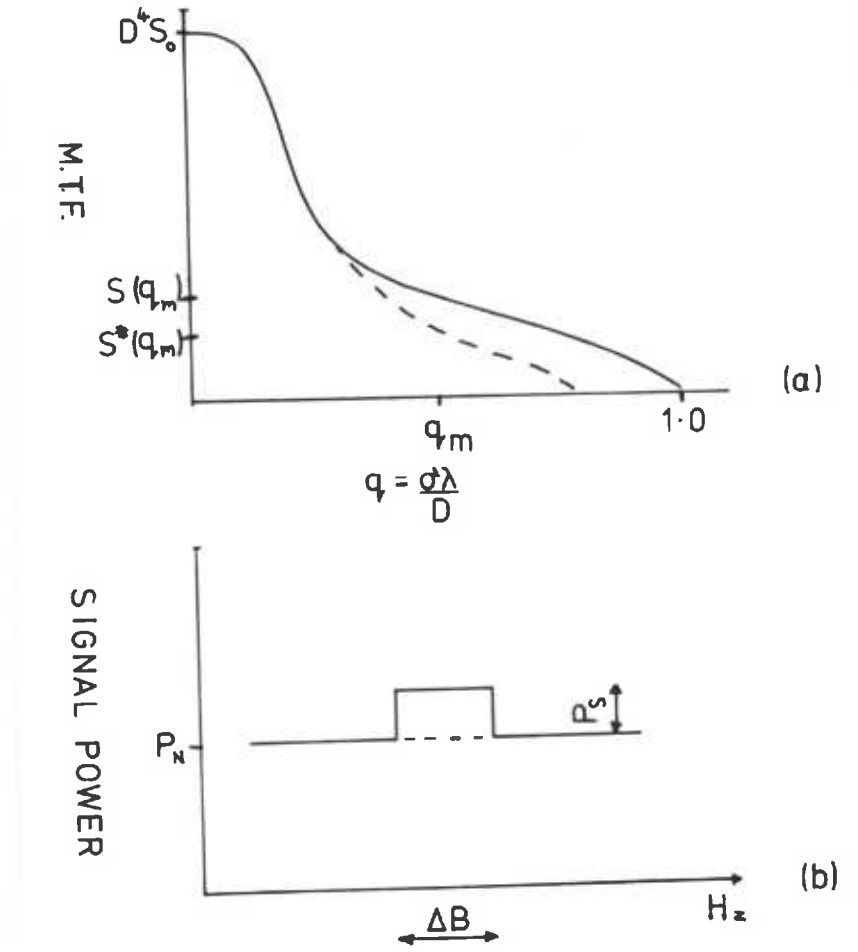

Fig. 3.2 a) $S(q)$ Point spread transfer function

$S^*(q)$ Transfer function of source extended to diffraction limit $\Delta\theta_D = \lambda/D$

S_o is the total squared intensity normalized to a 1m diameter telescope.

b) Signal power spectrum for measurement of $S^*(q_m)$ when $S^*(q_m) = P_S \Delta B$.

Where S_o is the image intensity squared for a one metre diameter telescope, corresponding to the speckle limiting magnitude. The factor β is included to take account of the optical filter bandwidth $\Delta\lambda$ selected using the criterion of Chapter 2 ie $\Delta\lambda = \frac{\lambda^2}{D\Delta\theta_s}$ where $\Delta\theta_s$ is the seeing angle size

If $\Delta\lambda_{phot}$ is the normal photometric bandwidth associated with the width of the infrared atmospheric window then

$$\beta = \left(\frac{\Delta\lambda}{\Delta\lambda_{phot}} \right)^2 \qquad \text{for } \Delta\lambda < \Delta\lambda_{phot} \qquad (3.12)$$

otherwise $\beta = 1$

It may be assumed that the temporal frequency power spectrum of the signal associated with the measurement of $S^*(q)$ takes the form as shown in Figure 3.2 b.

The signal power (Hz^{-1}) P_S is superimposed on the detector and background noise power (Hz^{-1}) P_N.

It is assumed that the bandwidth ΔB containing the signal power is governed by the temporal coherence in the image where $\Delta B = 1/t_c$ (see later chapter for discussion on and measurement of to).

It is shown in Appendix 3 that the signal to noise ratio for a measurement of total noise power P taken over a bandwidth ΔB is given by $(\tau\Delta B)^{\frac{1}{2}}$, where τ is the post-detection integration time. For the measurement of $S^*(q_m)$ we have

$$S^*(q_m) = P_S \Delta B \qquad (3.13)$$

with a signal to noise ratio

$$S/N = \frac{P_S (\tau\Delta B)^{1/2}}{((P_S+P_N)^2+P_N^2)^{1/2}} \qquad (3.14)$$

or in the case where $P_S << P_N$

$$S/N = \frac{P_S}{P_N} (\tau\Delta B/2)^{1/2} \qquad (3.15)$$

The above equation takes into account that in order to find $P_S \Delta B$ it is necessary to measure the background noise power over a total bandwidth of ΔB taken on either side of the signal passband.

In the next chapter it will be shown that for the detector noise limited case

$$m_{DL}(D) = 1.25 \log (S_{oo}^2 \beta\tau D^4/P_D) \qquad (3.16)$$

where β has been introduced to represent the optical bandwidth of the filter used.

In the background limited case we have

$$m_{BL}(D) = 1.25 \log (S_{oo}^2 \tau D^2/P_B) \qquad (3.17)$$

where S_{oo} is the intensity from a zero magnitude star using a 1m telescope.

The total noise power (Hz^{-1}) from the detector may be expressed as

$$P_N = P_D + P_B \qquad (3.18)$$

or $$= 10^{-0.8m_{BL}} \cdot S_{oo}^2 \tau D^2 + 10^{-0.8m_{DL}} \cdot S_{oo}^2 \beta\tau D^4$$

Now in order to resolve the difference between $S^*(qm)$ and $S(q_m)$ with a signal to noise of unity we require that

$$\left(\frac{P_S}{P_N}\tau\frac{\Delta B}{2}\right)^{\frac{1}{2}} = \frac{S^*(q_m)}{S(q_m) - S^*(q_m)} \qquad (3.19)$$

and if we assume that the extended source has a gaussian angular profile with an equivalent width $\Delta\Theta_o = \lambda/D$

then

$$S^*(q_m) = \exp(-2\pi q^2 S(q)) \qquad (3.20)$$

So that we have from Equations 11-20, that the speckle limiting magnitude is given by

$$m_S^* = 1.25 \log \left[\frac{(1-\exp(-2\pi q_m^2) T_D(q_m) r_o^2 \beta(\tau t_o/2) D^2}{10^{-0.8m_{DL}} + \beta^{\frac{1}{2}} D^2 10^{-0.8m_{BL}}} \right] \qquad (3.21)$$

and for background limited conditions we have

$$m_S^* = m_{BL} + 1.25 \log (0.21 r_o^2 (\beta t_o \tau)^{\frac{1}{2}}) \qquad (3.22)$$

where the value $q_m = 0.5$ has been used. This is in fact approximately the optimum value for q_m. However as indicated in Figure 3; which shows

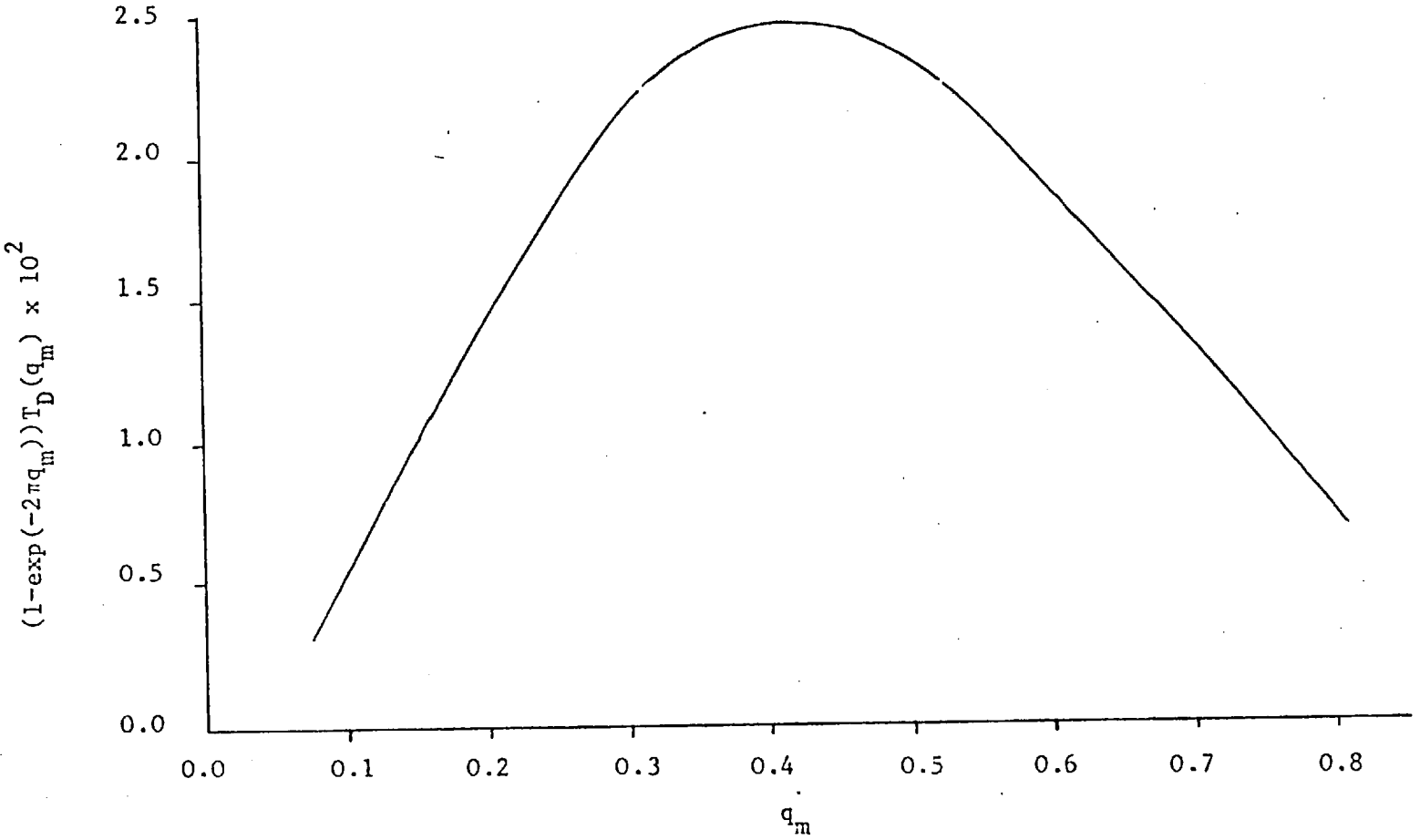

Fig 3.3 Optimum value for normalized spatial frequency q_m

($D/r_o = 3$, $\lambda = 2.2\mu m$)

the value of $(1-\exp(-2\pi q_m^2)T_D)$ plotted against q_m, the value of m_s^* is not particularly sensitive to changes in the value of q_m. Figure 3.3 was calculated using Korff's model for $T_o(q_m)$ (3.3).

The speckle limiting magnitudes have been computed from Equation 3.21 and are given in Table 3.1 along with the filter details and photometric magnitude limits for the 1.5 telescope. Measured parameters found on the 1.5m telescope were used together with the following relations (see later chapters for details).

$$r_o = \frac{(0.5)^{-1/5}\ \lambda^{6/5}}{\Delta\theta_v} \times 10^6 \text{ m}$$

$$t_o = 0.04\ \lambda^{\frac{1}{2}} \text{ secs}$$

where $\Delta\theta_v$ is the seeing angle in the visible in radians and λ is the wavelength in microns.

It should be stressed that the theory will only apply if $r_o << D$, which should be valid for large telescope diameters and short infrared wavelengths but progressively becomes more approximate for small telescopes at longer wavelengths.

The predicted speckle limiting magnitudes are particularly sensitive to changes in the infrared atmospheric background and the visible seeing angle which will depend on the telescope site.

Comparison of Two Methods of Spatially Filtering

The success of the method described above must ultimately depend on the stability of the atmospheric modulation transfer function over the period in which the spatial filters are used sequentially.

An alternative method which has been suggested would aviod this requirement by sampling all spatial frequencies in the image simultaneously. This method involves scanning the image across a narrow slit rather than a grating. If the slit is very narrow then the output signal from the detector contains information about all spatial frequencies of interest, although the higher spatial frequencies do suffer some attenuation due to the fall-off of the transfer function of the slit.

In order to compare the two methods I shall consider the case where the image, of size $\Delta\theta_s$, consists of a simple fringe pattern. If the slit is of width $\Delta\theta_o$ where $\Delta\theta_o$ is the resolution limit of the telescope, then both methods will produce a signal which is spread over a bandwidth $\Delta B = 1/t_o$ where t_o is the temporal correlation scale of the image,

However in the case of the slit the total power received will be reduced by a factor $\Delta\theta_o^2/\Delta\theta_s^2$ compared with the total power

Table 3.1

Speckle limiting magnitudes for the infrared filters J,H,K,L and M.

	J	H	K	L	M
m_{BL}	15.4	15.3	14.0	10.0	7.0
m_{DL}	14.0	13.7	13.2	12.3	10.9
m^*_S	11.3	11.8	12.0	9.6	7.1

received by the grating.

If we now define the ratio A such that

$$A = \frac{S/N \quad (\text{grating})}{S/N \quad (\text{slit})}$$

then from Equation 15 we have

$$A = \frac{\Delta\theta_s^2 \ (P_D + P_B \ \Delta\theta_o/\Delta\theta_s)}{\Delta\theta_o^2 \ (P_D + P_B)}$$

where account has been taken of the reduction in the background noise through the slit,

It may now be noted that the resolution width in the power spectrum is equal to $1/\Delta\theta_s$ whereas the total bandwidth available in the MTF is equal to $1/\Delta\theta_o$ so that the number of resolution elements in the transfer function is given by

$$N = \frac{\Delta\theta_s}{\Delta\theta_o}$$

so that

$$A = N^2 \ \frac{(P_D + P_B/N)}{P_D + P}$$

However since the number of resolution elements in the transfer function is N, then the slit method is capable of giving N measurements simultaneously. It can be said then that approximately the ratio of the signal to noise for the grating method divided by the signal to noise ratio for the slit method, for the measurement of an established source is given by :-

$$A^* = \frac{A}{N^{\frac{1}{2}}}$$

In the detector noise limited case then

$$A^* = N^{3/2}$$

while in the background limited case

$$A^* = N^{\frac{1}{2}}$$

This simple treatment then, indicates that the grating method offers higher signal to noise than the slit method, the advantage in fact, being even greater since all the resolution elements in the power spectrum do not carry the same amount of information.

Chapter 4 Instrumentation

Introduction

In this chapter I shall describe the equipment which has been developed to perform speckle interferometry in the near-infrared, from 1 to 5μm.

As discussed in Chapter 3 the method involves oscillating an image across a spatial filter before spectrally filtering and reimaging onto a single element detector.

The detector, the filters, the gratings and the apertures are all cooled to liquid nitrogen temperatures in order to reduce the infrared background radiation and in the following sections the detector cryostat will be described in some detail.

The Detector Cryostat

The instrument was initially designed for use at the cassegrain focus of the 1.5m flux collector at Tenerife. The optical configuration adopted was one where the beam from the telescope secondary is turned through 180^{o}, so that the focal plane of the telescope is parallel to and 5.4" above the photometer baseplate, as shown in Figure 4.1.

The cryostat then is designed to be downward looking with its focal plane 5.4" from its base. In this configuration the beam used if F/12 and the plate scale is $10\hat{''}$ to 1mm.

The arrangement inside the cryostat is shown schematically in Figure 4.2, the individual components being described in the following section. The cryostat and the photometer are shown in Figure 4.3.

The Detector

A single element 0.5mm diameter Indium Antimonide photovoltaic detector supplied by Santa Barbara Research Corporation, California was used.

The pre-amplifier circuit, which was designed by A.D.MacGregor at Imperial College, is based on that described by Hall et al (4.1) and is shown in Figure 4.4 .

The value of the feedback resistor can be selected using the latching relay LR1, so as to avoid saturating the preamplifier in high background situations (L,M,Filters) while allowing maximum

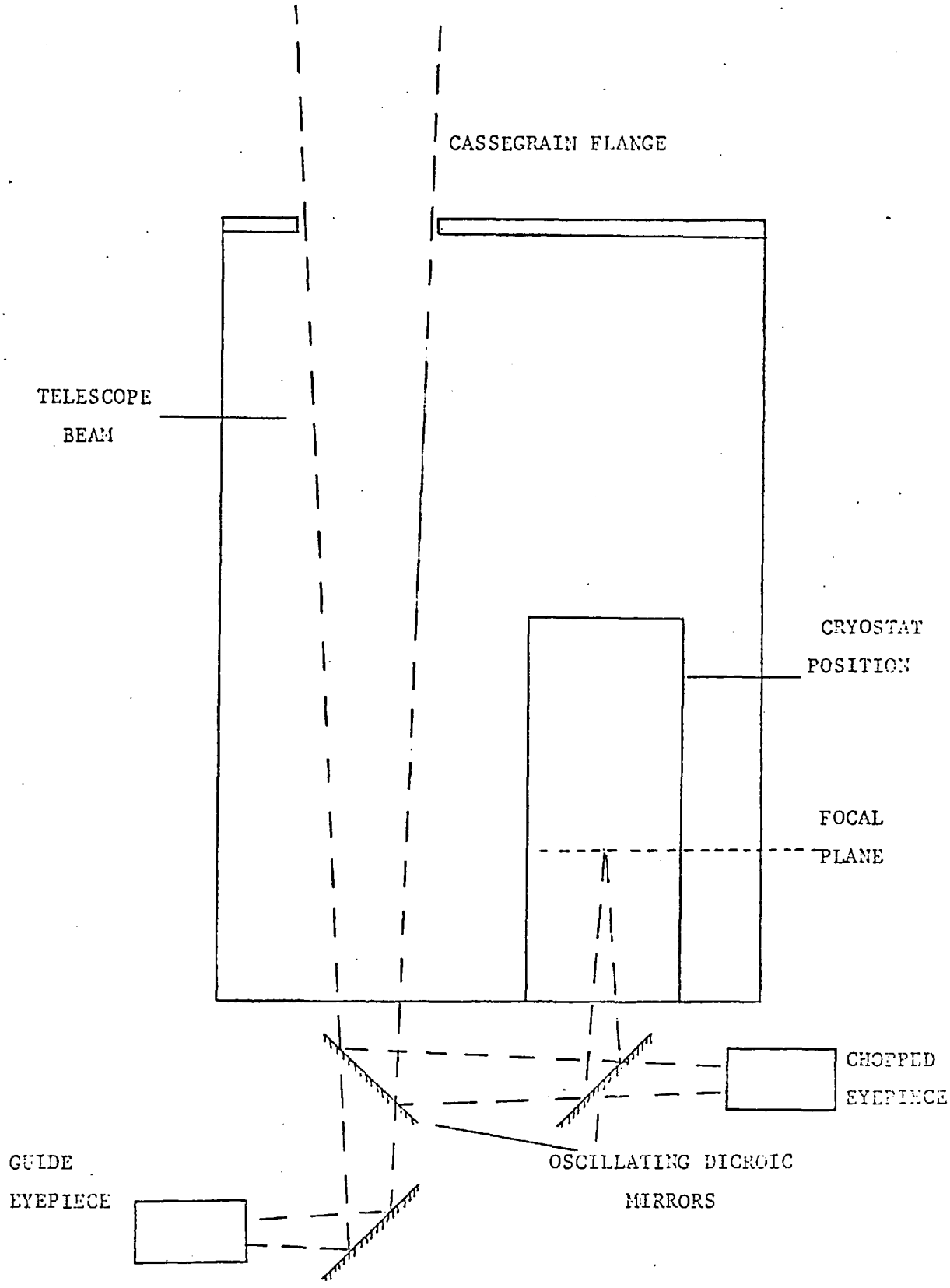

Fig. 4.1 Optical configuration of photometer

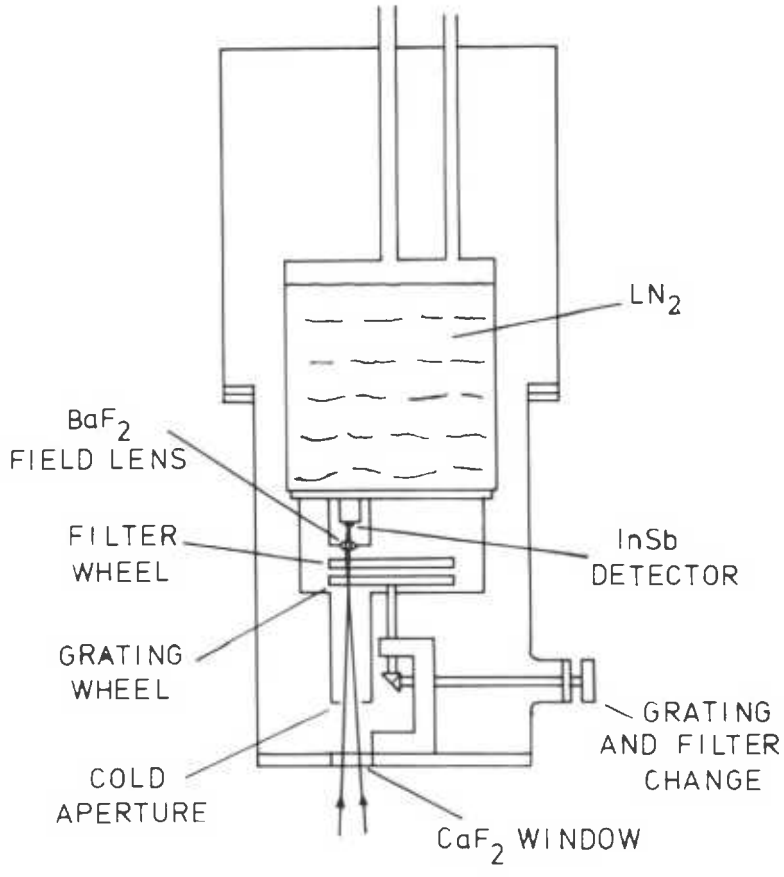

Fig. 4.2 Detector Cryostat

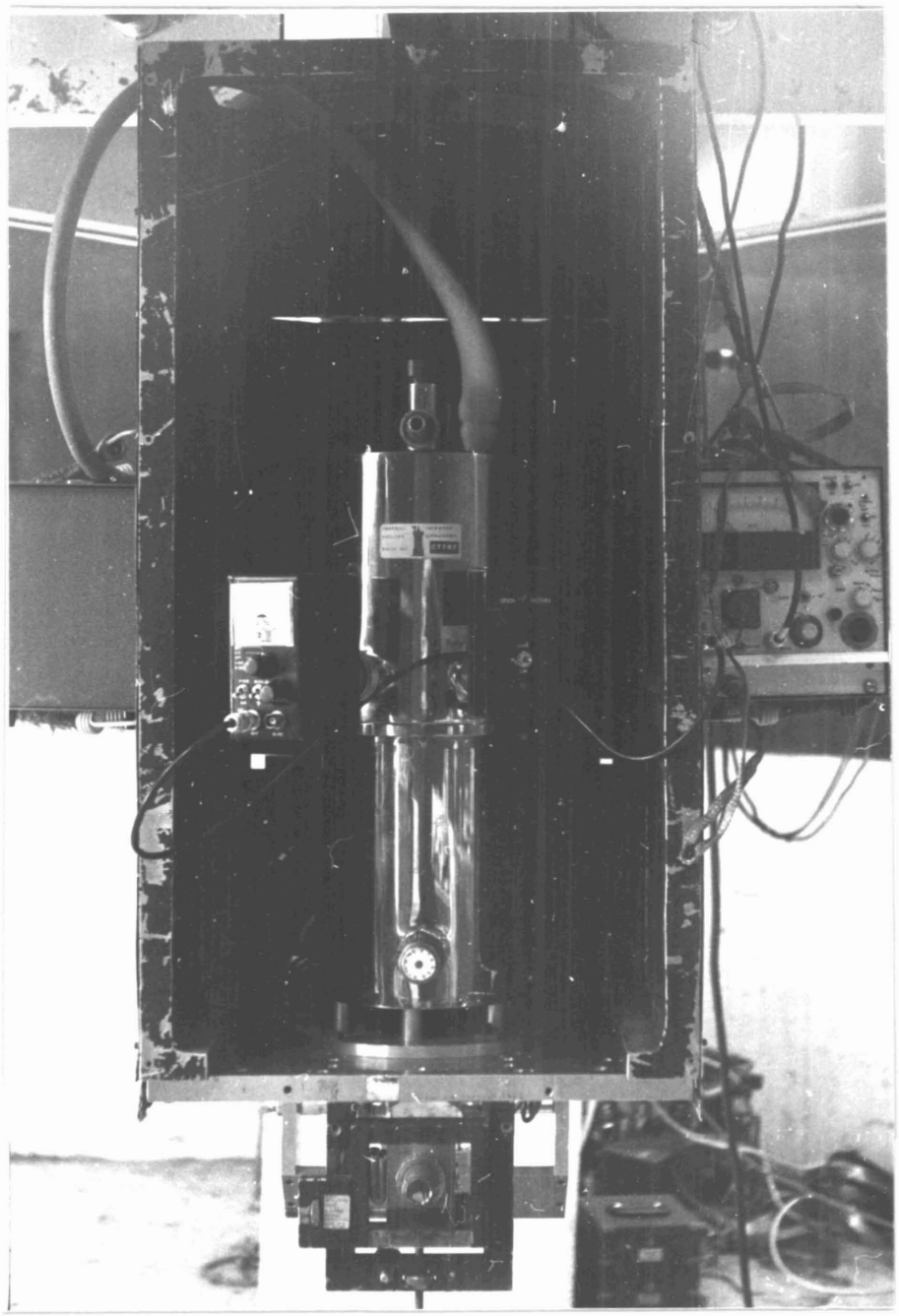

Fig. 4.3 Cryostat and Photometer

sensitivity in low background situations (J,H,K Filters).

In the normal mode of operations the circuit is set up to give zero bias across the detector.If the bias across the detector exceeds a few millivolts,excess noise appears (4.1).It is found that the noise power approximately doubles if the bias across the detector is increased to 10mv.

The zero bias condition is achieved by the following procedure.The detector is allowed to look at a metal blank at liquid nitrogen temperature,thus giving approximately zero background.With SW1 earthed the amplifier is then trimmed using VR2 to give zero DC output as measured on a DVM.Feedback now constrains the gate of FET 1 to remain at zero volts so long as the gate of FET2 is at zero volts.In fact the voltage at G1 follows exactly the voltage at G2 and this property is used to measure the diode curve of the detector and hence determine its impedance.This is achieved by setting SW1 to $\pm$ V,the voltage at G2 can now be varied via VR1,between about +30mV and -30mV.If the voltage across the detector is V_B and the detector impedance is R_D then there is a current i_D flowing through the detector.Now due to the high input impedance of the FET,i_D is constrained to flow through the load resistor R_L.However,if the output voltage is Vout then the current through R_L is given by

$$i_L = \frac{Vout - V_B}{R_L} \qquad (4.1)$$

but $$i_D = i_L$$

so that $$i_D = \frac{Vout - V_B}{RL} \qquad (4.2)$$

Thus we can plot the diode curve of the detector by changing V_B and monitoring Vout.

Now for the linear part of the curve we can say

$$i_D = \frac{V_B}{R_D} \qquad (4.3)$$

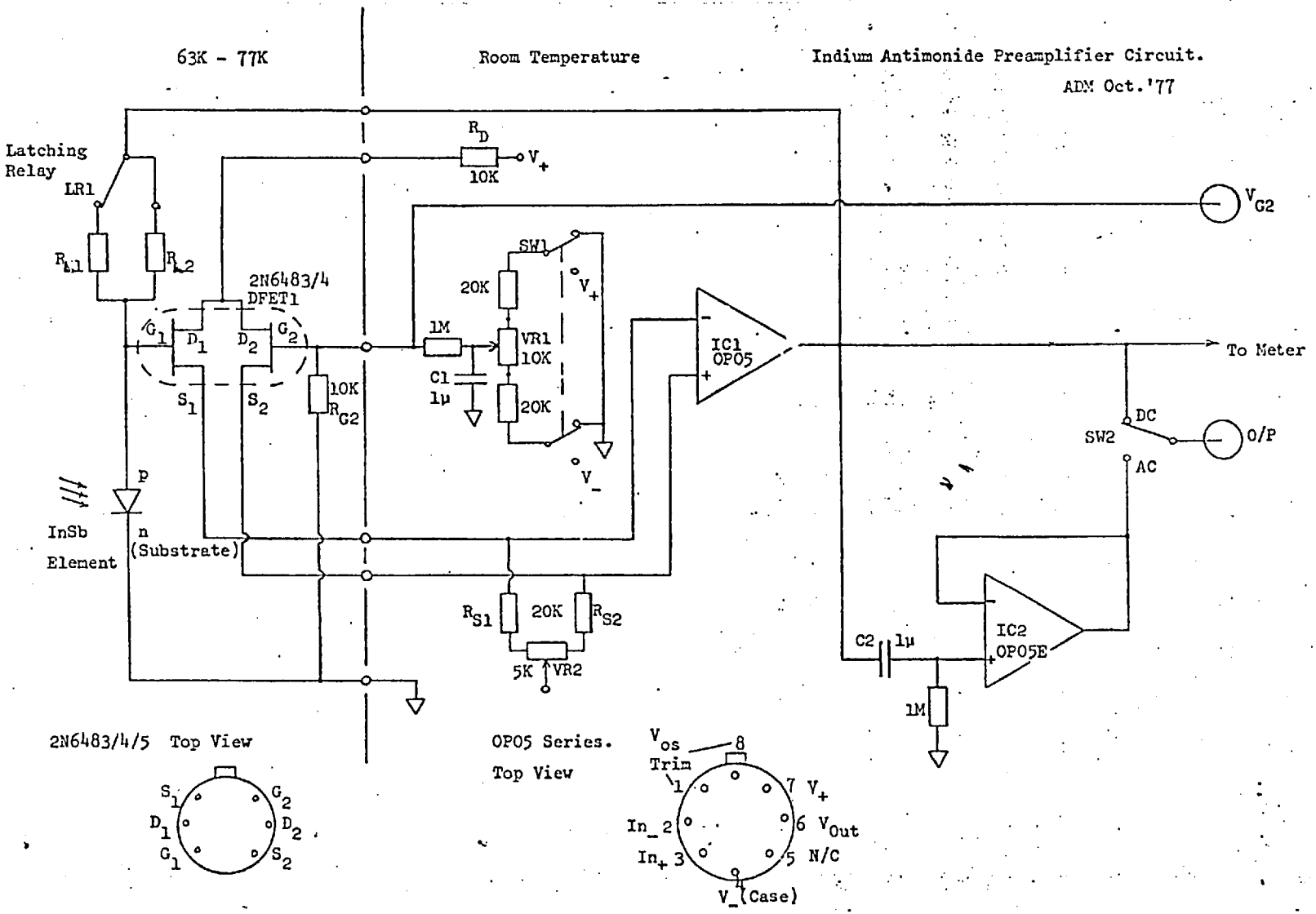
63K - 77K
Room Temperature
Indium Antimonide Preamplifier Circuit.
ADM Oct.'77
Latching Relay
LR1
R_{L1}
R_{L2}
R_D
10K
V_+
V_{G2}
2N6483/4
DFET1
G_1
D_1
D_2
G_2
S_1
S_2
10K
R_{G2}
SW1
20K
1M
VR1
10K
20K
C1
1μ
V_+
V_-
IC1
OP05
To Meter
SW2
DC
AC
O/P
P
InSb
Element
n
(Substrate)
R_{S1}
20K
R_{S2}
5K
VR2
C2
1μ
IC2
OP05E
1M
2N6483/4/5 Top View
OP05 Series.
Top View
V_{os} Trim
1
8
7 V_+
6 V_{Out}
5 N/C
In_- 2
In_+ 3
V_- (Case)

Fig. 4.4

so that $$\frac{V_B}{R_D} = \frac{Vout - V_B}{R_L} \qquad (4.4)$$

and since $Vout >> V_B$

$$R_D \simeq \frac{V_B}{Vout} \times R_L \qquad (4.5)$$

Figure 4.5 shows a typical diode curve obtained in this way. On this occasion the load resistor used was 5×10^9 so that the detector impedance was $\sim 10^8$.

Detector NEP

The Noise Equivalent Power (NEP) of a detector is defined as the input signal which produces unity signal to noise when noise is measured as the r.m.s value in unity bandwidth.

For an ideal photovoltaic detector, one electron - hole pair emerges per absorbed photon.

$$\therefore \text{Current responsivity} = \alpha\, e/h\nu$$
$$= 0.8\lambda\alpha A.W^{-1}$$

here α = quantum efficiency
e = electronic charge
$h\nu$ = photon energy

Now the Johnson noise current i_n at 64^oK (pumped LN_2) is given by

$$i_n = \left[\frac{4kT}{R_{//}}\right]^{\frac{1}{2}} \quad A.\ H_z^{-\frac{1}{2}}$$

$R_{//}$ = effective resistance of detector and feedback circuit
= parallel combination of detector resistance and feedback resistance

so that $$i_n = \frac{6 \cdot 10^{-11}}{R_{//}^{\frac{1}{2}}} \quad A.\ H_z^{-\frac{1}{2}}$$

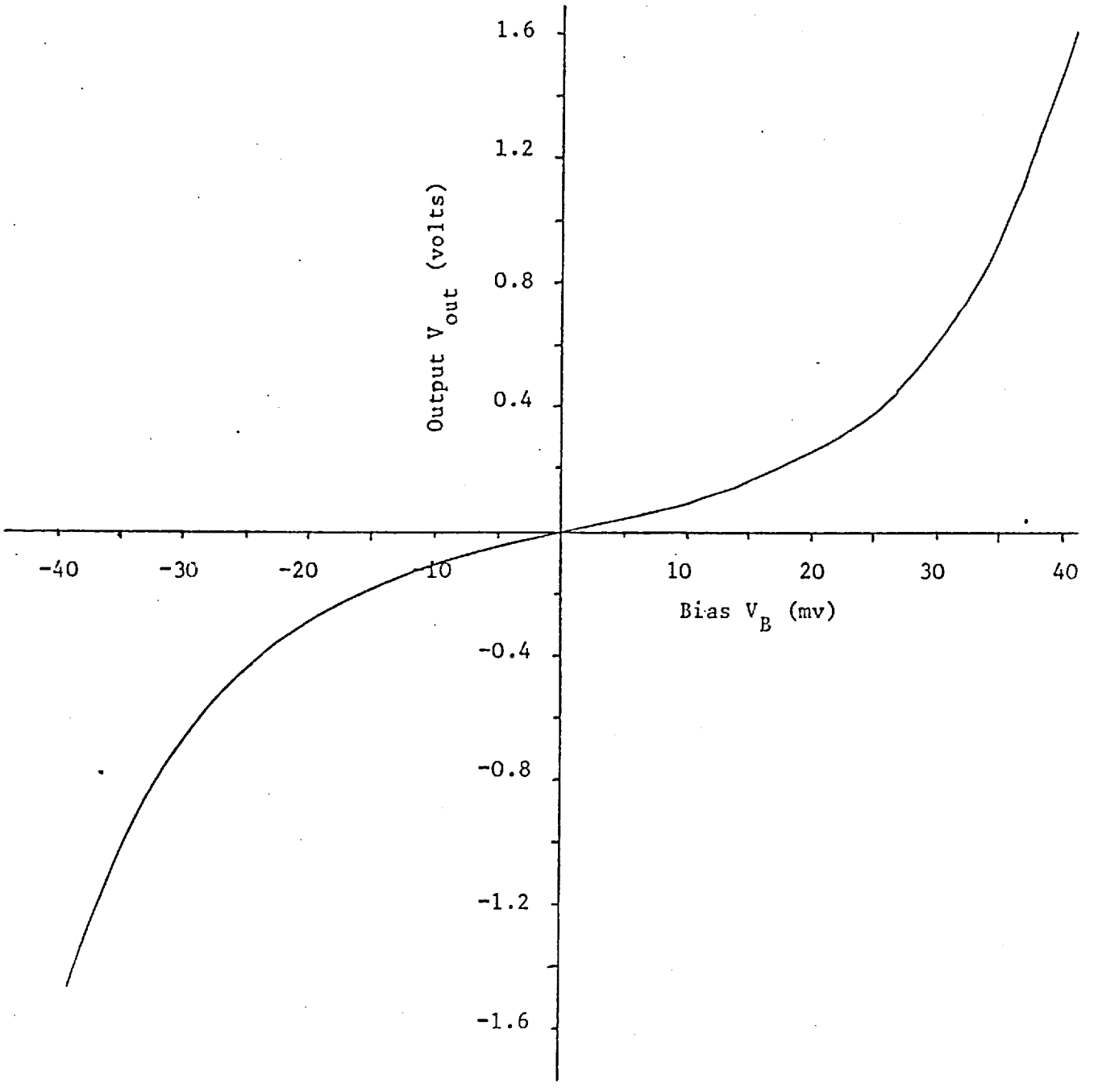

Fig. 4.5 Typical diode curve

Now we wish to know the number of watts of input which will give the same current as the Johnson noise i_n, so that

$$\text{NEP} = \frac{\text{Johnson noise current}}{\text{current responsivity}}$$

$$\text{NEP} = \frac{7.5.\ 10^{-11}}{R_{//}^{\frac{1}{2}}} \quad \text{WHz}^{-\frac{1}{2}} \qquad (4.6)$$

where for a typical InSb detector $\alpha = 0.5$ and $R = 5 \times 10^9 \Omega$.

Measurements have been made by Imperial College of the background shot noise using the 1.5m telescope at Tenerife and a 15" aperture.

The values obtained for the infrared filters J,H,-K,L,M together with the detector NEPs from Equation 4.6 are given in Table 4.1

Table 4.1

Filter	Shot Noise $\text{WHz}^{-\frac{1}{2}}$	NEP $\text{WHz}^{-\frac{1}{2}}$
J	3.5×10^{-15}	1.7×10^{-15}
H	2.2×10^{-16}	1.3×10^{-15}
K	3.8×10^{-16}	1.0×10^{-15}
L	5.1×10^{-15}	6.0×10^{-16}
M	1.7×10^{-14}	4.4×10^{-16}

As can be seen the system is shot noise limited at J,L,M.

Photometric Magnitude Limits

The total squared noise power for a 1m telescope with a 15" beam can be expressed as

$$P_N = P_D + P_B$$

where P_D = Squared intrinsic detector noise power NEP^2

P_B = Squared shot noise from sky background from 15" beam

So that for a telescope of diameter D and beam W" we have

$$P_N = P_D + P_B D^2 \left[\frac{W}{15}\right]^2$$

Now if $P_D >> P_B D^2 \left[\frac{W}{15}\right]^2$ then we are said to be detector noise limited

While if $P_D << P_B D^2 \left[\frac{W}{15}\right]^2$ then we are said to be background shot noise limited.

In the following discussion a $15''$ beam will be assumed. For the detector noise limited case we can define the limiting magnitude obtainable in time τ as

$$m_{DL}(D) = 1.25 \log \left[\frac{So^2 \tau D^4}{P_D}\right]$$

where So is the flux received from αlyr using a 1 metre telescope. In the background shot noise limited case we have

$$m_{BL}(D) = 1.25 \log \left(\frac{So^2 \tau D^2}{P_B}\right)$$

System Bandwidth

The bandwidth of the system is restricted primarily by the feedback resistor and the stray capacitance across it and from it to the ground,Bandwidth measurements were made by observing the system response to short light pulses.These were produced by chopping the radiation from a small pea lamp using a rotating disc with a single,narrow,radial slit near to its edge.Using this method it was possible to obtain a square pulse of about 1ms duration. The frequency response of the system obtained in this way is shown in Figure 4.6.The resulting value of 1/RC is approximately 200Hz, this could be increased by decreasing the value of the feedback resistance but this would result in an increased NEP.

Field Optics

The detector is mounted on a copper column to provide good thermal contact with the LN_2 worksurface,and has the field lens mounted directly above.

The field lens is Barium Fluoride and images the primary mirror onto the surface of the detector element.This reduces

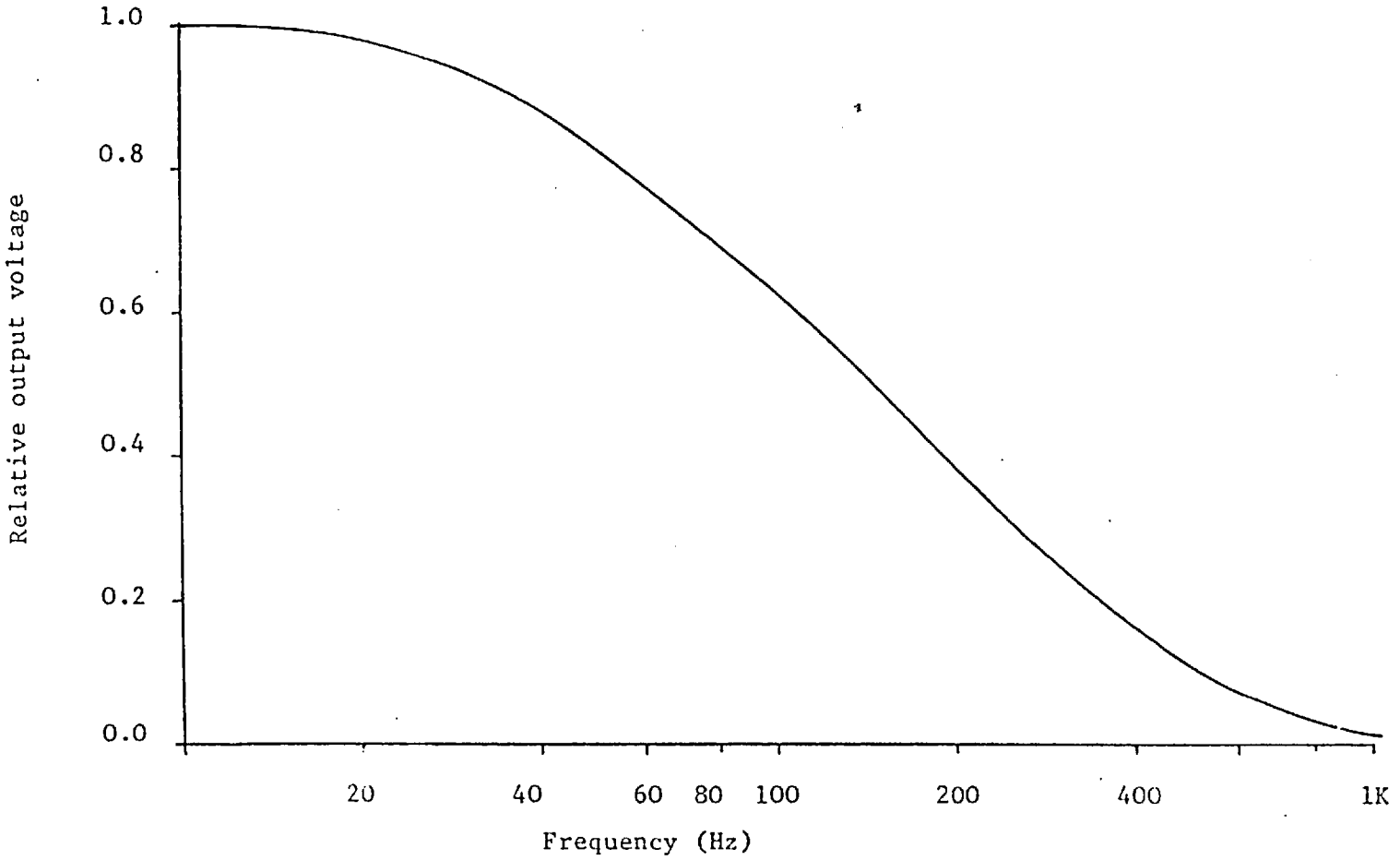

Fig. 4.6 System Bandwidth

the danger of spurious signals being produced by changes in sensitivity across the active area of the detector.The focal length of the lens is designed so that it produces an image which is the same size as the detector element.For an F/12 system with a 0.5 mm detector the lens has a focal length of 6mm.The detector mount and field lens can be seen in Figure 4.7 along with the cold pre-amp which is mounted alongside the detector column.

Grating and Filter Wheels

As indicated in Figure 4.2 the gratings and filters are mounted in separate wheels which enable the required combination to be placed in the beam of the telescope.In fact the gratings lie in the focal plane of the system,with the filters between the gratings and the field lens.

Rotation of the gratings wheel is accomplished by rotating a knob on the outside of the cryostat which is linked(Fig 4.8) via a flexible coupling and a set of anti-backlash gears to the axle of the grating wheel.Thermal isolation is achieved by means of a slotted drive plate on the axle of the wheel which meshes with two small pins on the drive shaft.The drive being direct,it is then possible to determine the position of the wheel by observing marks on the control knob.

In order to avoid the complexity of two drive systems the filter wheel is driven via the grating wheel.This is achieved by a pair of steel pins,one in each wheel,which enable the grating wheel to push the filter wheel to the required position.Once the filter has been selected the grating wheel can be rotated in the opposite direction,thus leaving the filter wheel in position and allowing the selection of the required grating.Determination of the position of the filter wheel is accomplished by having a small pointer behind the control knob which is pushed round by a pin on the knob thus mimicking the action inside the cryostat (Figure 4.9).In order to accurately locate the wheels,each has indentations on its circumference into which a small nylon wheel drops when the wheel is in the correct position.The nylon wheel is spring loaded and acts also as a switch to turn on an LED warning light outside the cryostat when the wheel is out of alignment.Figure 4.10 shows the filter and grating wheel assemblies while Figure 4.11 shows the cryostat with the pre-amp box on the left,the position warning light and load change box on the right and the control knob at the bottom.

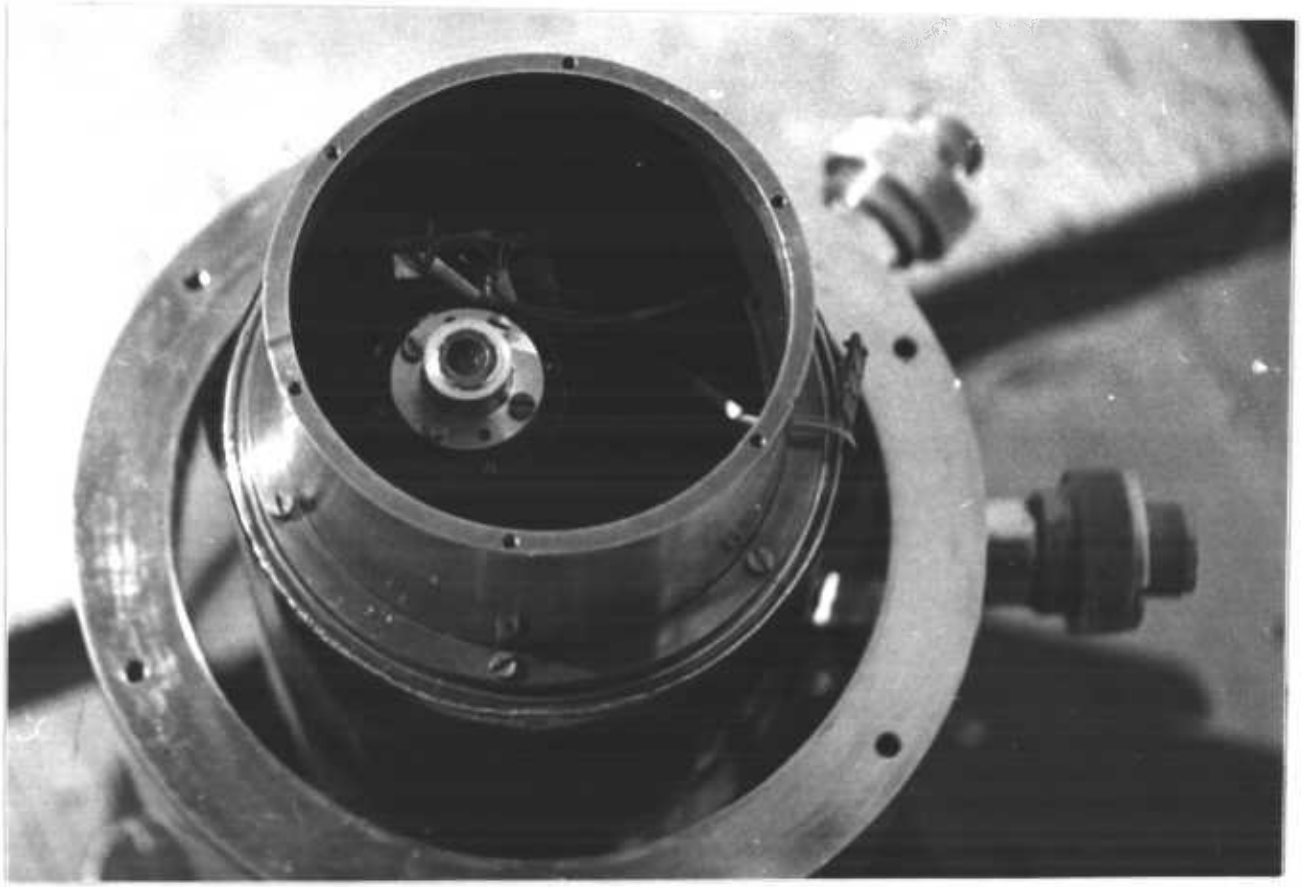

Fig. 4.7 Detector mount and field lens

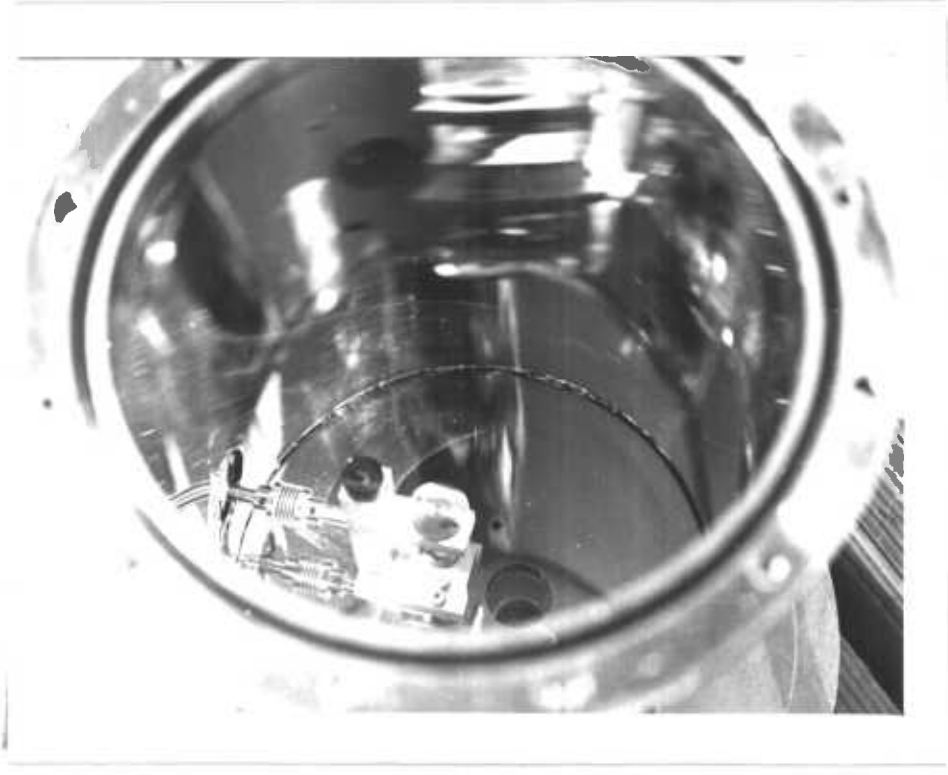

Fig. 4.8 Filter and Grating drive

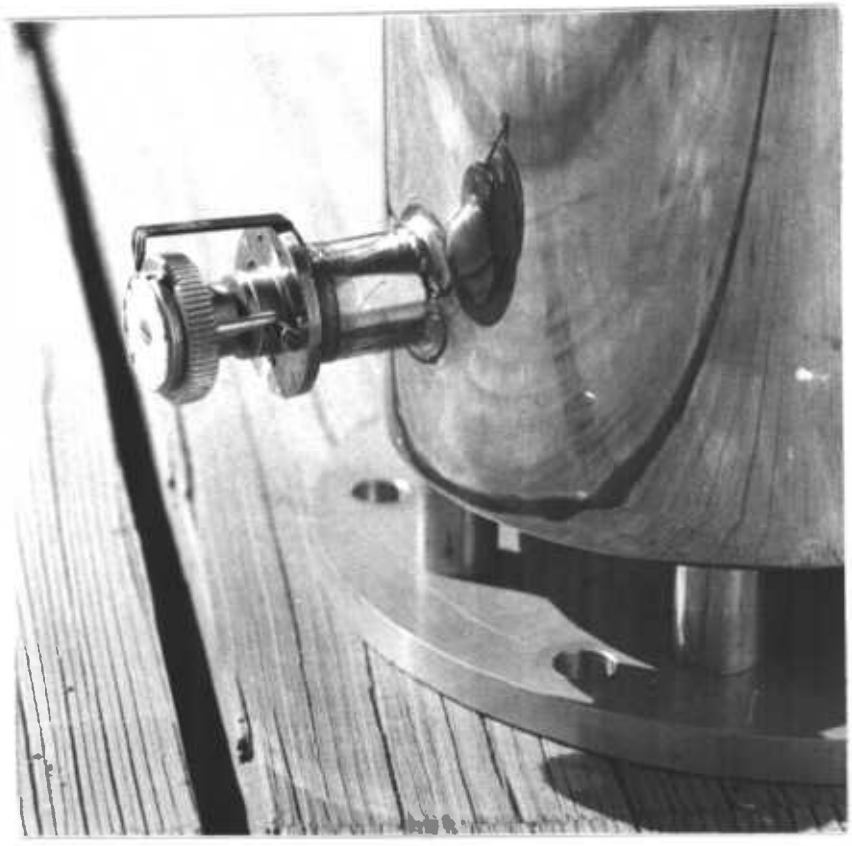

Fig. 4.9 Filter and Grating control knob

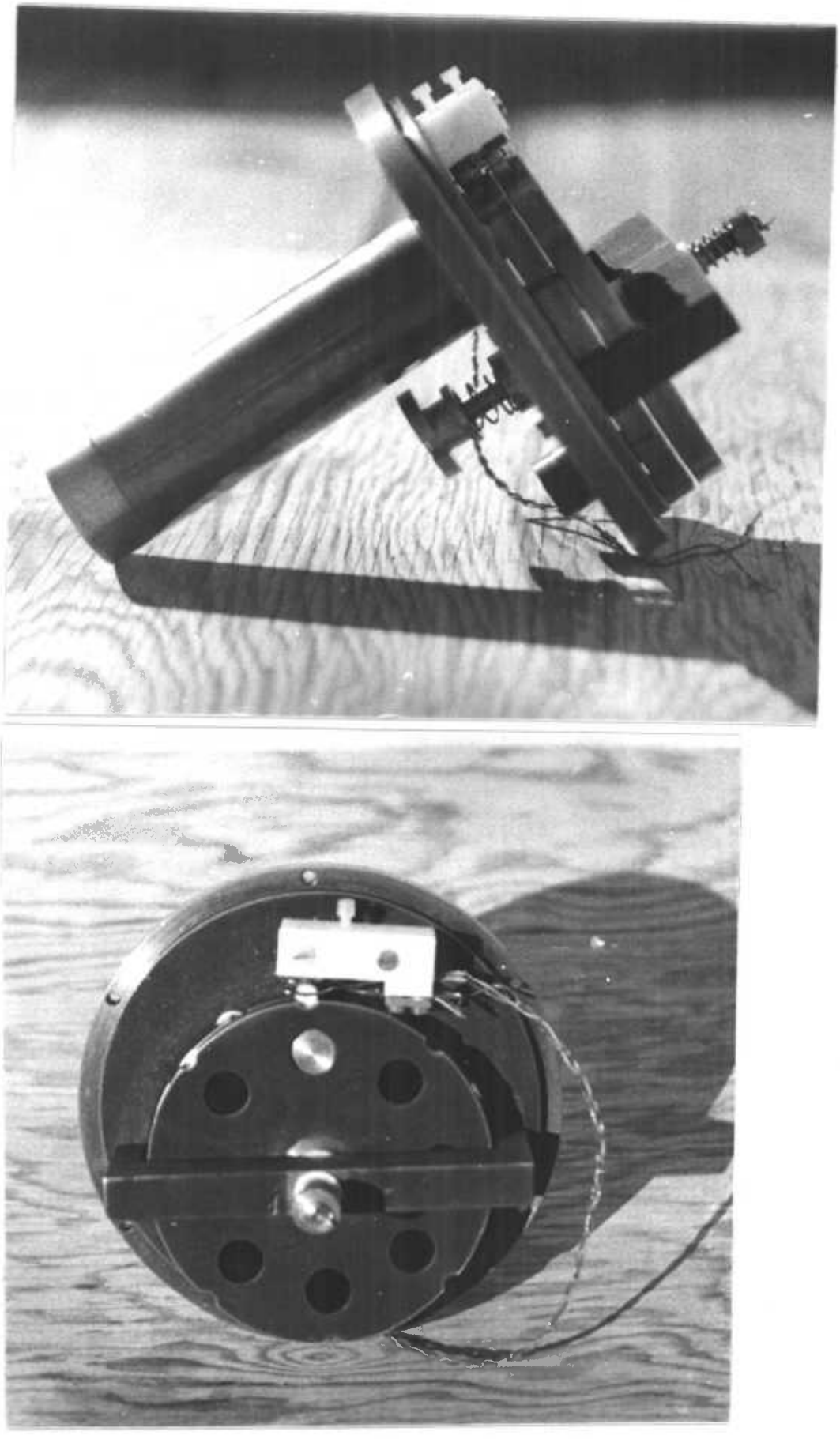

Fig. 4.10 Filter and Grating wheel assembly

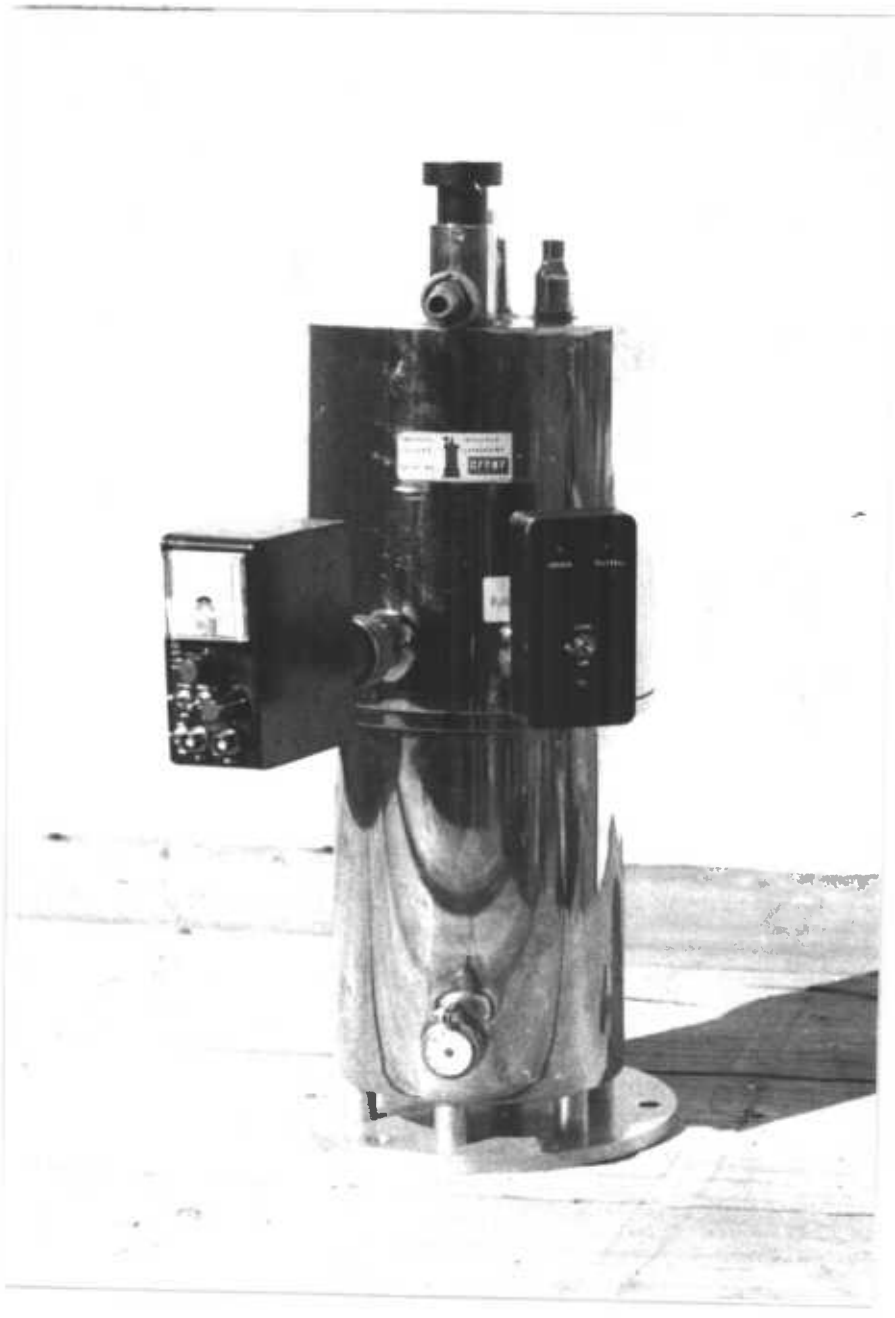

Fig. 4.11 BOC cryostat

Originally the bearings for the two wheels consisted of brass shafts running in PTFE bushes.However these bearings proved to be unsuitable for three reasons :

1) Due to the contraction of PTFE when cooled to liquid nitrogen,the bushes had to be made to be slack fitting on the shafts. The amount of slack was very difficult to judge and meant that the system was very difficult to set up at room temperature.

2) The PTFE bushes tended to pick up tiny particles of dirt and metal which subsequently caused seizing of the bearing.

3) PTFE acts as a thermal insulator thus hampering the initial cooling of the gratings and filters.

The bearings were therefore redesigned,the construction used being stainless steel shafts running directly into copper bushes, the bearing being lubricated using molybdenum disulphide powder.These bearings have proved to have been very successful at liquid nitrogen and show none of the problems encountered with PTFE.

Gratings

The gratings were produced from Barium Fluoride discs of 1cm diameter and 1mm thickness.The lines are aluminium and were produced by the following procedure.

The discs were first thoroughly cleaned using alchohol,water being avoided since this attacks the surface of the BaF_2 .A totally opaque coating of aluminium was then vacuum deposited onto one face of each disc,which was then given a thin coating of Shipley AZ Positive Working Photoresist.This was accomplished by spinning the disc at approximately 4000 r.p.m and then placing two drops of the resist onto the centre of the disc.After baking at $50^{o}C$ for 15 minutes the discs were then contact printed in a UV vacuum frame for approximately 30 seconds with the required, photographically produced master grating.The discs were then developed using the recommended Shipley developer,thus removing the resist from the exposed areas.In order to remove the aluminium from these areas the discs were then etched in a 30% solution of Phosphoric Acid. Finally the remaining photoresist was removed using acetone to leave just the aluminium lines on the BaF_2 substrate.

A few points should be noted about the above procedure.

1) Good coatings of photoresist are essential if high resolution is required.Micro resist should be used (in this case Shipley AZ 1275) and should be thinned before use 50/50 with cellulose thinner.

2) During photoresist coating dust should be avoided as this will leave tracks in the coating after spinning.The photoresist should,if possible,be strained through a micro-mesh filter before being used.

3) The etching process should be monitored closely to avoid undercutting and pitting of the lines due to over-exposure to the etchant.

4) BariumFluoride may be repolished using Ceasium Oxide after contamination with water.

Aperturing

The arrangement of cold apertures in the system serves two purposes.Firstly a focal plane aperture selects the size of the field of view,This is accomplished by mounting apertures in the grating wheel,so that the plane of the apertures lies directly on top of the opaque lines of the gratings.

Secondly,the apertures ensure that while all the available radiation is collected,the detector cannot 'see' unwanted radiation from the telescope structure.The main aperture is mounted on a column about 3" away from the focal plane.This aperture allows each part of the focal plane field to 'see' an F/12 beam.This beam is in fact larger than the secondary of the 1.5m,which in turn is undersize to prevent the possibility of looking at the edge of the primary (the sky giving a much lower and uniform background than the telescope's structure).It is the telescope secondary therefore which acts as the principal stop of the system,the purpose of the cold aperture being to ensure that the detector does not see a beam larger than F/8 which would hit the edges of the hole in the primary and thus cause unwanted chopping signals.

The focal plane aperures are 2mm in diameter thus giving a field of view 20" in diameter.Other size apertures are placed in spare locations in the grating wheel for setting up and photometry purposes.

Chopping System

In the following sections the design and operation of the chopping system.used to produce the motion of the image across the grating,will be described.The chopper used is of the two-mirror type,similar to that described by Jorden et al (4.2) but designed

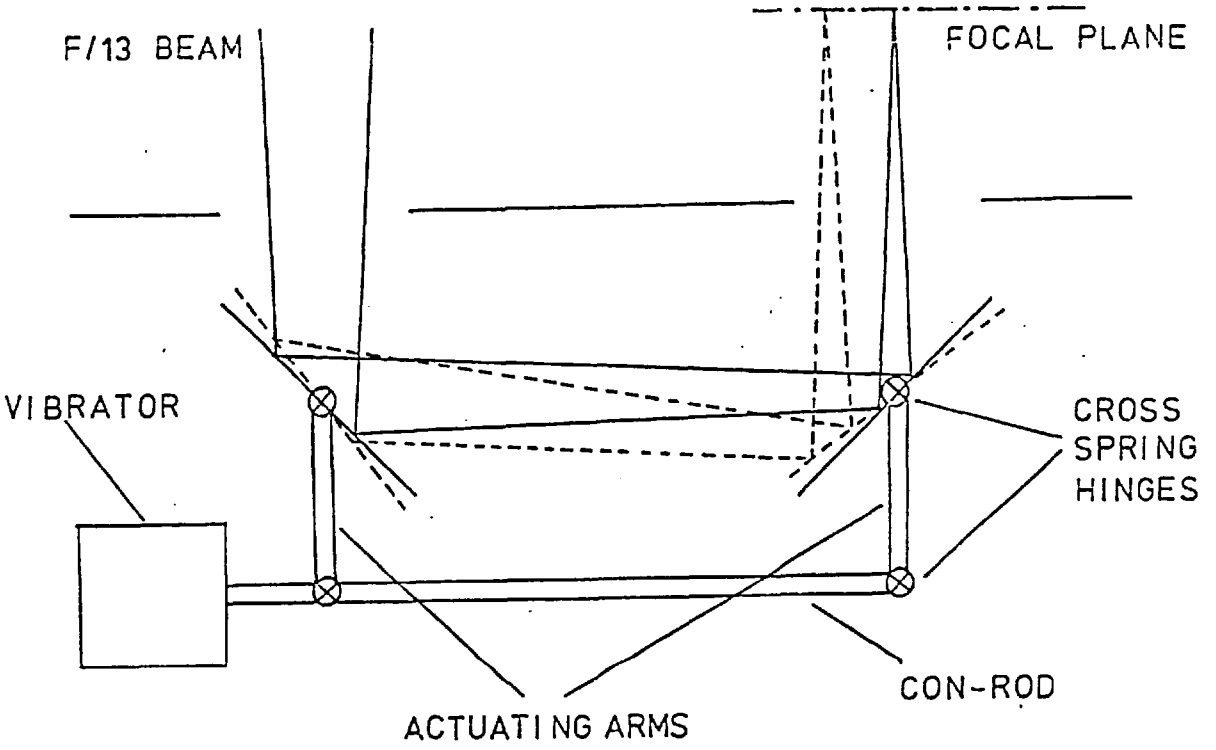

Fig. 4.12 Two-Mirror Chopping System

for use at low frequencies under servo-control.

Principle of the Two-Mirror Chopper

As shown in Figure 4.12 the mirrors are mounted on cross-spring hinges, the angle between them being maintained at 90^{o} by the parallelogram arrangement of the cam-rods and actuating arms.

With reference to Figure 4.13 let the distance between the mirrors be D while the angle of rotationof the mirrors is θ.

Now let $z = D-x$ (4.6)

So that $y = z \tan 2\theta$ (4.7)

and $x = z(\tan 2\theta)\tan (45 + \theta)$ (4.8)

Now $$\tan 2\theta = \frac{2\tan\theta}{1 - \tan^2\theta}$$

Or for small θ $\tan 2\theta = 2 \tan \theta$ (4.9)

and $$\tan (45+ \theta) = \frac{1 + \tan \theta}{1 - \tan \theta}$$ (4.10)

Equation 4.8 then becomes

$$x = z2\tan\theta \frac{1 + \tan\theta}{1 - \tan \theta}$$ (4.11)

but for small θ $\tan^2\theta \to 0$

So that $$x = \frac{2z}{\cot \theta - 1}$$ (4.12)

Again for small θ and noting that $D \gg x$

we have $$\underline{\underline{x = 2D\theta}}$$ (4.13)

In the chopper used D =6" and a typical displacement = 1mm so that $\theta = 3.25 \times 10^{-3}$ radians.

It is now easy to show that the charge in the optical path length is negligable for small θ

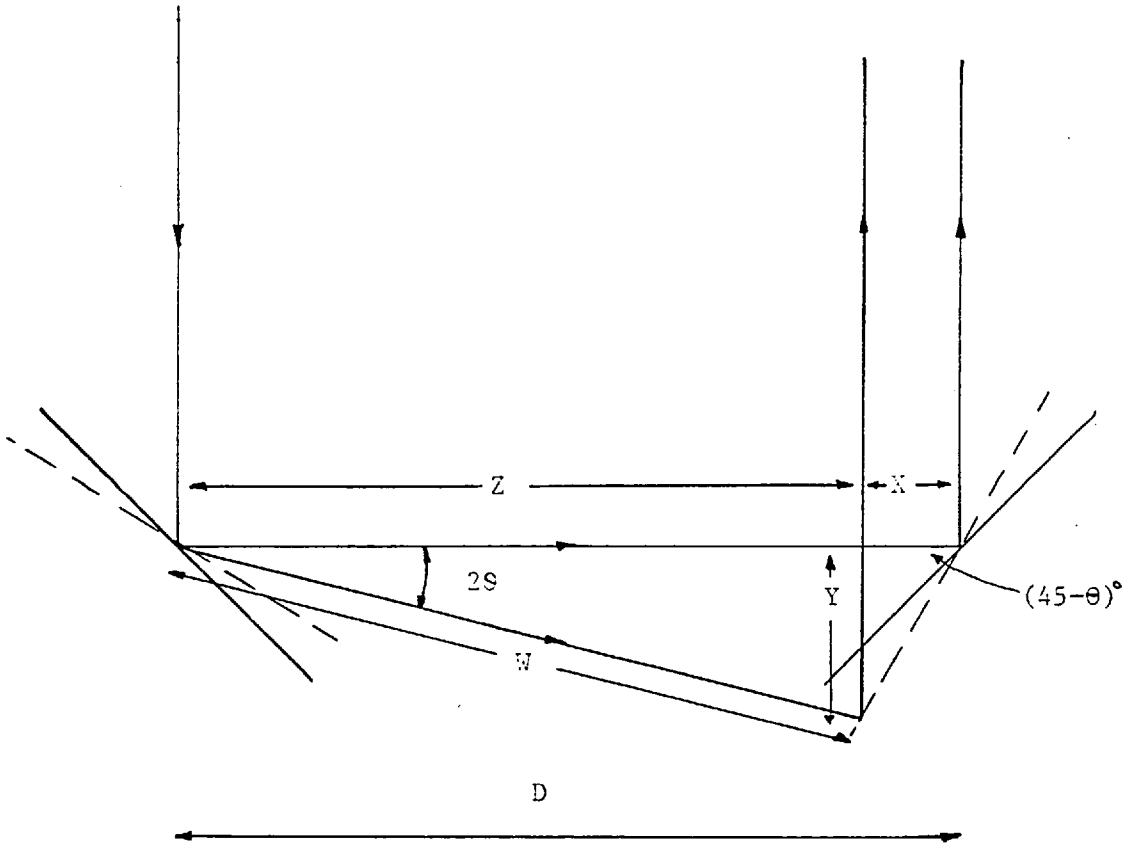

Fig. 4.13 Geometry of Two Mirror Chopper

Change in path length $\delta d = (z + x) - (w + y)$ (4.14)

$$= (z + x) - \left(\frac{z + x\tan (45-\theta)}{\cos 2\theta} \right) \quad (4.15)$$

and for small θ $$\delta d = (z + x) - \left(z + x \left[\frac{1-\tan\theta}{1 + \tan\theta}\right] \right) \quad (4.16)$$

$$= \frac{x \tan \theta}{1 + \tan \theta} \quad (4.17)$$

and so to a first approximation

$$\underline{\delta d \approx x\theta} \quad (4.18)$$

For $x = 1\text{mm}$ $\delta d \simeq 3.25 \times 10^{-3}\text{mm}$

Equations 4.14 and 4.19 represent the two major advantages of thetwo mirror chopper for this application.From Equation 4.14 it can be seen that large chops can be obtained from small motions of the mirrors,while Equation 4.19 demonstrates the negligable defocusing of the image during the chop.

It has been pointed out in two papers (4.2,4.3) that it is possible,by a slight modification of the chopper design, to ensure that during chopping the detector is always viewing the same point on the primary.This then reduces the chopping signal due to motion across the primary.

The modification consists of rotating one of the mirrors through a slightly larger angle than the other and hence pointing the hypothetical beam from the detector at the same place on the primary.

This differential rotation is produced by making one of the pairs of actuating arms slightly longer than the other.

With reference to Figure 4.14 which shows the geometry of the 1.5m,the image of the primary is formed 40.3 inches behind the secondary.

If ℓ is the distance from the chopper mirror to the image of the primary and if x is the displacement of the beam, then the beam must be turned through an angle

$$\delta\theta = x/\ell$$

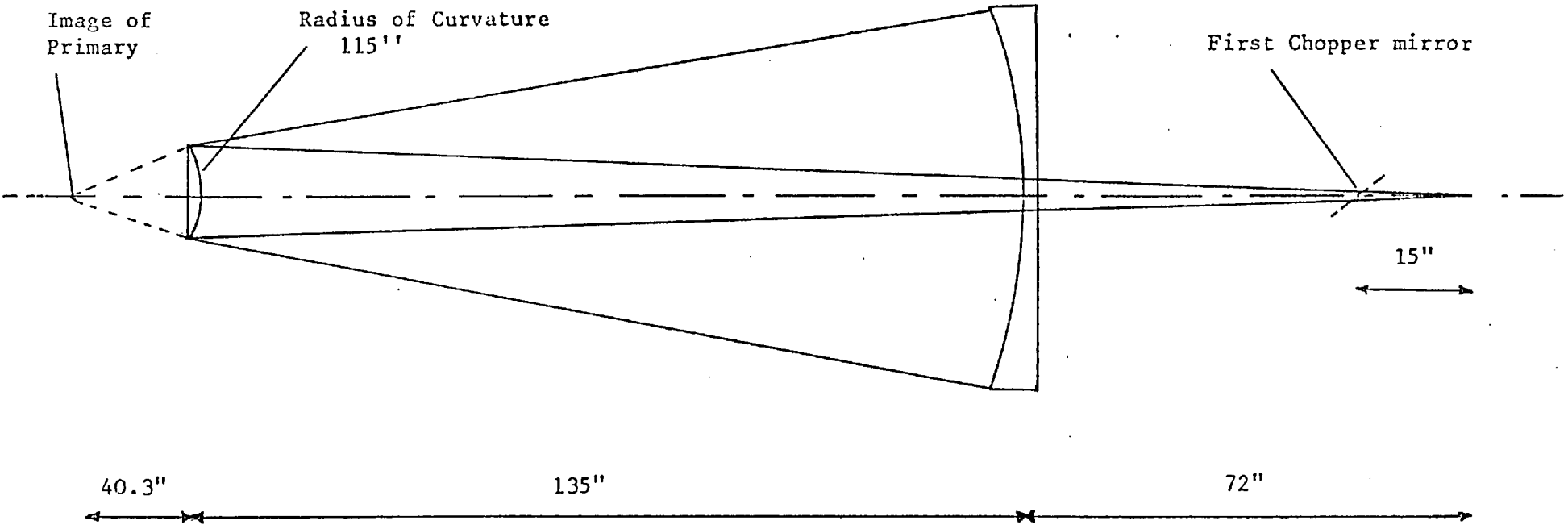

Fig. 4.14 Geometry of the 1.5m Flux Collector

but $x = 2D\theta$

So that $\delta\theta = \frac{2D\theta}{\ell}$

The required angular motion of the mirror then is only half this i.e $D\theta/\ell$ and it is easily seen that this angle must be added to the normal motion of the mirror.

Now the angle θ is inversely proportional to L where L is the length of the actuating arm. So that is L^1 is the modified arm length then

$$\frac{L^1}{L} = \frac{\theta}{L + \frac{D\theta}{\ell}}$$

and hence

$$L^1 = \frac{L}{1 + D/\ell}$$

In the chopper used L = 0.75". D = 6" and ℓ = 233" so that L^1 = 0.73".

Gold Coatings for Chopper Mirrors

As mentioned previously and with reference to Figure 4.1 the chopper mirrors are made semi-reflecting in order to provide visual images for guiding purposes.By using gold coatings it is possible to obtain high reflection in the infrared (≥90%) while allowing up to 50% transmission in the visible,see Figure 4.15 (due to P.R.Jorden(4.4))

For use in the photometer system of Figure 4.1 the first mirror (on the left in Figure 4.1)is given a coating which allows about 40% transmission in the visible,to give the normal stationary guiding image.The second chopper mirror allows about 10% transmission in the visible to give a chopped guide image as a monitor of the chop.

The procedure for cleaning and coating the mirrors is described in Appendix 4.

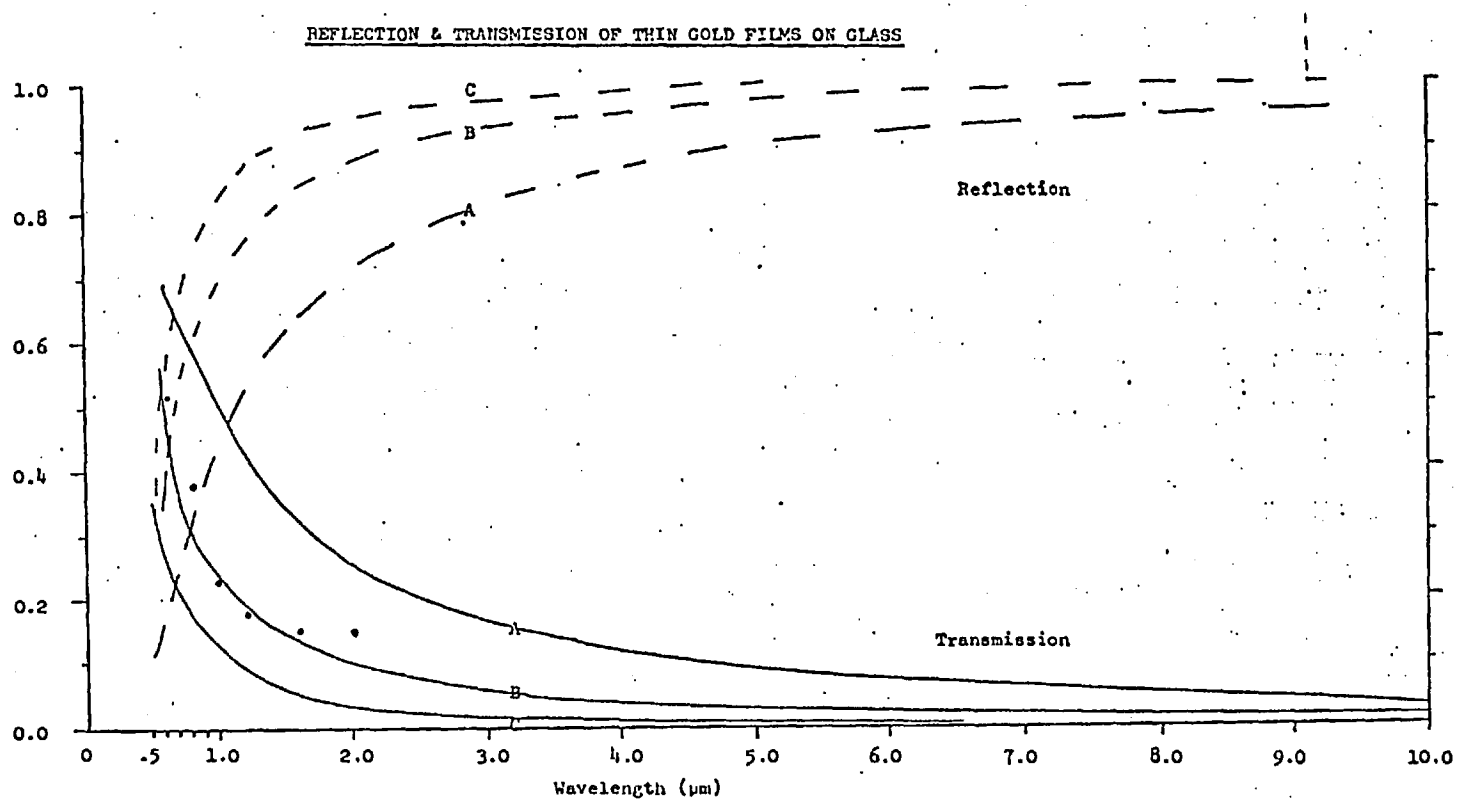

The Dots show measured values of Transmission of a sample with 55% Transmission @ 5500 Å

Theoretical Curves	A	0.009μm layer of Gold on glass (absorption beyond 1μm is not shown),	T=70% @ 5500 Å
	B	0.016μm layer	T=50% @ 5500 Å
	C	0.023μm layer	T=35% @ 5500 Å

Fig. 4.15

Servo-Control for Chopper

The circuit which provides servo-control for the two-mirror chopper is shown in Figure 4.16.It is based on a circuit designed by Lemke et al (4.5) and provides,proportional differentional and integrational feedback.

Feedback is via a magnetic resistive transducer (type FP 2002100) the magnet being mounted on one of the actuating arms of the chopper.

Figure 4.17 shows the power op-amp circuit which provides the drive to the coil,the amplifier is a National Semi-conductors LH 0021CK and is capable of producing 2A output.

The sevo control and drive are mounted in a control box which can be seen strapped to the photometer frame in Figure 4.18. The control box also contains the waveform generator which provides the reference for the servo-control.

The reference unit is capable of providing either a square wave for normal photometry or a triangle wave for speckle work.As mentioned in Chapter 3,in the speckle mode the frequency of the chop must be changed when the grating is changed in order to maintain the same modulation frequency on the detector.This is accomplished by having several pre-programmed chop frequencies which can be selected via a control on the front panel of the box.

Figure 4,19 shows the reference unit,the circuit being derived from Tobey et al (4.6)

The system was tested by observing the feedback signal while the reference signal was

a) a square wave of frequency 20Hz
b) a triangle wave of frequency 20Hz

In both cases the chopper was giving a throw of about 1mm.

The results of these tests are shown in Figure 4.20 for the three different damping conditions,i.e underdamped,overdamped and critically damped.

The damping is provided by the differential feedback section,the gain of which is adjustable on the front panel of the unit.

The integrational feedback is included to avoid such long term errors as gravity scanning as the telescope changes its orientaion.The time constant used is≥10 seconds so that there is little effect on the normal chop frequencies while the high gain of the section ensures a stable mean position.

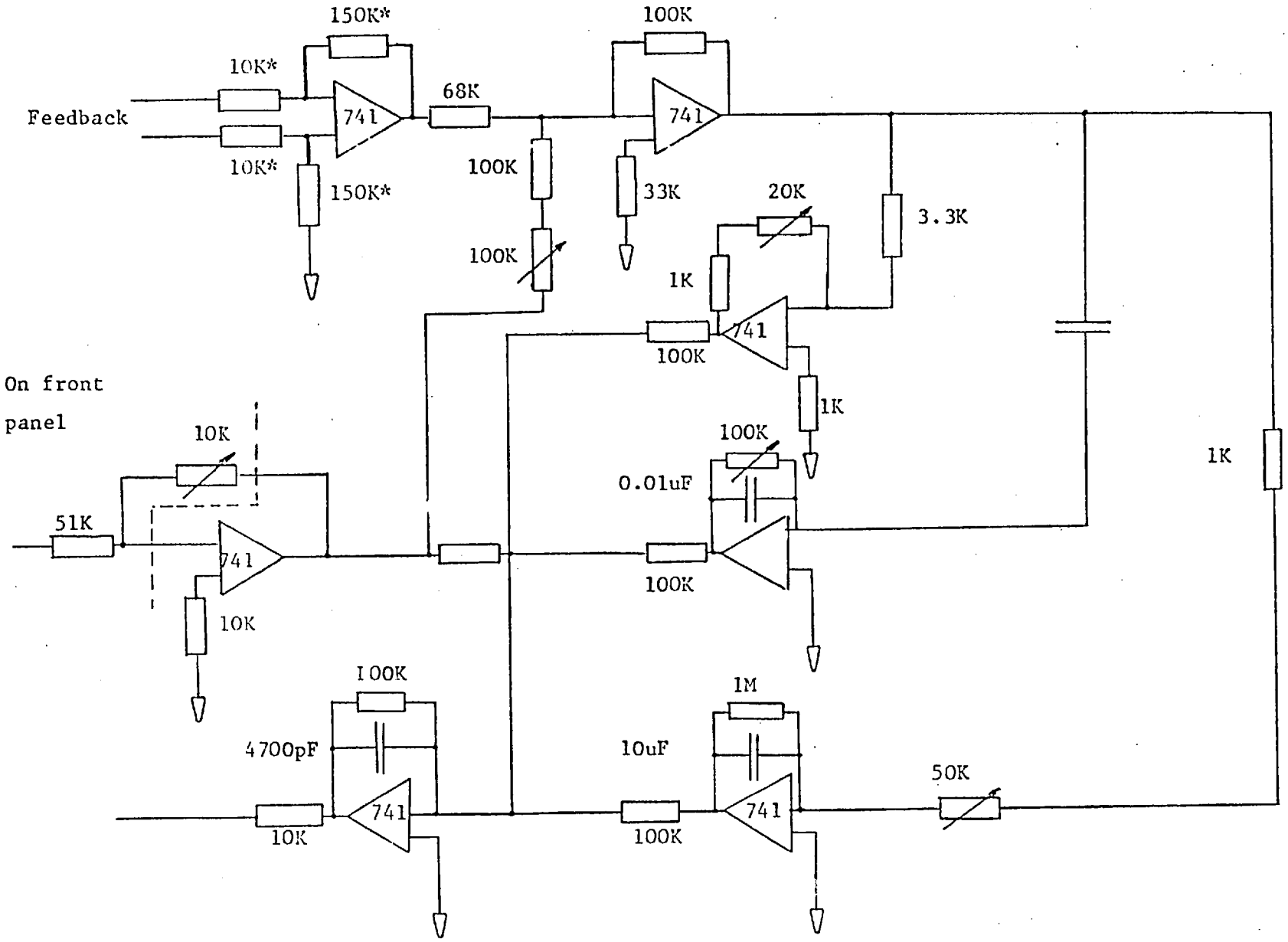

* Matched resistors

Fig. 4.16 Servo-control for Two-mirror Chopper

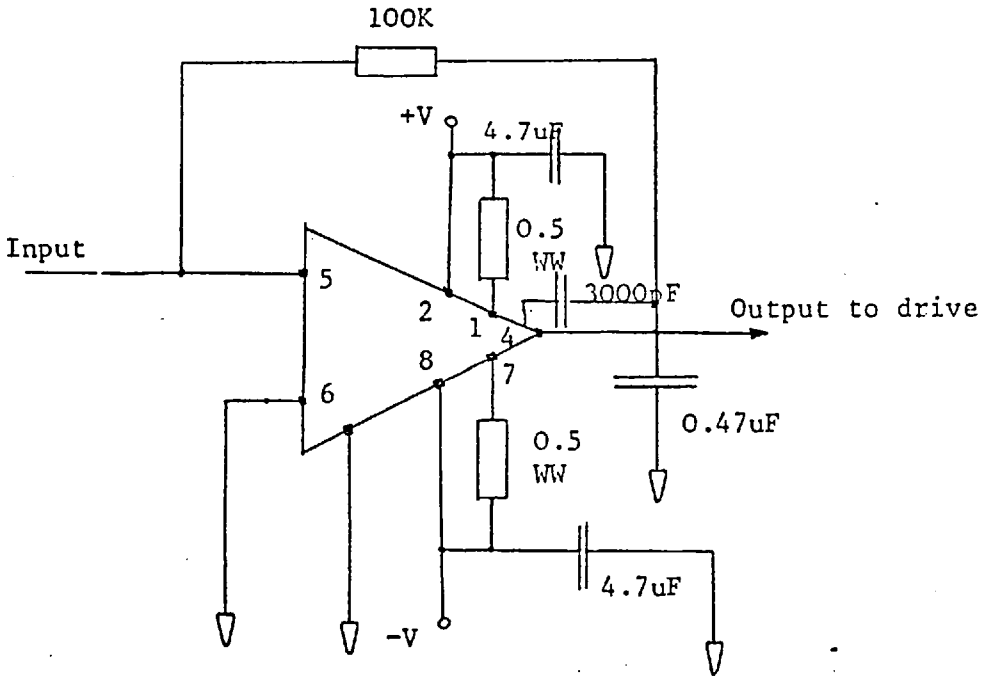

Fig. 4.17 Power op-amp for chopper drive

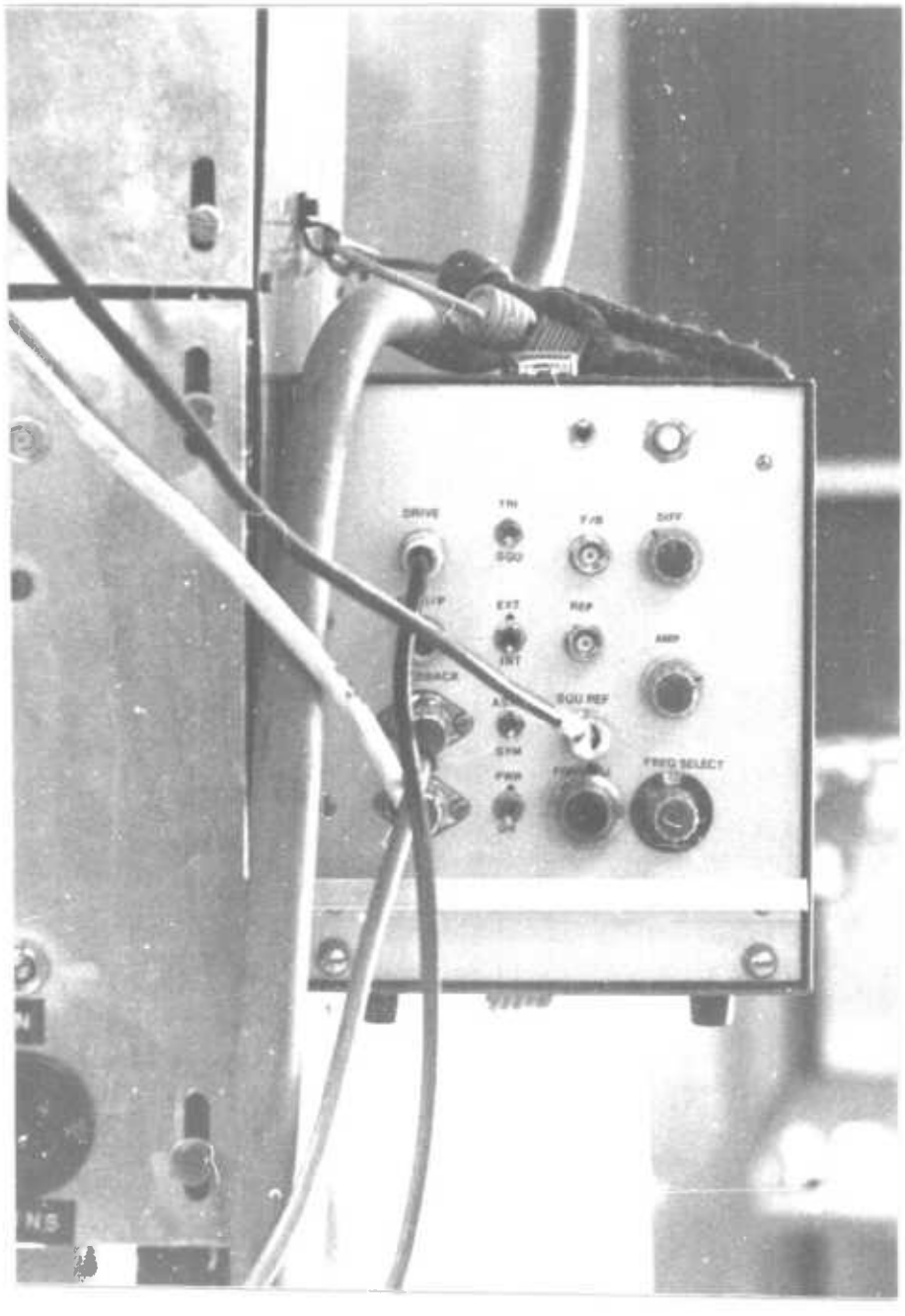

Fig. 4.18 Chopper control box

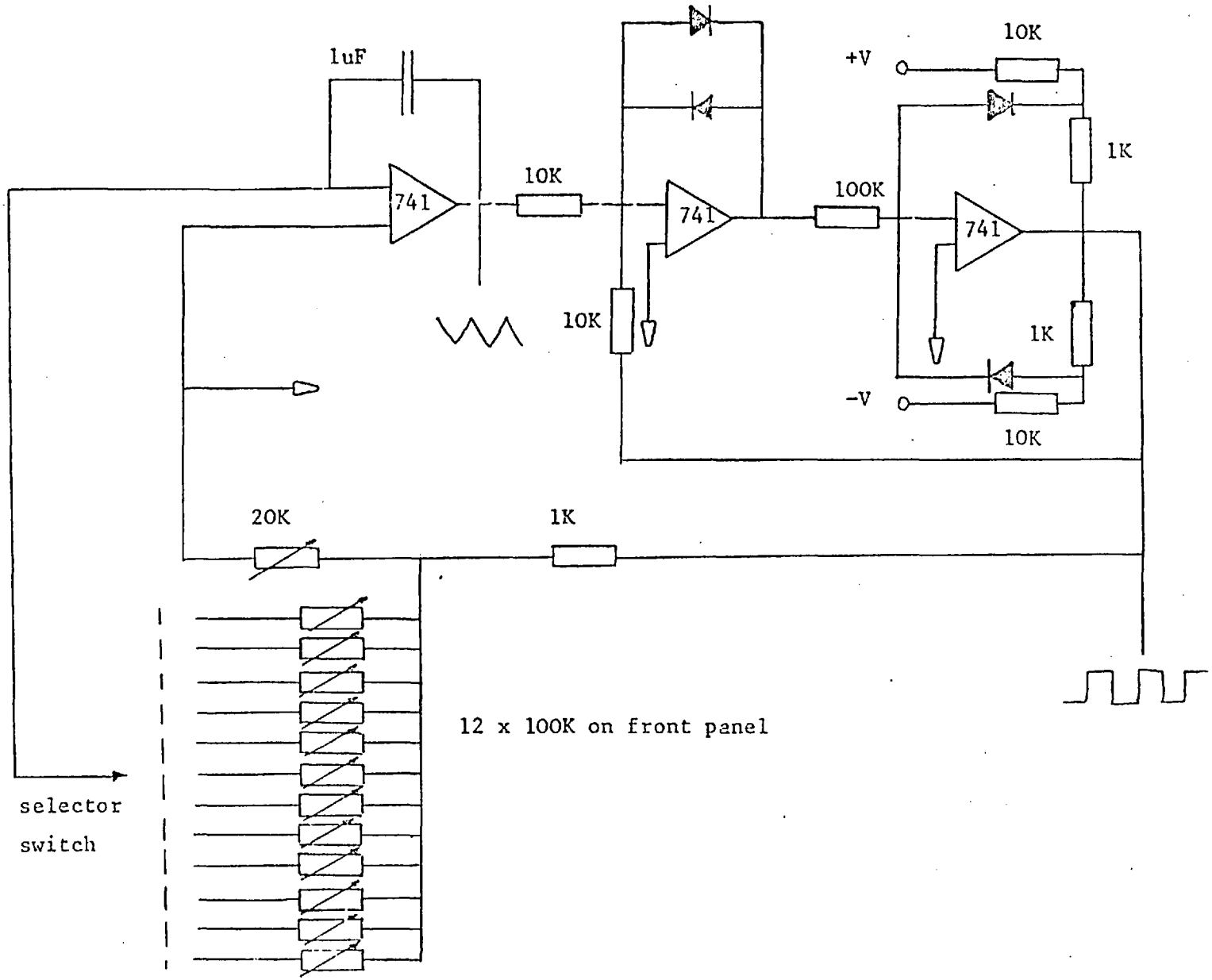

Fig. 4.19 Chopper control reference unit

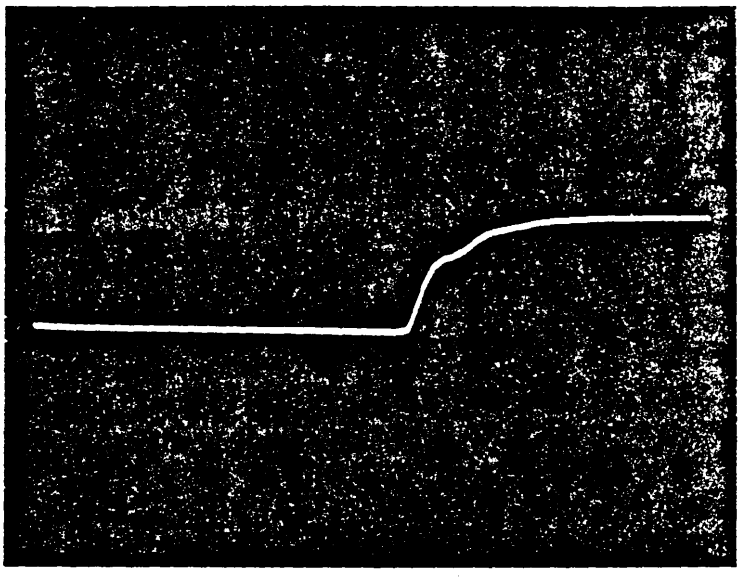

(i) 5ms

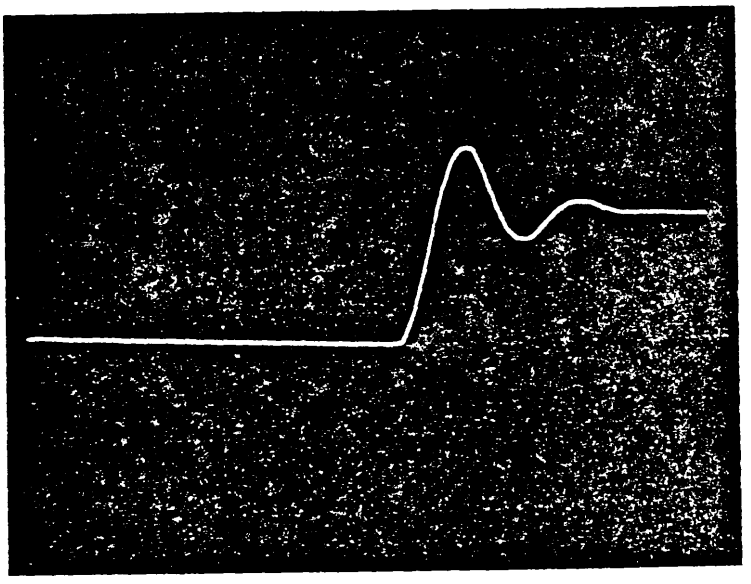

(ii)

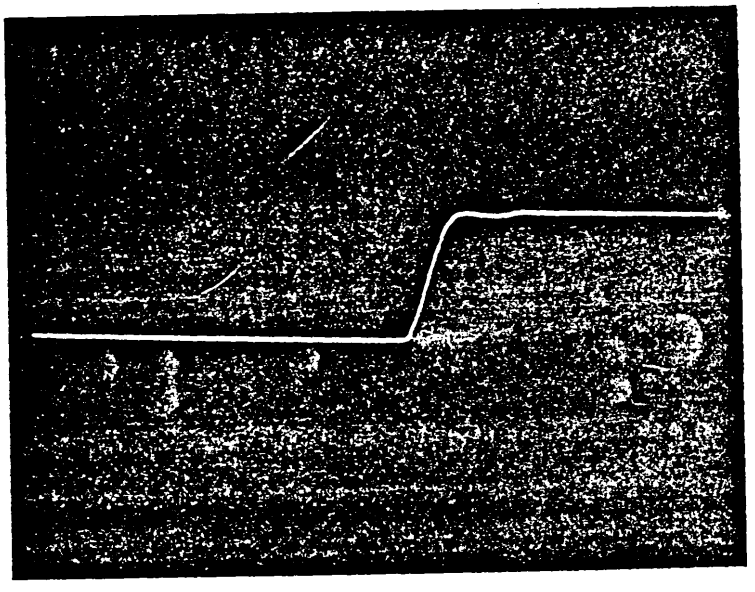

(iii)

Fig. 4.20 a) Chopper response to 20Hz square wave
i) over ii) under iii) critical damping

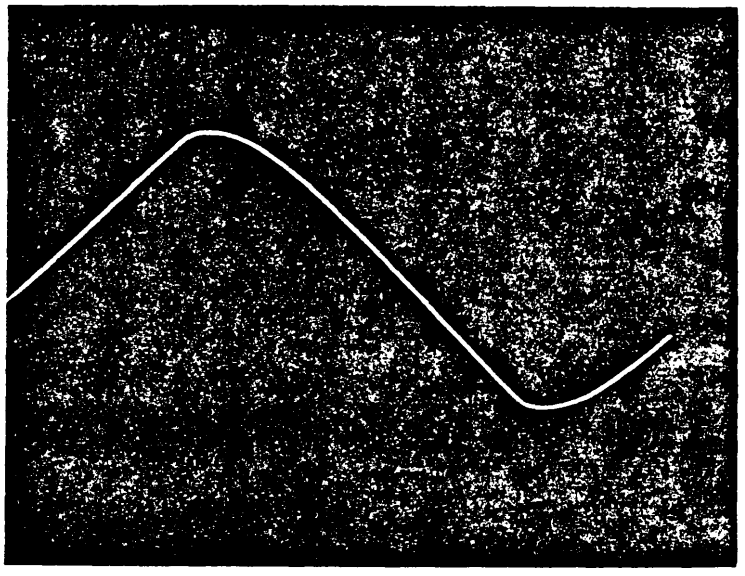

(i)

5ms

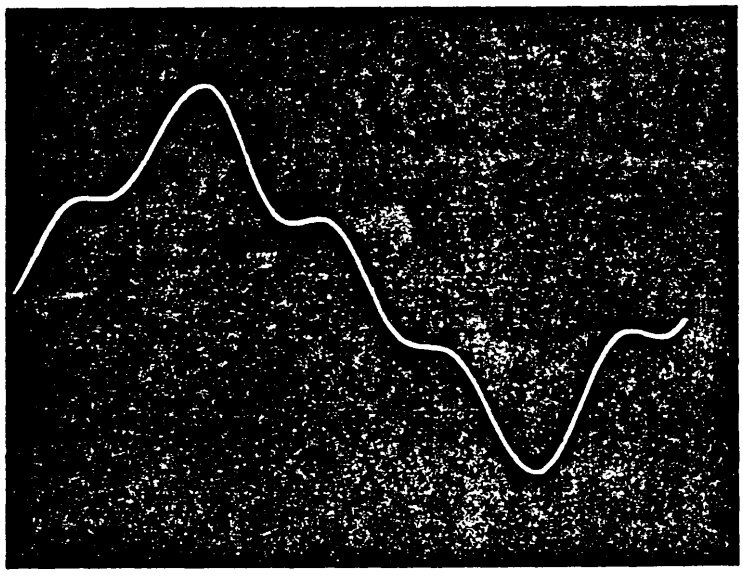

(ii)

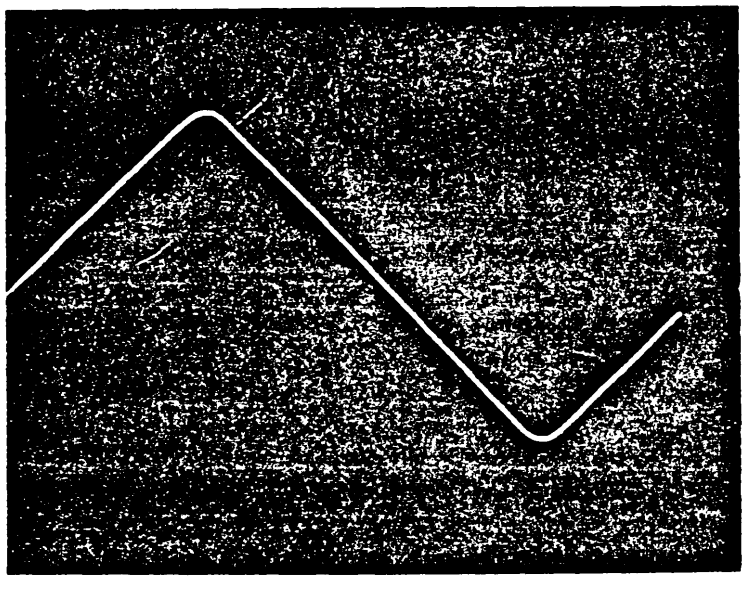

(iii)

Fig. 4.20 b) Chopper response to 20Hz triangle wave
i) over ii) under iii) critical damping

As can be seen in Figure 4.20 the rise time for the critically damped square wave is about 4 ms so that for a 20 Hz chop 16% of the time is lost between positions.The figure seems to be slightly less for the triangle wave cases.

On-Line Data Analysis

As will be discussed in the next chapter the signals from the detector for any one grating are recorded on magnetic tape in analogue form,for later analysis at Imperial College.However,in order to provide a certain degree of 'quick look' on-line analysis of the data on low cost,computer controlled spectrum analyser has been developed.

Principle of Simple Spectrum Analyser

In its simplest form a spectrum analyser can be seen as just a tunable filter.However since the design and control of narrow bandwidth tunable filters is not easy,a method has been used which allows the use of a single narrow bandwidth bandpass filter.

Consider the input signal

$$S(t) = A \cos (2\pi f_o t + \phi)$$

Where ϕ is an arbitrary phase angle.

If we multiply the signal by a second sinusoide of frequency f then we obtain

$$\begin{aligned} S\ (t) &= A \cos (2\pi f_o t + \phi)\ B \cos (2\pi f t) \\ &= \tfrac{1}{2} AB \cos (2\pi t(f_o - f) + \phi) + \tfrac{1}{2} AB \cos(2\pi t(f_o + f) + \phi) \end{aligned}$$

This signal can then be passed through a bandpass filter so that if $(f_o - f)$ falls within the bandpass then it gets through the system.The ouput of the filter can then be rectified and smoothed in order to measure the power in the band of frequencies passed by the filter.

By scanning the frequency f and measuring the change in the power measurement,the power spectrum of the signal S(t) can be measured.

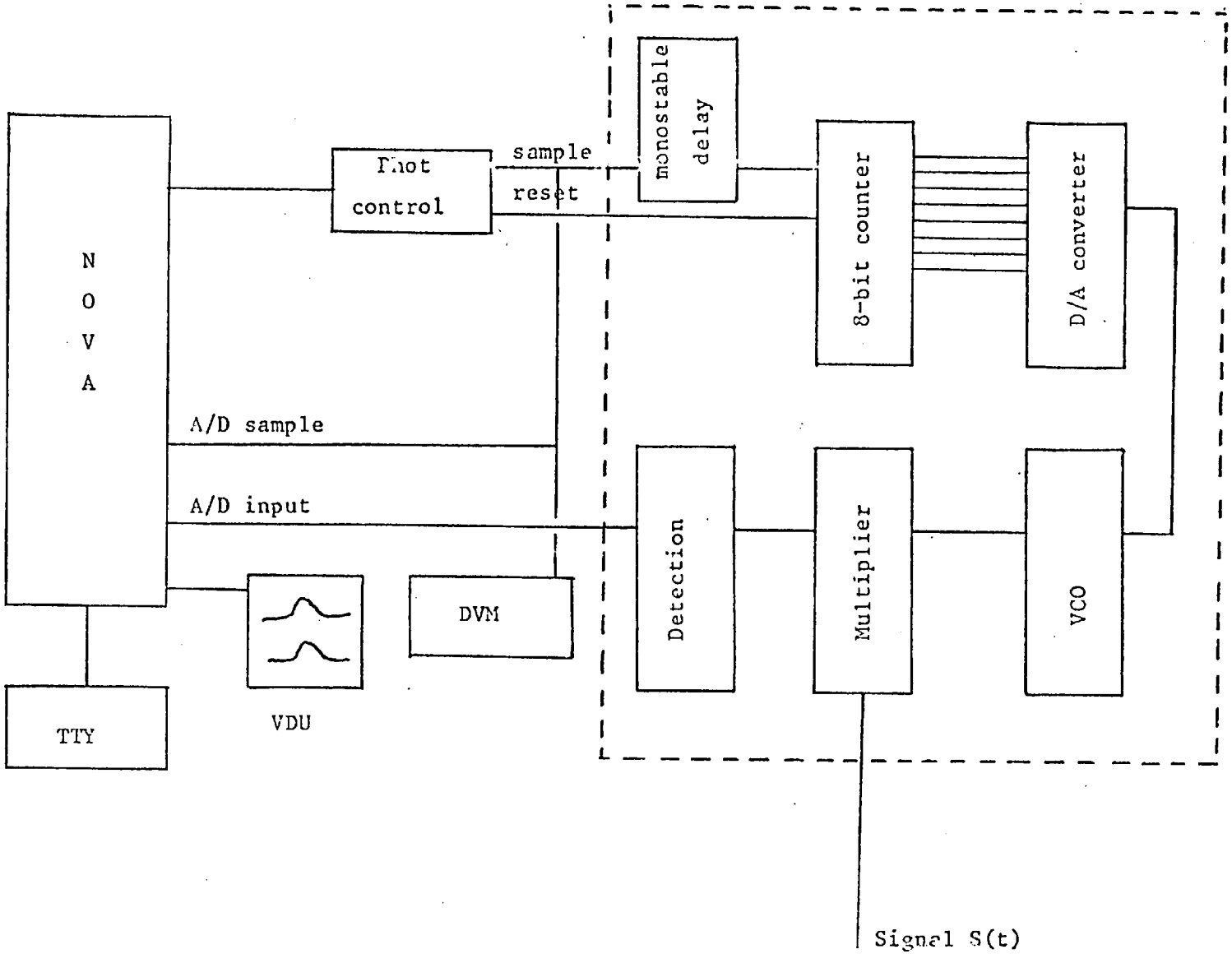

Fig. 4.21 Simple computer controlled spectrum analyser

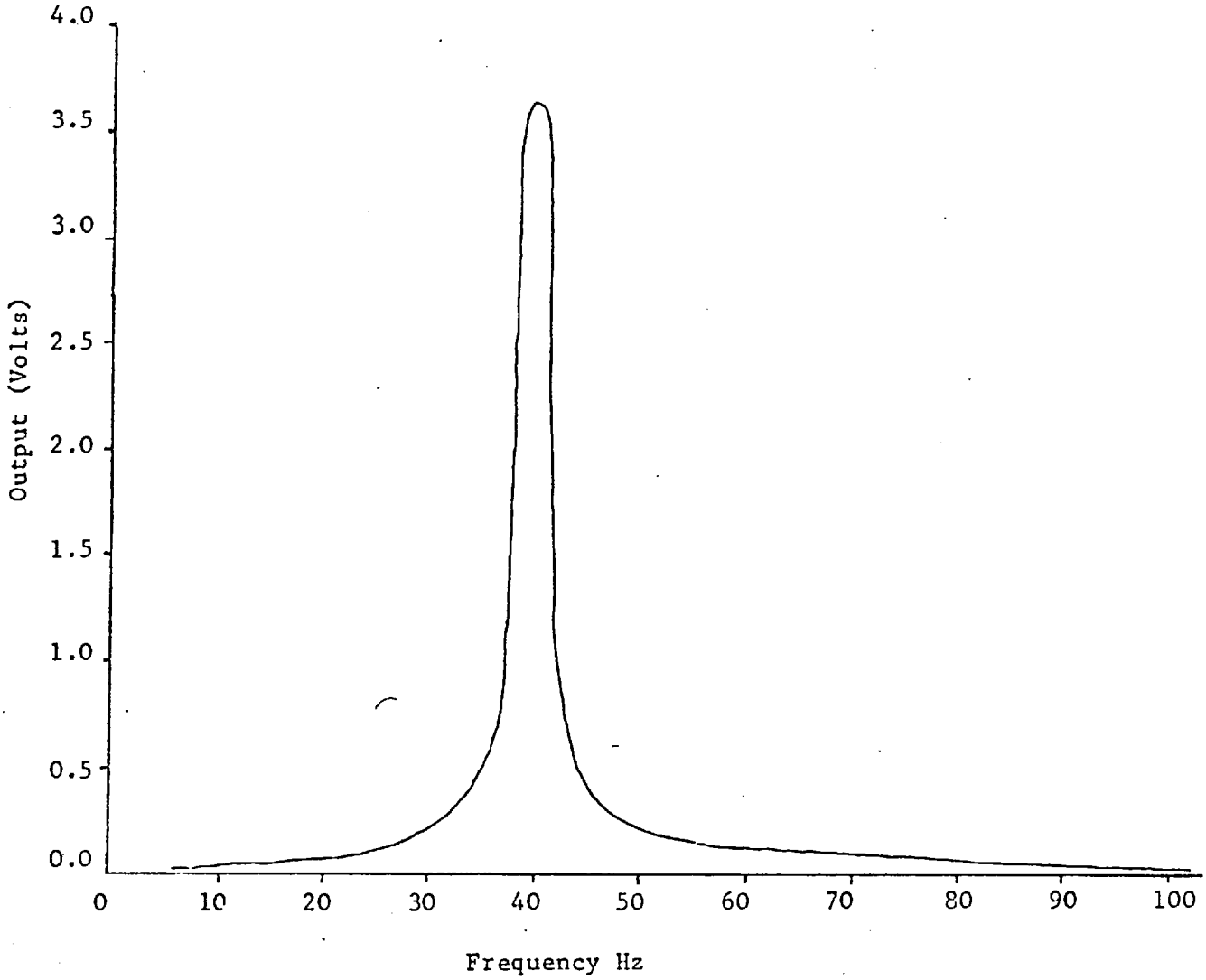

Fig. 4.22 Profile of filter for spectrum analyser

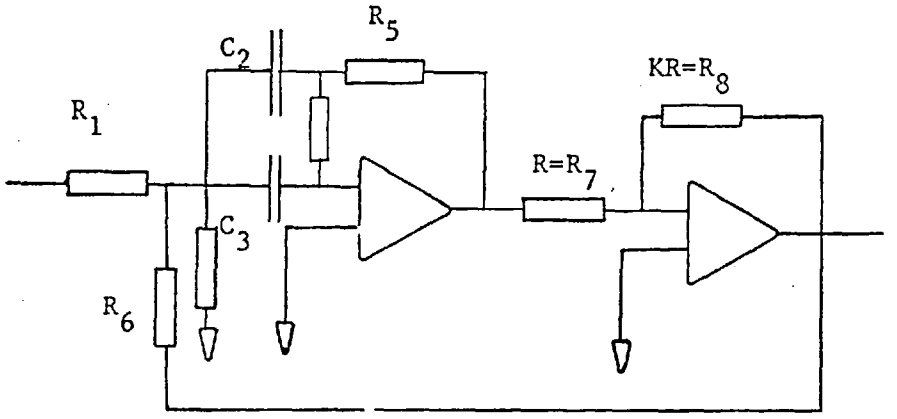

$R = Q/\omega_o C$ $\qquad R_6 = RKQ/(2Q-1)$

$G_2 = 1/R_2 = 1/R \times (Q-1-2/K+1/KQ)$

Fig. 4.23 Bandpass filter circuit

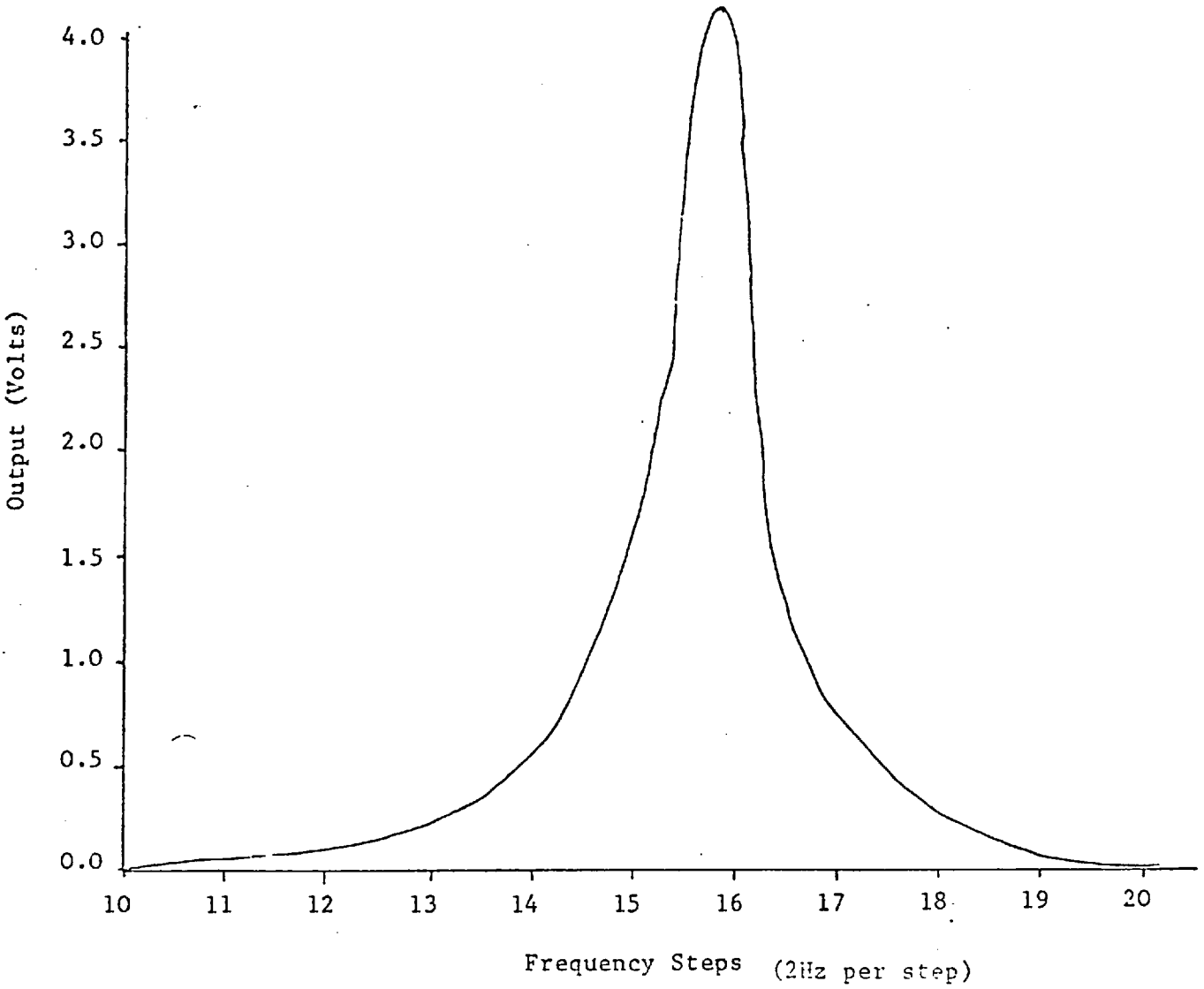

Fig. 4.24 Response of spectrum analyser to 120Hz sine wave input (2V pk-pk)

Realization

Figure 4.21 shows schematically the realization of a simple computer controlled spectrum analyser.

With reference to Figure 4.21,computer control comes via the Data General Nova on Tenerife.The computer controls the operation of the photometry sampling box which is used by the Imperial College group to provide sample pulses for a DVM and nod pulses for the telescope after a preset number of samples.The design and operation of the Photometry Box has been described by P.R.Jorden (4.4)

When used with the spectrum analyser samples from the control box go both to the Digital Vallmeter Sample Control and to the spectrum analyser.The pulse to the spectrum analyser is delayed by 20ms to allow the DVM and A/D of the NOVA to sample the ouput of the Spectrum Analyser before a frequency step occurs.Frequency stepping is achieved by driving a voltage controlled oscillator (VCO) from a D/A converter which in turn is controlled by an 8-bit binary counter which counts the sample pulses.The nod pulse from the photometry control box is used to reset the counter after a complete scan.

The Nova then receives scans of the spectrum in the form of sets of samples from the A/D converter in a Camac interface.The latest scan is displayed by the Nova via Camac on a CRT display unit in the dome,along with the sum of all previous scans.When the signal to noise on this sum is judged sufficient the points of the spectrum are printed out on the TTY along with the total power in the signal.

Figure 4.22 shows the profile of the bandpass filter the circuit of which is shown in Figure 4.23 (circuit derived from Tobey et al (4.6))

Figure 4.24 shows the response of the spectrum analyser to a 120Hz sine wave input.

The computer control programme was written in Basic with extensions developed at Imperial College for the control fo Camac.For reference the control programme is listed in Appendix5 .

Setting up and Observing Procedure

At the beginning of an observing trip the photometer and chopper must be correctly aligned in order to reduce the background and ensure that chopping signals are not produced.This is done with the aid of a He-Ne laser which is reflected vertically down from the

position where the detector would normally be.Thus the laser is reflected by the chopper back up to the secondary of the telescope.The chopper can then be aligned so that the beam from the detector hits the centre of the secondary.The laser is then removed and an artificial star is placed in the photometer so as to give a small image at the position of the detector,after reflection by the chopper.The exact position of this image is set by use of a perspex column gauge which sits in place of the cryostat.At this stage both eyepieces are aligned with the artificial star image.The column gauge is then removed and the cryostat is placed on the photometer,By monitoring the DC signal from the detector the position of the cryostat is set,this is done with a small focal plane aperture (0.5mm) in position so as to give the greatest accuracy.

The artificial star is then removed and the telescope is pointed at a bright calibration star.The infrared image is found by searching around the centre position as indicated in the guide eyepiece.Once the image is located,the eyepiece can then be reset to the correct position.The error in the intital setting up using the artificial star is usually found to be within $5^{\prime\prime} = 0.5$mm.

The following procedure is followed at the start of each nights observations and periodically during the night.

The telescope is focused by oscillating the image across a grating whose spacing is approximately equal to the seeing disc size,the telescope focus being adjusted to give maximum modulation of the signal.The visual image is then scanned around in the guide eyepiece with the chopper off,to check the location and shape of the aperture function.This gives an indication of the accuracy of alignment of the system.

The observing technique normally adopted is to select an object of interest and a suitable,nearby calibration star which is as close to the object as possible,After deciding at which infrared wavelength the observations are to be made,a sequence of measurements are made at that wavelength on the calibration star.This sequence consists of measuring the signal from each grating in turn,and then repeating the measurement again.This gives an indication during the data analysis of whether the MTF of the atmosphere was changing during the time period of the observations.After two runs on the calibration star the same procedure is followed on the object of

interest before returning and making a further set of measurements on the calibration star.

Using this observing technique much time is spent not observing the object of interest but rather observing calibration stars.However,the accuracy of the method is very dependant on the accuracy with which the atmospheric MTF is determined,especially if the function changes during the observations.

All data is recorded in analogue form on low noise magnetic tape cassettes using an Aiwa 1250 tape deck.It is important therefore during observing to note where and on what cassette a piece of information was recorded.Therefore for each observation a sheet is filled out which contains the following information. : Object name,reference,date,infrared filter used,siderial time at start of observation,comments on weather tape,tape position at start of each grating,gain of amplifiers.

A typical sheet is shown in Figure 4.25.

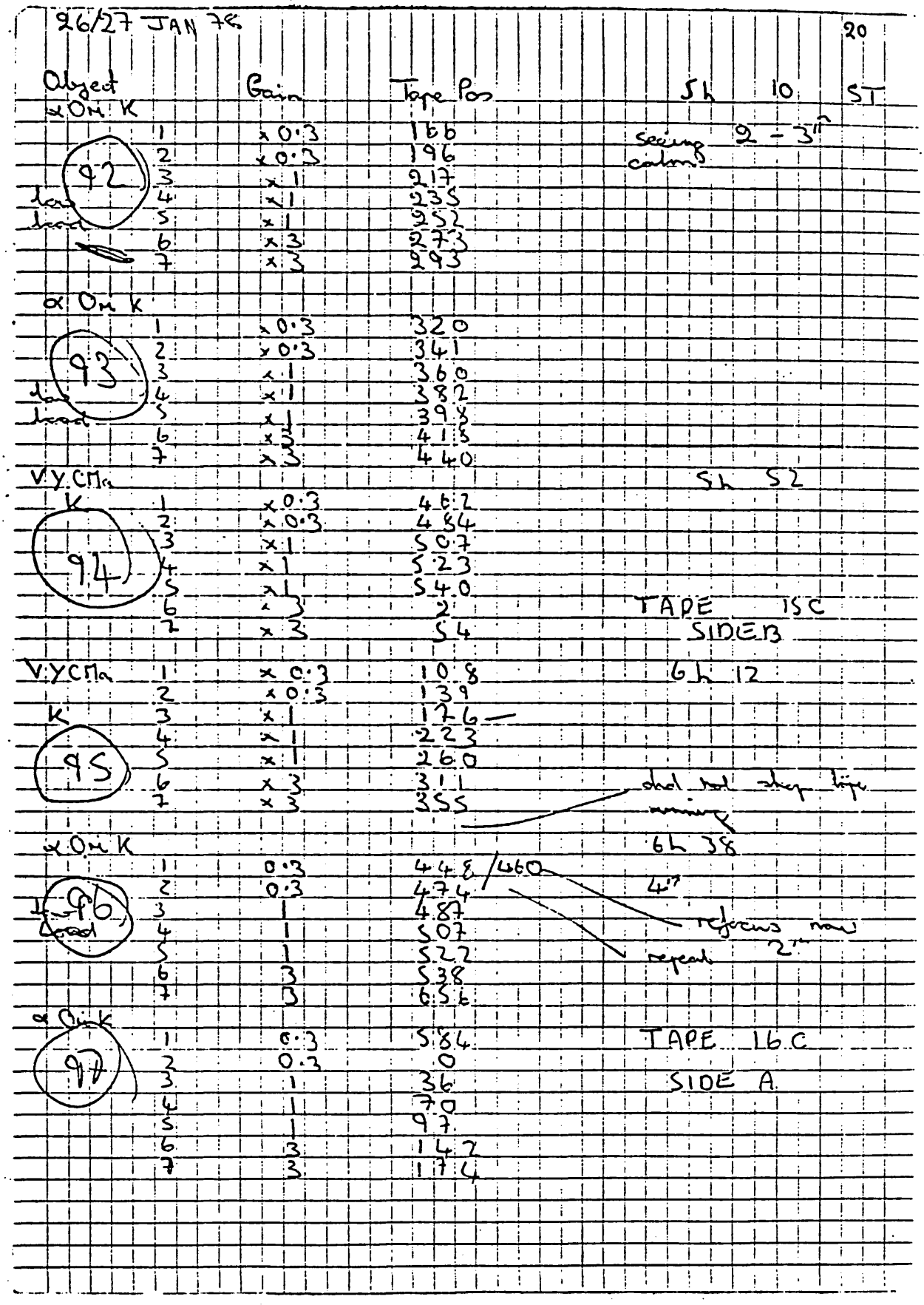

Fig. 4.25 Typical observing sheet

Chapter 5 Data Reduction

Introduction

As mentioned in the previous chapter the amplified signals from the detector are recorded in analogue form on magnetic tape for later analysis at Imperial College.In this chapter I shall discuss the method by which this is carried out.

It was shown in Chapter 3 that due to the oscillatory motion of the chopper the signal from the detector is periodic so that its power spectrum is a line spectrum with harmonic spacing equal to the chop frequency.For the coarse gratings this line spectrum is easily visible due to the higher chop frequencies.For the fine gratings however a spectrum with a characteristic bandwidth is obtained.Typical power spectra for both coarse and fine gratings are shown in Figure5·1.These were obtained by running the signals from the tape directly into a Hewlet-Packard Spectrum Analyser (Model 3580A).

In order to calculate the power in the signal on any one grating without including excess noise it is necessary to calculate the power spectrum of the signal.It is found that most of the power is contained within the bandwidth 0-200 Hz so that the data must be sampled at at least 400 Hz in order to avoid aliasing.Typical bandwidths ΔB for the signal power spectra are found to be $\simeq$ 20 Hz (see Figure4·1 and Chapter 6) so that a figure of 5 Hz is a reasonable target for the resolution in the power spectrum.In order then to give a smooth curve which may be easily and accurately integrated,the sample period in the spectrum is chosen to be 1 Hz.

Calculation of Power Spectra

The power spectrum of a function f(t) may be obtained in two ways.The function may be Fourier transformed and then squared to give the power transform $P(\omega)$.Alternatively the function may be auto-correlated to give $(f(t)* f(t)) = \phi(t)$ which may then be cosine transformed to give the power spectrum i.e

$$P(\omega) = (\mathrm{FT}\{f(t)\})^2 = \mathrm{FT\ (cosine)}\{f(t) * f(t)\}$$

where FT $\{\ \}$ represents the Fourier transform.

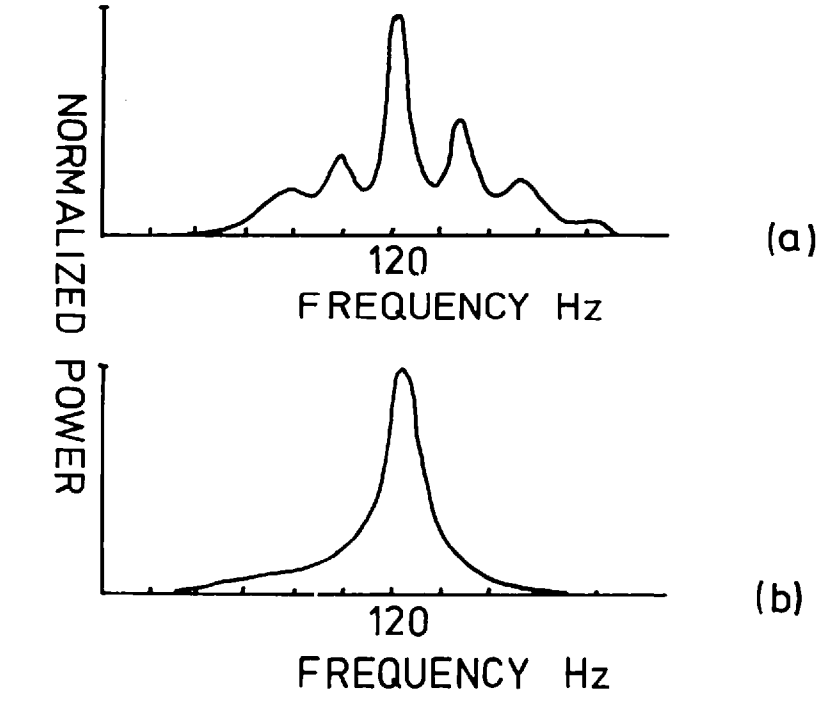

Fig. 5.1 Power spectrum of signal from detector for
a) grating with 2 lines per mm.
b) grating with 7 lines per mm.

Using the first method it would be necessary to calculate the Fourier transform of 40 points and then square the result, ten times per second.Now the number of multiplications required to perform a Fast Fourier Transform on N data points is of the order of $2N \log_2 N$ (5.1).We require then 424 multiplications to perform the FFT on 40 data points plus 200 squaring operations to form the power transform.The total number of multiplications per second is therefore of order 6,240.

Alternatively using the second method an autocorrelation with a 40 point range may be found which may then be cosined transformed after the total integration time.Here the number of multiplications required per second would be 1,600 with the same number of additions.

The autocorrelation method is clearly the faster of the two methods.Because of this and the simplicity of the algorithms required,the autocorrelation method was chosen for the data analysis.

The Algorithm

Assuming we have data with the following characteristics

Power spectrum $P(\omega)$

Autocorrelation $\phi(t)$

Maximum frequency f_{max}

Resolution in power spectrum ΔW

The autocorrelation of a function I(t) may be expressed as

$$\phi(t') = < I(t+t')I(t) > \qquad (5.1)$$

now if we sample at a rate $1/\Delta t = 2f_{max}$ so that $t' = m\Delta t$ then

$$\phi(m) = \sum_{n=1}^{N} I(m+n)I(n)/(N+1) \qquad (5.2)$$

Now for a resolution ΔW in the power spectrum

$$t'_{max} = m_{max}\Delta t = 1/2\Delta W$$

and since

$$\Delta t = 1/2f_{max} \qquad m_{max} = f_{max}/\Delta W$$

so that for $f_{max} = 200$ Hz and $\Delta W = 5$Hz

$$m_{max} = 40$$

Now the power spectrum is given by

$$P(f) = 2\int_0^{\infty} \phi(t)\cos(2\pi ft)\,dt \qquad (5.3)$$

$$\simeq 2\sum_{m=0}^{m_{max}} \phi(m)\cos(2\pi fm\Delta t) \qquad (5.4)$$

let $f = k\Delta f$

$$P(k) = 2\sum_{m=0}^{m_{max}} \phi(m)\cos(2\pi km\Delta f\Delta t) \qquad (5.5)$$

if $f = 1Hz$

$$P(k) = 2\sum_{0}^{m_{max}} \phi(m)\cos(\pi\, km/200) \qquad (5.6)$$

The Computer

The computer used at Imperial College for data analysis is an Interdata 70 with 16K words of core and 2 x 2½ megabyte disc drives.Interfacingis via a CAMAC crate and system periferals include : line printer,CRT display,VDU,TTY,fast paper tape reader and fast paper tape punch.

FORTH - a new high level interactive language

The task which we require the computer to perform is not an easy one for a conventional programming language.Since the data is read in from magnetic tapes which contain sets of data of different lengths,the control language must be interactive.An interactive language such as BASIC however is not fast enough to permit the rapid digitalization and data storage required here.It was decided therefore to write all the data analysis programmes in the new high level interactive language;FORTH.

FORTH - and English - like language

FORTH is a new language (5.2) designed to avoid mini-computer users having to programme in assembler code.It is an English-like language in that it has a dictionary containing 'verbs'and 'nouns'. Verbs cause sequencies of computer operations to occur while nouns are the objects operated on (variables,constants,array elements). Starting from a few basic definitions the user defines new words and stores them in the dictionary.As with English the simple words are defined first and the complex words are defined in terms of previously defined words.

The Stack

Communication between the user and the words he uses and between one word and another is provided by a push down stack. He may for example place numbers on the stack (by entering them on the VDU) and then type a word which acts on the stack to produce the desired result. For example typing 3 8 *4/. will return the value 6,the sequence of operations can be seen in Figure42.

Key Board Entry	Stack
3	3
8	8 3
* (multiply)	24
4	4 24
/ (divide)	6
. (print result)	Empty

Blocks

A key factor in the way FORTH may be used to handle and store data in the existance of 1024 byte blocks.These blocks are sections os disc storage which may be used to store either text or data.The text contains the definitions which can be compiled into the dictionary by loading the blocks.Data is stored either as 512 integer numbers or 256 floating point numbers.A block of data may be moved by the use of a single command into a 1024 byte buffer in core.The disc then becomes an extension of the core.If a block is altered while in a buffer then it is rewritten onto the disc when the buffer is required for another block.

Operation of CAMAC under FORTH

The control of the CAMAC interface under FORTH is achieved by defining words which refer to the address of a given module in the crate.The function codes for the module are then defined as FORTH words so that for example

INTER CLEAR SA

clears the interrupt register (SA refers to a Single Action CAMAC operation).

Implementation of Data Analysis

I shall describe here the analysis of the signal from the detector for any one grating,from it being read off the magnetic tape to a value for the power being printed out.

The analysis falls into three sections which take the form of three separate operations with three points of interaction with the operator.

These are -:

a) Data input, digitization and storage.

b) Calculation and display of the power transform.

c) Summation over the relevant bandwidth and calculation of the power in the signal.

a) Data Input

The word DATA -IN is used to digitize the data from the tapes and then store the numbers in blocks (512 per block).DATA -IN then returns the number blocks stored to the operator.The only input required is the number of the block which the operator wishes to be the start block of the data.

So that 150 DATA-IN stores data in blocks 150 onwards. The analogue to digital converter module is a GEC - Elliot ADC 1201. Triggering is by inverted TTL pulses (the 1 state for CAMAC being 0v) from a Wavetek model 185 waveform generator.

As a test of the maximum data input rate the word T-RUN may be used to count the number of clock pulses sent to the ADC using a Harwell model 7039-1 preset counting register module.512 pulses only are sent to the ADC so that if the programme misses any pulses the block is not filled,which can easily be detected.It is found the maximum input rate is 700 Hz.Thus the required 400 Hz is well within the capability of the system.

In order to test how many pulses are lost between blocks the number of pulses required to fill a given number of blocks is determined.It is found that 5 % of the data is lost between the blocks.

b) Calculation of Power Spectrum

The word POWER is used to calculate the autocorrelation of each block,co-add and then cosine transform to produce the power spectrum.The result is then normalized (the normalization being stored for later use) and then displayed,via a Harwell 7011-2 display driver, on a CRT.The inputs required for POWER are ; the number of blocks, the

the number of the first of these blocks and the destination of the autocorrelation function.The power spectrum is stored two blocks from this block.

So that 50 150 250 POWER calculates the autocorrelation of 50 blocks from 150 to 199 and stores the co-addition in block 250. The normalized power spectrum is stored in block 252.

The next step in the analysis depends on the amount of noise in the spectrum.On a bright source there is normally little or no background noise on the spectrum (P_N of Figure 4.2 (b)).On weak sources however the background must be removed from the spectrum.This is done by fitting a straight line (using the word ST-LN) to points in the spectrum on either side of the modulation passband and then adjusting the data so that this line coincides with the axis.

c)Calculation of the Total Power in the Signal

The word INFO is used to calculate the area under the power spectrum.This area is then divided by the number of blocks used and the square of the amplifier gain at the time of the observation,finally it is multiplied by the normalization factor generated during POWER. INFO then records on the line printer : a run reference,the number of blocks used,the normalization factor,the area under the power spectrum and finaly the power of the signal.The input requirements for INFO are : a run reference and the square of the amplifier gain.

So that 1cc. 1 INFO gives the information on run 1 for which the gain was 10.

Sequence of Analysis Operations

Below is a typical conversation between an operator and the computer.Computer responses are underlined and the operator actions are shown on the right.

Conversation	Operations to start tape running
OK	
150 DATA-IN	Monitor signal on oscilloscope and press button 1 of interrupt register at end of data set
50 BLOCKS STORED ON DISC	

(Cont)

OK — Stop tape running

50 150 250 POWER

I AM NOW WORKING ON THE FT

OK — At end of calculation power spectrum is displayed on CRT press button 1 of interrupt register after inspection

100. 1 INFO

OK

INFO now prints the results of the calculation on the line printer,below is a typical output

RUN REF	1
NO OF BLOCKS	50
NORM IS	1.0000
AREA IS	1.0000E2
POWER IS	2.0000E-2

The Programmes

For reference the complete text used for data analysis and system testing is listed in Appendix 6 .This list is not meant to be self explanatory although the experienced FORTH programmer should be able to understand the functions of most words

DATA -IN can be found in block 138
POWER can be found in block 144
INFO can be found in block 144

Chapter 6 Observations

Introduction

The results described in this chapter have been obtained using the 1.5m Infrared Flux Collector on Tenerife in the Canary Islands.The telescope is situated at a height of about 2500m on a dry mountain site (the amount of precipitable water vapour being as low as 1mm).The site is positioned at latitude $28^{o}\ 17'\ 32''$, longitude $1^{h}\ 05^{m}\ 48.1^{s}$.Observations were made during August'77 and January'78 .The telescope was designed to give images of about $2''$, to allow a light weight and hence very cheap construction.The observed images during the observing trips were slightly astigmatic but a line image could be selected so as to give images of sub-arcsecond width in the direction perpendicular to the grating lines.Typical seeing at the site is about $2''$ so that the criterion of being able to resolve the seeing disc can normally be met and hence the aberrations of the telescope should not affect the resolution of the speckle technique.

Optical Filters Used

The infrared filters used for the observations were the standard photometry filters,the effective wavelengths and bandwidths of which are given in Table 6.1.As mentioned in Chapter 2,in order to avoid any loss of speckle visibility the filter bandwidths should meet the criterion

$$\Delta\lambda < \lambda^{2}/\Delta\theta_{S}D \qquad (6.1)$$

where $\Delta\theta_{S}$ is the seeing size in radians.The ideal bandwidths from Equation 6.1 are listed in Table 6.1.As can be seen the shorter wavelength filters are wider than required,the J-filter being approximately twice the required width.

Due to the extended bandwidths used each speckle will be spread due to the astronomical refraction.If this spread is larger than the diffraction limit then the resolution will be reduced. The amount of astronomical refraction may be calculated from the relation (6.1,6.2).

$$\text{Astronomical Refraction} = (\mu_{o}-1)(1-H_{o})\tan\alpha-(\mu_{o}-1)(H_{o}-\tfrac{1}{2}(\mu_{o}-1))\tan^{3}\alpha \qquad (6.2)$$

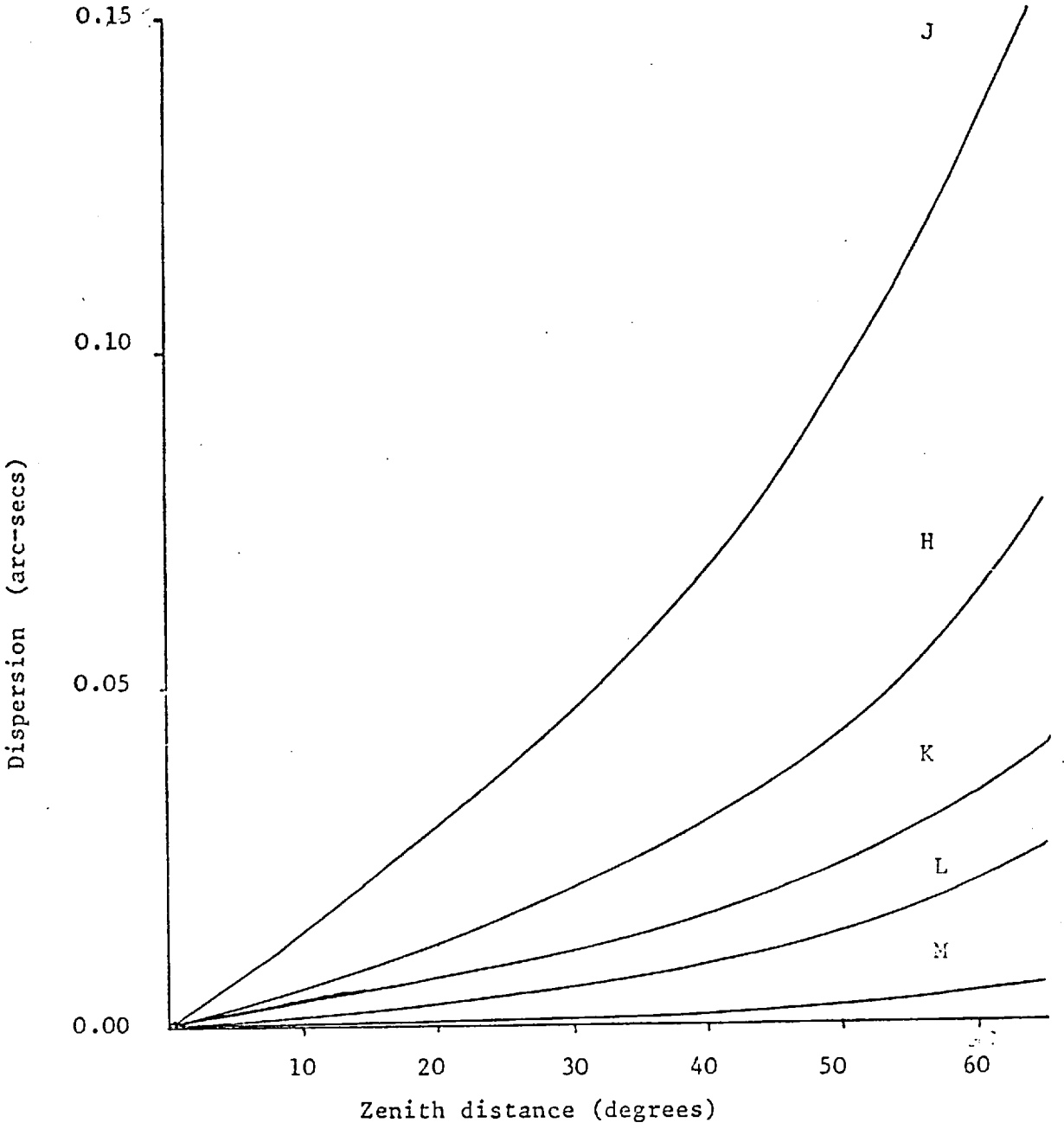

Fig. 6.1 Dispersion over bandwidths of filters

Table 6.1

Details of infrared filters used.
The dispersion is for zenith distance = 60°
while the resolution $\Delta\theta_D = \lambda/D$ where D = 1.5m

	J	H	K	L	M
λ_{eff}(μm)	1.23	1.65	2.23	3.45	4.94
$\Delta\lambda_{phot}$(μm)	0.24	0.30	0.41	0.57	0.80
$\Delta\lambda=\lambda^2/D\Delta\theta_s$(μm)	0.12	0.24	0.46	1.20	2.65
Dispersion ($\hat{\pi}$)	0.123	0.062	0.033	0.021	0.0034
Resolution ($\hat{\pi}$)	0.17	0.23	0.31	0.47	0.68

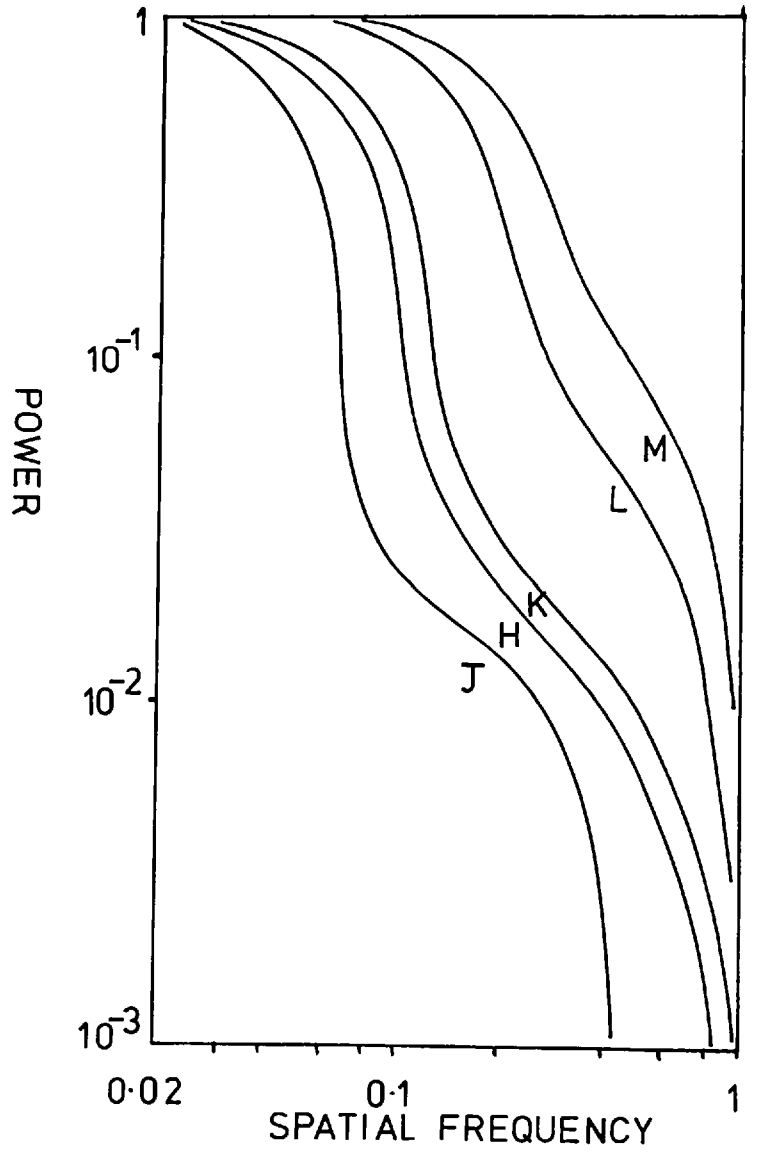

Fig. 6.2 Spatial frequency power spectra of the point source μ UMa at five infrared wavelengths. Spatialfrequency normalized to 1 at $\sigma = D/\lambda$

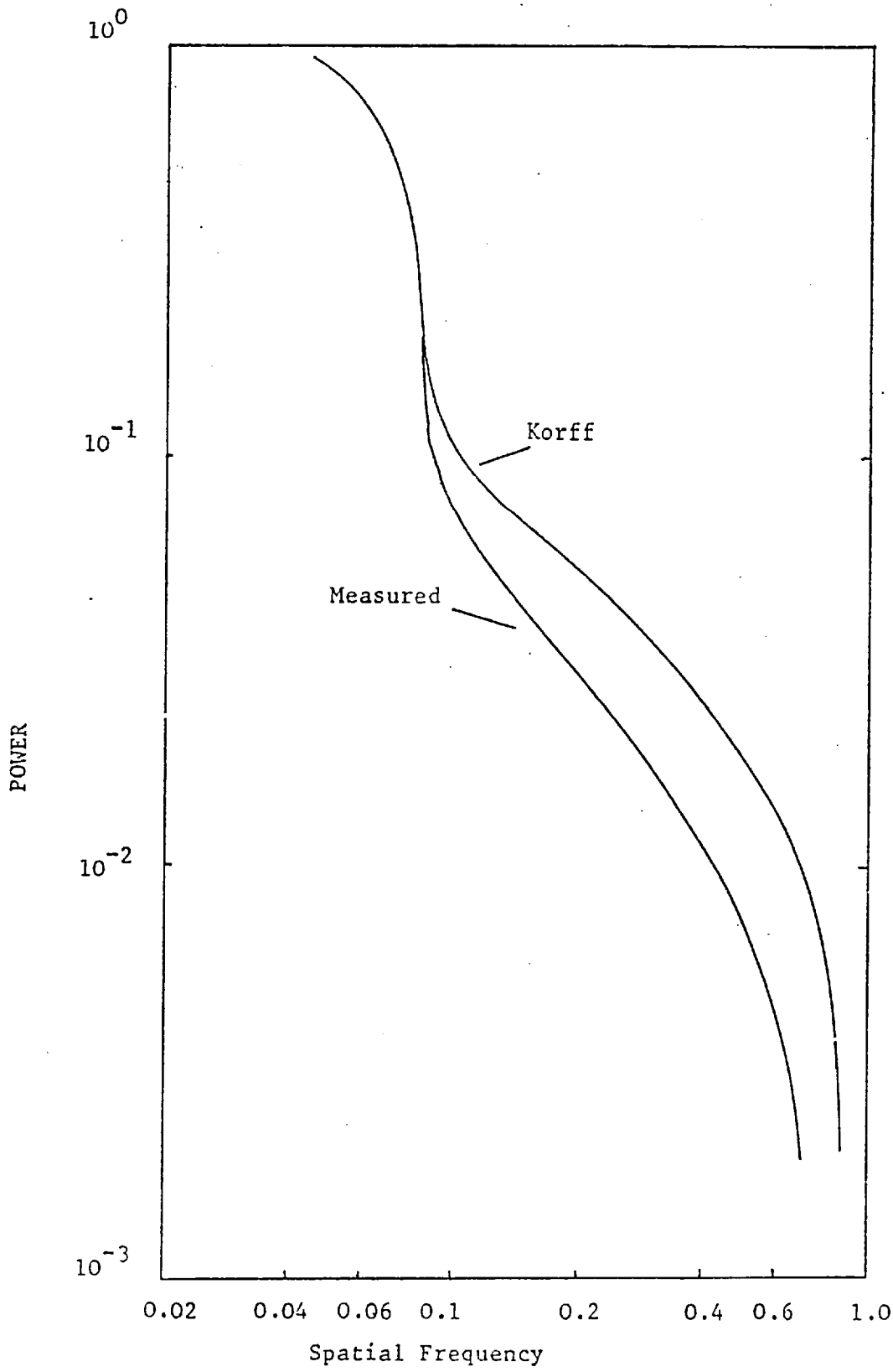

Fig. 6.3 Measured and predicted MTFs at 2.2μm

where α is the zenith distance of the observation

and Ho = $\frac{\text{height of atmosphere}}{\text{radius of earth}} \simeq 0.0125$

Using the refractive index values given by Allen (6.3) the spread in the image over the filter bandwidths have been calculated and are shown in Figure 6.1.In Table 6.1 the refraction at zenith distance 60^{o} for each filter is listed.The spread is small compared to the resolution limit of the 1.5m telescope which is also listed in the Table.

Measurements of MTF's

Measurements of the atmospheric MTF have been made by observing bright calibration stars.Figure 6.2 shows a set of such measurements for the five infrared filters taken over a period of one hour.Here the spatial frequency axis has been normalized to 1 at the diffraction limit.The curves clearly consist of two componants as predicted by Korff (6.4) and by Dainty (6.5),diffraction limited information being retained on all but the J (and to some extent the H) filter.The fall-off at J is thought to be due to the overlarge optical bandwidth of this filter.The MTFs are a little lower then those predicted by Korff,consistent with the findings of Karo and Schneiderman (6.6) at visible wavelengths.Figure 6.3 shows a measured MTF at 2.2um fitted at low spatial frequency to one predicted by Korff (6.4).

Measurement of r_o

Recalling Fried's model for the short exposure MTF of the atmosphere telescope system we have

$$\langle T(\sigma)\rangle_{SE} = T_o(\sigma)\exp(-3.44(\sigma\lambda/r_o)^{5/3}(1-(\sigma\lambda/D)^{1/3}) \qquad (6.3)$$

where σ = spatial frequency in the image plane (cycles/radian)

$T(\sigma)$ = transfer function of the telescope

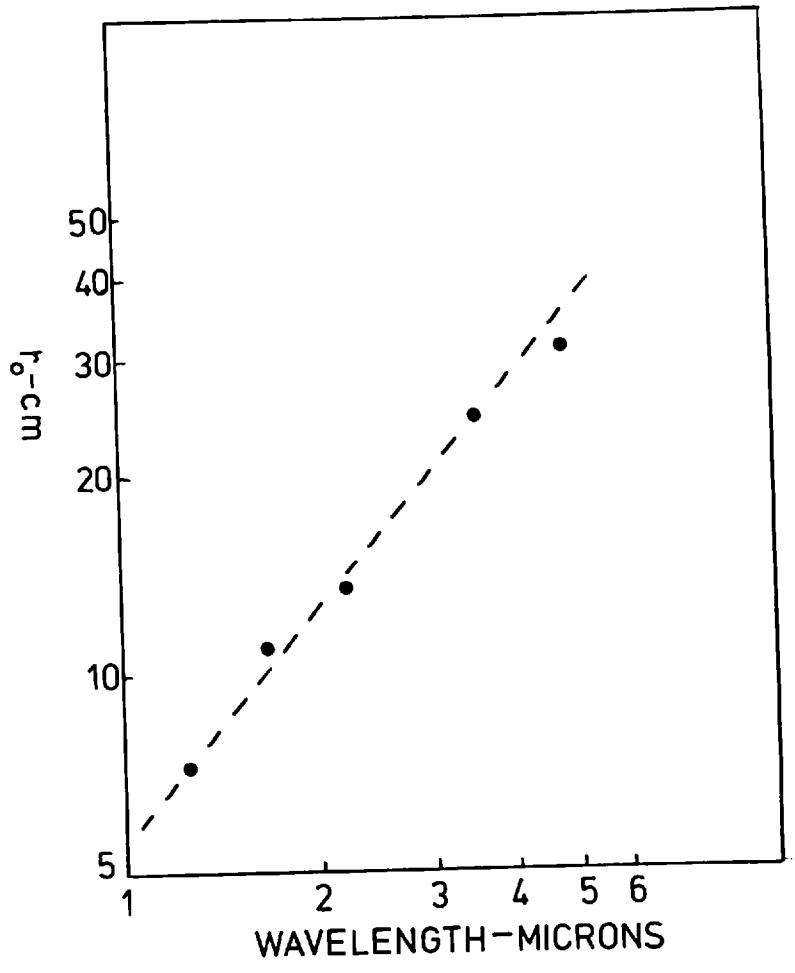

Fig. 6.4 r_o vs. λ ; The line shown reprisents a 6/5 power law.

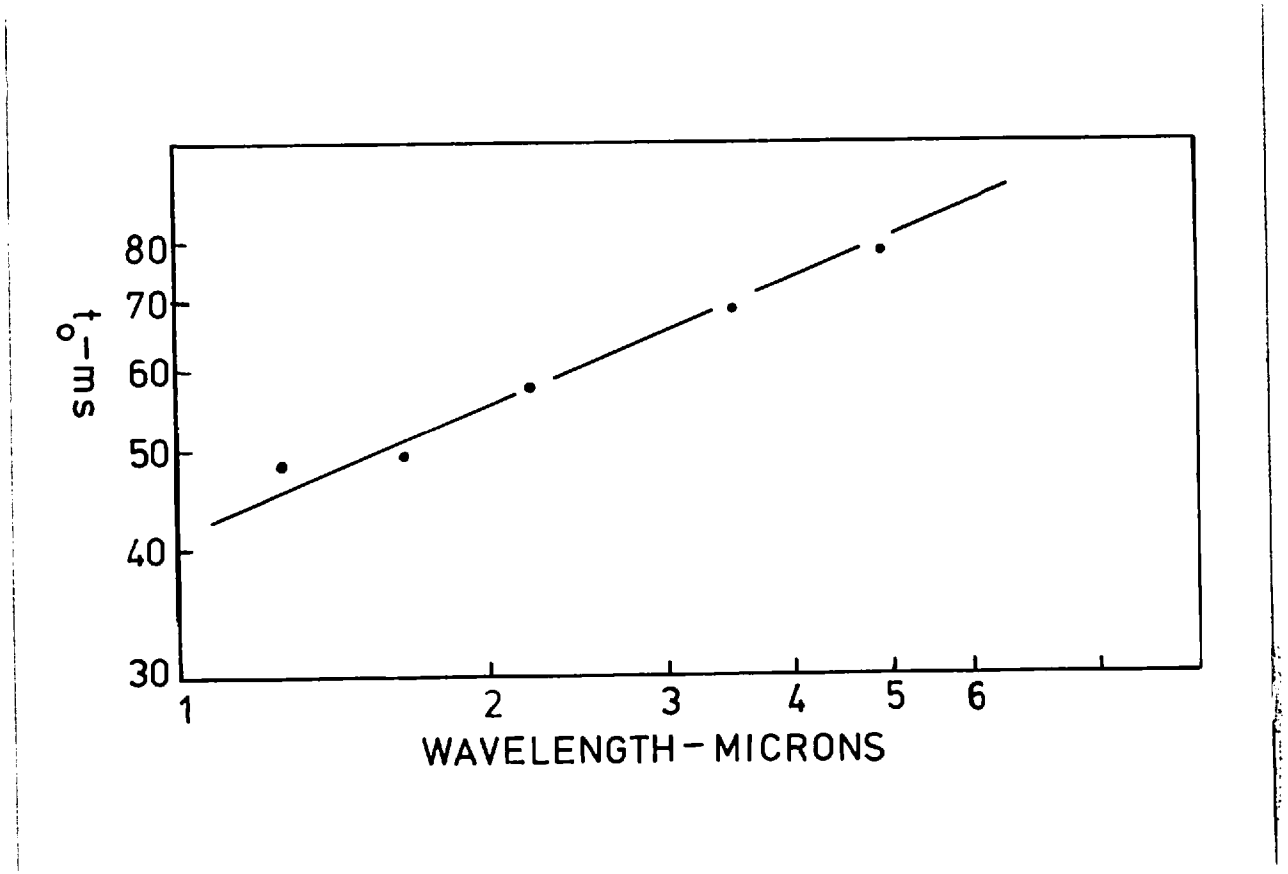

Fig. 6.5 Temporal correlation width t_o vs λ ; the line shown is approximately a half power law.

Now as discussed in Chapter 1 Fried defines r_o as

$$r_o = \left(\frac{6.88}{A}\right)^{5/3}$$

where $A \propto \lambda^{-2}$

so that $r_o \propto \lambda^{6/5}$

Values of r_o were obtained by fitting theoretical predictions from Equation 6.3 to measured transfer functions. Figure 6.4 shows a set of such results for the different infrared wavelengths, taken over a one-hour period.

The data can be seen to be in reasonable accord with the 6/5 power law shown. The visual seeing was estimated during the observations to be $\geq 3''$ which would lead us to expect the seeing at 2.2um to be $\sim 2.2''$ (from the 6/5 power law). This would give a value of r_o at 2.2um $\simeq$ 20cm. This is in fact in reasonable agreement with, although a little higher than the measured value.

Measurement of the Temporal Correlation of the Atmosphere

For measurements of the power spectrum of an image at high spatial frequency (large compared to the reciprocal of the seeing disc diameter) the bandwidth of the resulting detector signal is spread predominantly by changes in the image over a characteristic time t_o. Thus the bandwidth of the signal gives a measure of t_o, the temporal correlation width of the image. Figure 6.5 shows values of t_o obtained in this way (adjusted to remove the effects of limited resolution in the power spectrum and limited chop amplitude of the image) for the different infrared wavelengths. The line shown is approximately a half power law. It has been suggested (6.7,6.8) that $t_o \simeq d/V$ where V is the wind velocity and d is a characteristic scale in the aperture, which is of the same order as r_o but is a function of spatial frequency. So that t_o should be proportional to $\lambda^{6/5}$. Some of the discrepancy is probably caused by the over large optical bandwidths used.

The Measurement of Extended Sources

From Chapter 2 it is clear that in order to determine an object's power transform the normalized power spectrum of its image intensity must be divided by the normalized power spectrum

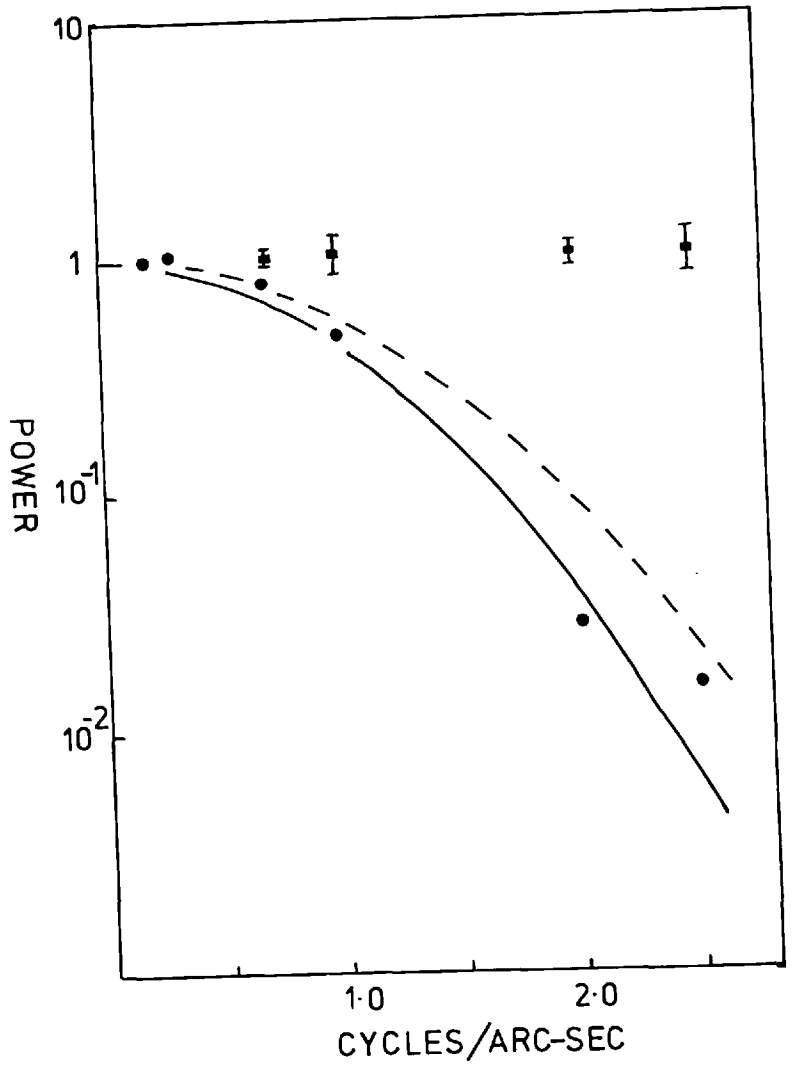

Fig. 6.6 Theoretically predicted power spectra for

a) source extended to the diffraction limit at 2.2μm (---)

b) source extended to .35″ (——), compared with experimental points for IRC +10216 at 2.2μm.

of a nearby point source.The feasibility of this method must ultimately depend on the stability of the atmospheric fluctuations during the measurement of the source and more importantly over the period including the calibration.Stars within 10^{o} of the source were selected and frequent comparisons were made.

As a test the mean was taken of the normalized power spectra of four calibration stars.Each power spectrum was then divided by this mean so that the spread in these points around unity represents changes in the atmospheric transfer function over a typical observation period.The results of the test are represented by the error bars of Figure 6.6.Also shown in Figure 6.6 is a set of data divided by the appropriate point spread transfer function for the extended source IRC + 10216 at 2.2μm.This source will be discussed in more detail in the next section.However,the data can be seen to be a reasonable fit to the gaussian profile of equivalent width $\cdot 35''$ shown in Figure 6.6.

In the remainder of this chapter I shall discuss two objects (1RC + 10216,VYCMa) which are somewhat representative of the types of objects which may be studied using the Infrared Speckle Technique.Some very preliminary measurements of their spatial structure will also be presented.

1RC + 10216

1RC + 10216 has a visual magnitude of about + 19 although at 5μm it is the brightest source outside the solar system. Frogel et al (6.9) reported that its mean 2.2μm magnitude was about zero but that it varied on a time scale of about 600 days over a range of at least 2mag.They also found that the energy distribution from 1.2 to 5μm fitted a 650^{o}K black-body although the longer wavelength data seemed to fit a cooler source.The nature of the source was interpreted as a central star surrounded by a dust shell. Because of the similarity of its variability to late type Miras,they suggested such a variable as a possible candidate for the central energy source.The similarity of the source to other objects thought to be protostars suggested an alternative description of the source but its position (out of the galactic plane) and the lack of any gas,dust or other young stars in the surrounding region pointed away from this explanation.

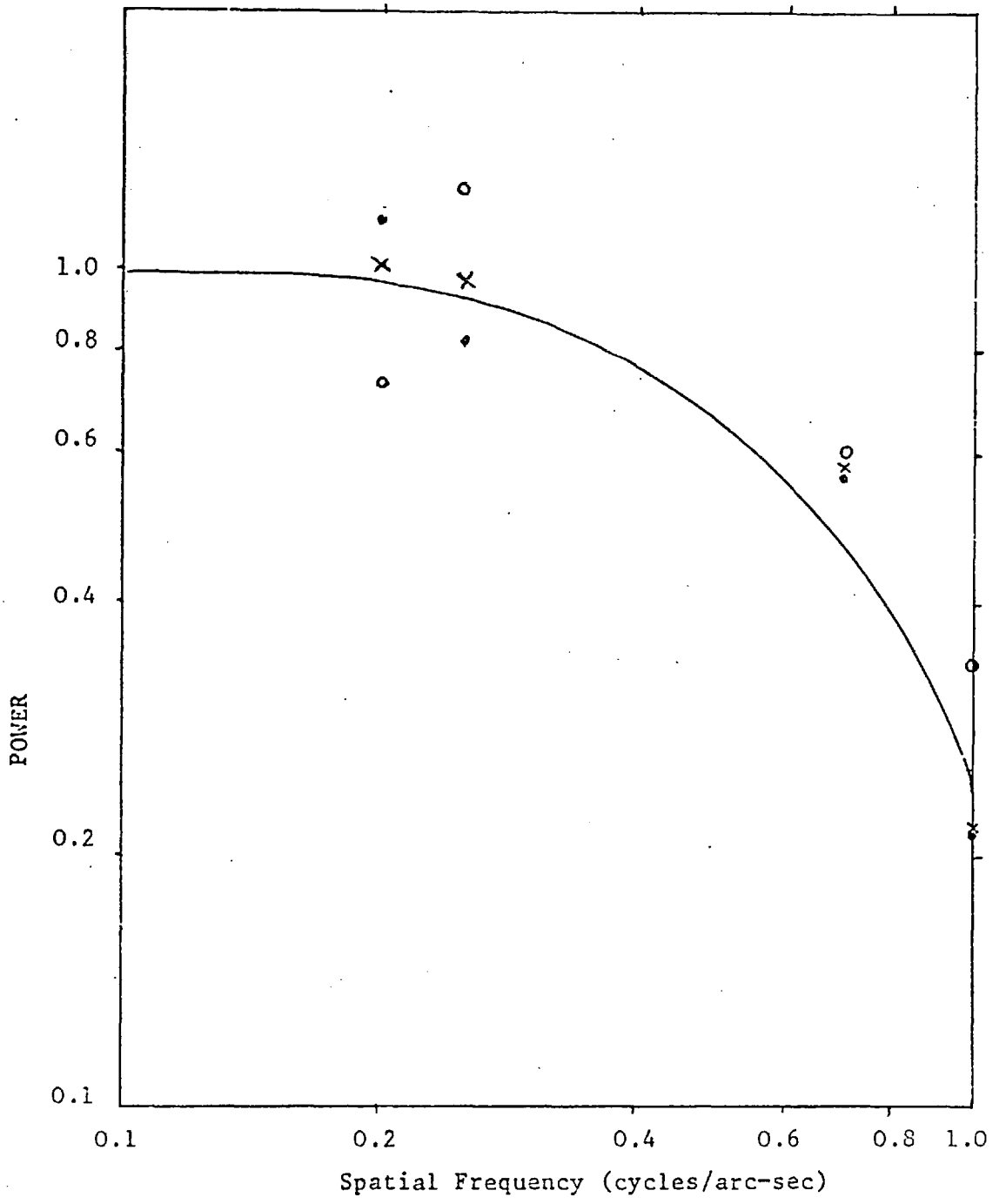

Fig. 6.7 Comparison of 2.2μm (o); 3.5μm (•) and 4.8μm (×) data for IRC +10216. Also shown is the power spectrum of a Gaussian profile of equivalent width 0.5″

Observations by Miller (6.10) in the spectral range .7 - 1.1μm indicated the presence of absorption features identified as CN bands, together with an underlying 1250°K black body continuum. This led to the identification of the source of IRC + 10216 as a carbon star rather than a Mira variable.

During the winter of 1970-71 IRC + 10216 underwent two occultations by the moon. Observations of these occultations by Toombs et al (6.11) at 2.2, 3.5, 4.8 and 10μm confirmed the presence of an extended dust shell around the central star. The occultation data in fact suggested that a two shell model was appropriate. Toombs et al deduced a schematic model of IRC + 10216 as a late type carbon star surrounded by a dust shell which scatters some of the starlight, but probably absorbs and thermally re-emits the majority of it. This dust shell may be represented by two components; a bright optically thick central component with a characteristic diameter of 0.4″ and temperature 600°K, and at a less luminous optically thin outer component having a characteristic diameter of 2″ and a temperature around 375°K. Observations at 8.3, 10.2 and 11.1 μm by McCarthy et al (6.12) using the Michelson type interferometer suggest a dust shell diameter of 0.9″ with diameter increasing with wavelength.

At visible wavelengths IRC + 10216 appears as a nebula with marked asymmetry, the axis being 2″ x 4″. Recent observations by McCarthy et al (6.13) suggest that this asymmetry is also present at near infrared wavelengths.

As mentioned previously and with reference to Figure 6.6 the 2.2μm data obtained using the Infrared Speckle Technique gives a reasonable fit to a single gaussian profile of equivalent width .35″. Figure 6.7 shows a comparison of 2.2, 3.5, and 4.8μm data. Also shown in the figure is the power spectrum of a gaussian profile of equivalent width 0.5″. Although thedata are limited there are some interesting features worth noting. In common with the findings of Toombs et al the 3.5 and 4.8μm profiles are very similar while the 2.2μm data suggest that the central 0.4″ component is not optically thick but that a temperature gradient is being observed.

The data may be modelled by several geometries, however the best fits are obtained using simple gaussian profiles rather than the two component shell models suggested by other observers.

This could be explained as being due to the outer part of the dust cloud,manifesting itself as the wings of the gaussian profiles used here.The two-shell models previously used are slightly unrealistic as they assume two uniform discs of diameter $0.4''$ and $2''$.However, since the outer shell is clearly optically thin and as mentioned above,the inner shell is not definitely optically thick,uniform disc profiles would not be expected.

VYCMa

Optically VYCMa appears as a multiple star surrounded by a reflection nebula.The brightest component was observed to be a visual binary of separation $0.65''$ (6.14).The spectrum was photographed by Joy in 1942 (6.15) who determined a type M3-4 irregular variable.Later Studies however by Wallerstein (6.16) suggested that the central component was a M5eIb-II double.

Infrared observations by Hyland et al (6.17) show VYCMa to have an excess at wavelengths longer than about 3μm over that from α Her which on the basis of optical spectra should be similar. In fact the flux from VYCMa cannot be fitted by any single black-body curve.Hyland et al suggest that a second black-body of temperature less than $300^{\circ}K$ is required to fit the infrared data.

VYCMa is found to be a source of both OH and H_2O maser radiation.Observations of the 1612MH$_z$ OH line (6.18) suggest a two velocity system which when combined with the data on the infrared excess may be interpreted as being due to a central star surrounded by an expanding dust shell.

The model of VYCMa proposed by Hyland et al was of pair of M5Ib stars surrounded by a thick spherically symmetric circumstellar dust shell.

The question again is whether VYCMa is a contracting protostar or an evolved star.The dust shell cannot be used to distinguish as both evolutionary states can possess one.The presence of the 1612MH$_z$ OH maser line led Hyland et al to favour the evolved star although the proposed protostar in Orion also possessed this line,Herbig (6.19) on the other hand favoured the model of a circumstellar envelope around a very young star.This was based on the source being positioned in a nebulous region containing other young stars.Herbig also suggests the distance to the objects as 1.5Kpc and explains previous higher estimates as being due to observation

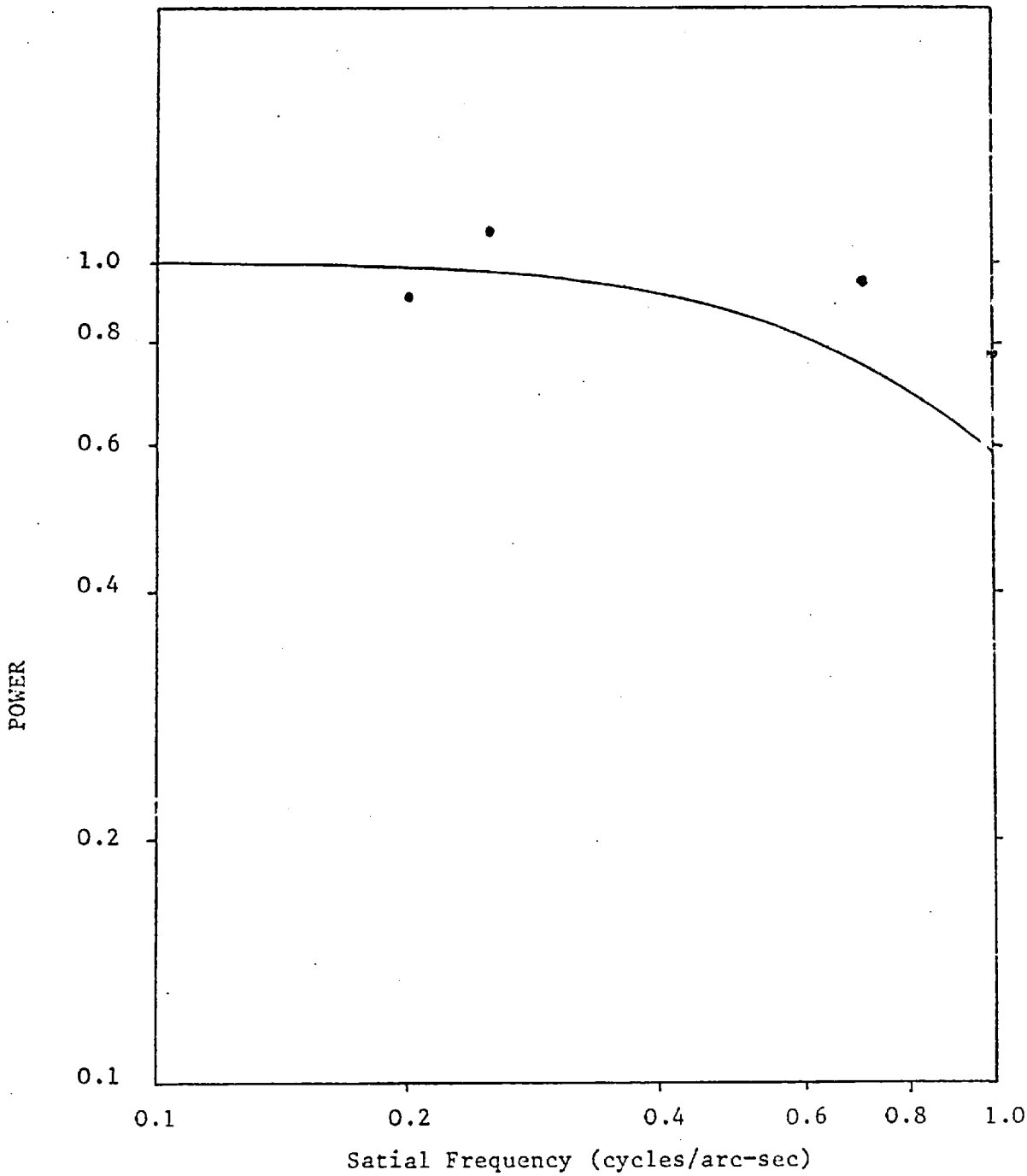

Fig. 6.8 4.8um data for VY CMa compared with power spectrum of a uniform disc of diameter 0.45"

of condensations (Knots) in the dust cloud rather than a binary system.Herbig's model is of a M3-5I star surrounded by dust,but in the form of an equatorial disc rather than a spherical shell.

The dust shell of VYCMa was first resolved by McCarthy and Low (6,20) at 5μm.They made measurements in a east-west position angle and interpreted the object in terms of a circular disc with angular diameter approximately 0.45". They noted that later longer wavelength measurements (6.12) were not consistent with simple models of the temperature profile of the dust,and that this may be due to the disc-like structure of unknown position angle.

The measurements using Infrared Speckle Interferometry were all made at a N-S position angle so that one would expect to see evidence for asymmetry in the object compared to the results of McCarthy and Low.Figure 6.8 shows the 4.8μm compared with a profile corresponding to the uniform disc used by McCarthy and Low. Clearly the extension of VYCMa is less in this position angle than in that measured previously.Furthermore the results at shorter wavelengths show evidence of a complex structure which the present range of spatial filters is unable to resolve,however the changes in the form of the results at different wavelengths indicate the presence of temperature gradients in the dust.Clearly a more detailed study of this object is required at a number of different position angles and with greater resolution in the power spectrum,before any clear description of its structure can be given.

Conclusion

It has been shown in this Thesis that diffraction limited information may be retrieved when using the whole aperture of a large telescope,despite the presence of atmospheric turbulence. A method has been suggested by which this technique may be extended to the near infrared and the implementation of this method has been discussed.Finally some preliminary results which suggest that the theory of atmospheric turbulence may be extended to the near infraredand that the method may indeed produce diffraction limited information, have been presented.

There are several areas where the implementation could be improved,most obviously in thearea of data reduction.The present system has been developed because of the limited computing power available in Tenerife.This has made complete on-line data analysis imposible.However it is planed to use the technique on the 3.8m UKIRT in the near future,where the computer will be able to handle the vast majority of the data on-line.A second limitation imposed by the use of the 1.5m Flux Collector is the limited resolving power available.This will of course be improved by a factor of about 2.5 when moving to the 3.8m ,provided the images are of sufficient quality.

Clearly the astronomical results so far achieved are of a very preliminary nature and need extending both on the objects already studied and on a whole range of other sources.Further more even when using the largest available single aperture telescope the resolution is not sufficient to resolve stellar diameters. A long baseline (50m) Speckle Interferometer has therfore been

proposed by M.J.Selby and will hopefully be constructed on a natural polar angled slope in Tenerife in the not too distant future.

REFERENCES

Introduction

0.1) Cohen,M.H. Proc IEEE,61,1192 (1973).

0.2) Johnson,M.A,Betz,A.L.,Townes,C.H. Phys Rev (Letters) 33,1617,(1974).

0.3) Michelson,A.A.,Pease,F.G. Ap.J 53,249,(1921).

0.4) Hanbury-Brown,R.,Davis,J.and Allen,L.R. Mon Not R.Astr.Soc 137,375,(1969).

0.5) Hanbury-Brown,R.,Davis,J.and Allen,L.R. Mon Not R.Astr.Soc 137,393,(1969).

0.6) Blackwell,D.E.,Shallis,M.J, Mon Not R.Astr.Soc 180,177,(1977).

0.7) McCarthy,D.W and Low,F.J. Ap.J.202,L37,(1975).

0.8) Toombs,R.T.,Becklin,E.E.,Frogel,J.A.,Low,S.K.,Porter,F.C., and Westphal,J.A., Ap.J.173,L71,(1972).

0.9) Ridgway,S.T.,Wells,D.C., Astron J,82,414,(1977).

Chapter 1

1.1) Sir Isaac Newton.,Optik Bk 1,1730.(Dover,New York 1952),

1.2) Tatarski,V.I,Wave Propagation in a Turbulent Medium. (McGraw-Hill Book Co.New York 1961).

1.3) Kolmogarov,Doklady Akad.Nauk SSSR 30.301 (1941).

1.4) Born,M.,Wolf,E.,Principles of Optics (Fifth Ed.Pergamon Press 1975).

1.5) Fried,D.L.,J.Opt.Soc.Am,Vol 56,1372,1966.

1.6) Hufnagel,R.E and Stanley,N.R. J.Opt.Soc.Am 54 52 1964.

1.7) Zwang,L.R. Bull Acad Sci USSR.Geophysic Series No.8,1960,1117.

1.8) Gifford,F.A. J.Atmospheric Sci. 19,205 (1962).

1.9) ARDC Standard Atmosphere (1959).

1.10) Scaggins,J.R.,Proceedings of National Symposium on Winds for Aerospace Vehicle Design.(USA FCRL 1962).

1.11) Hosfeld,R. Measurements of the size of Stellar Images. AFCRC-TN-55-873.Joint Scientific Report 2.1955.

1.12) Hufnagel,R.E. Restoration of Atmospherically Degraded Images. Woods Hold Summer Study 2.(Also appeared in Ref 1.13).

1.13) Brookner,E. Appl Opt.10 1960.(1971).

1.14) Fried,D.L.,Mevers,G.E. Appl Opt 13 11,1974.

1.15) Hoag,A.A. Bull Astron 24 Part 2,269 (1964).

1.16) Meinel,A.B. Final Report on the Site Selection Survey for the National Astronomical Observatory.Contribution from the Kitt Peak National Observatory No.45. 1963.

1.17) Dainty,J.C.,Scaddan R.J. Mon.Not.Royal.Ast Soc. 170 519,1975.

1.18) Korff,D. J.Opt.Soc.Am.63,971,1973.

1.19) Low and Rieke. Experimental Phy. Vol 12. Pt A.

1.20) Andriesse,Wiersta. Astron and Astrophys. 24,1973.

Chapter 2

2.1) Labeyrie,A. Astron and Astrophys 6,85-87, (1970).

2.2) Gezari,D.Y.,Labeyrie,A. and Stanchnik,R.V. Ap J.173,LI-15 (1972).

2.3) Blazit,A.,Bonneau,D.,Koechlin,L. and Labeyrie.
Ap.J.214.L79-L84. (1977).

2.4) Lynds,C.R.,Worden,S.P.and Harvey,J.W. Ap J 207,174 (1976).

2.5) Beddoes,D.R.,Dainty,J.C.,Morgan,B.L,.Scaddon,R.J.
J.O.S.A. 66,11,(1976).

2.6) McAlister,H.A. Ap J.215,159-165, (1977).

2.7) Korff,D.,Dryden,G. and Miller,M.G. Opt Comm 5,187,(1972).

2.8) Dainty,J.C. Mon Not.Roy.Ast.Soc 169,(1974).

2.9) Dainty,J.C.Opt Comm 7, (1973).

2.10) Worden,S.P.,Lynds,C.R. and Harvey,J.W. J.Opt.Soc.Am 66,(1976).

2.11) Knox,K.T. J.Opt Soc.Am 66, (1976).

2.12) Laques,P. Advances in Electronics and Electron Physics.
Ed.J.D.McGee. Academic Press.London Vol 22B. p.755.

2.13) Born and Wolf. Principles of Optics.pg 485.

2.14) Reed,I.S. IEEE Transactions-Information Theory. IT-8,194,(1962).

2.15) Goodman,J.W. Laser Speckle and Related Phenomena.
Ed.J.C.Dainty. Springer Verlag (1975).

2.16) Dainty,J.C. Private Communication 1978.

2.17) Korff,D. J.Opt Soc.Am. 63,971,(1973).

2.18) Roddier,C.and Roddier,F. J.Opt.Soc.Am. 65,664,(1975).

2.19) Dainty,J.C. Laser Speckle and Related Phenomena.
Ed.J.C.DAinty. Springer Verlag.(1975).

2.20)Morgan,B.L.,Beddoes,D.R.,Scaddon,R.J., and Dainty,J.C.
Mon.Not.R.Ast.Soc. 183,701-710. (1978).

Chapter 3

3.1)M.J.Selby,R.Wade and C.Sanchez Magro. Mon Not R. astr Soc. (in press)

3.2) M.J.Selby private communication

3.3) D.Korff J.Opt.Soc.Am. 63 , 971 (1973)

Chapter 4

4.1) Hall,D.W.B.,Aitkens,R.S.,Jeyse,R. and McCurnin,T.
Appl Opt. 14,450,(1975).

4.2) Jorden,P.R,Long,J.F.,MacGregor,A.D. and Selby,M.J.
Astron and Astrophys, 49,421-424,(1976).

4.3) Koorneef,J.,Van Overbeeke,J. Astron and Astrophys 48,(1976).

4.4) Jorden,P.R. PhD Thesis.University of London.1977.

4.5) Fahmbach,M.,Haussecker,K.,Lemke,D. Astron Astrophys 33,265,(1974).

4.6) Tobey,G.E.,Graeme,J.G.,Huelsman,L.P., Operational Amplifiers-
Design and Applications.(McGraw-Hill Book Co).

Chapter 5

5.1) Brault,J.W., and White,O.R. Astron and Astrophys, 13,169,(1971).

5.2) Moore,C.H. Astron and Astrophys, 15,497,(1974).

Chapter 6

6.1) Smart,W.M. Sperical Astronomy. 6th ed.Cam.Uni Press 1977.

6.2) Humphreys,W.J. Physics of the Air.3rd ed. McGraw Hill .1940.

6.3) Allen. Astrophysical Quantities.

6.4) Korff,D. J.Opt.Soc.Am. 63,971,(1973).

6.5) Dainty,J.C. Mon.Not,Roy.Astro.Soc. 169,631,(1974).

6.6) Karo,D.P. and Schneiderman,A.M. J.Opt.Soc.Am 66,1252,(1976).

6.7) Roddier,C. and Roddier,F. J.opt.Soc.Am 65,664 (1975).

6.8) Karo,D.P. and Schneiderman,A.M. J.Opt.Soc.Am. 68,480,(1978).

6.9) Frogel,J.A.,Hyland,A.R.,Kristian,J., and Neugbauer,G.
Ap J 158,L133,(1969).

6.10) Miller,J.S. Ap.J. 161,L95,(1970).

6.11) Toombs,R.I.,Becklin,E.E.,Frogel,J.A.,Low,S.K.,Porter,F.C. and Westphal,J.A.
Ap.J, 173,L71,(1972).

6.12) McCarthy,D.W.,Low,F.J.,Howell,R. Ap J.214,L85,(1977).

6.13) McCarthy,D.W.,Howell,R.,Low,F.J., IAU colloq 50.(proceeding in press).

6.14) Warley,C. (1969 Private Communication with authors of 6.17)

6.15) Joy,A.H. Ap.J. 96,344,(1942).

6.16) Wallerstein,G. Pub.Ast.Soc.Pacific. 70,479,(1958).

6.17) Hyland,A.R.,Becklin,E.E.,Neugebauer,G. and Wallerstein,G.
Ap.J. 158,619,(1969).

6.18) Eliasson,B. and Bartlett,J.F. Ap.J,155,L79,(1969).

6.19) Herbig G.H. Ap.J. 162,557,(1970).

6.20) McCarthy,D.W.,Low,F.J. Ap.J. 202,L37,(1975).

APPENDIX 1

Random Fields see Tatarski ref (1.2)

Stationary Random Functions

Given the random function f(t) with mean $\overline{f(t)}$ we can define the correlation function as

$$B_f(t_1,t_2) = \overline{(f(t_1) - \overline{f(t_1)})(f^*(t_2) - \overline{f^*(t_2)})}$$

where f*(t) is the complex conjugate of f(t) so that for real functions of (t)

$$B_f(t_1,t_2) = B_f(t_2,t_1)$$

It is easily seen that the correlation function vanishes when the fluctuations at t_1 are statistically independent of the fluctuations at t_2.

A random function f(t) is called stationary if its mean value $\overline{f(t)}$ does not depend on the time and if its correlation function $B_f(t_1,t_2)$ depends only on the difference t_1-t_2

$$\text{i.e } B_f(t_1 - t_2) = B_f(t_1 - t_2) = B_f(t_1 - t_2) = B_f(\tau).$$

Random Functions with Stationary Increments

The mean values of meteorological variables of the atmosphere such as temperature,pressure and humidity,undergo comparatively slow and smooth changes.The difficulaty arises of which changes of the function f(t) are to be regarded as changes of the mean value and which are to be regarded as slow fluctuations. In order to avoid this difficulty we shall now introduce the concept of structure functions.

Given the non-stationary random function f(t) we can consider instead of f(t) the function $F_\tau(t)$ where

$$F_\tau(t) = f(t+\tau) - f(t)$$

For values of τ which are small compared to the rate of

change of f(t), the value of $E_\tau(t)$ is not affected by the changes in f(t). The function $E_\tau(t)$ can be regarded to a first approximation as a stationary random function. The function f(t) is then refered to as a random function with stationary increments.

We can now define the structure function of the random function f(t) as

$$D_f(\tau) = \overline{F_\tau(t)^2}$$

$$= \overline{(f(t+\tau)-f(t))^2}$$

Thus the value of $D_f(\tau)$ increases as the correlation over the period τ decreases.

Roughly speaking, the value of $D_f(\tau)$ characterises the intensity of those fluctuations of f(t) with periods which are smaller than or comparable with τ .

Locally Homogenous and Isotropic Random Fields

A random function of three variables (for example vector position in space) may be refered to as a random field, the concept of a random field being completely analogous to the concept of a random process. We can define the structure function of the random field $f(\vec{r})$ as

$$D_f(\vec{r}_1,\vec{r}_2) = \overline{(f(\vec{r}_1) - f(\vec{r}_2))^2}$$

The random field $f(\vec{r})$ is called locally homogeneous in a given region if the distribution functions of the random variable $(f(\vec{r}_1) - f(\vec{r}_2))$ are invariant with respect to shifts of the pair of points $\vec{r}_1, \vec{r}_2$ within this region.

A locally homogeneous random field is called locally isotropic in a given region if the distribution function of the quantity $(f(\vec{r}_1) - f(\vec{r}_2))$ are invariant with respect to rotations and mirror reflections of the vector $\vec{r}_1 - \vec{r}_2$ within this region.

so that we can say

$$D_f(\vec{r}) = \overline{(f(\vec{r} + \vec{r}_1) - f(\vec{r}_1))^2} = D_f(r)$$

APPENDIX 2

Form of the Power Spectrum of Signal from Spatial Frequency Filter

During one cycle of the chop motion the temporal frequency power spectrum of the signal may be written as

$$P'_{\sigma'}(f) = i_a^2(\sigma')\Delta\sigma^2 \left[2\int_0^{T/2} \cos(2\pi f_o t + \Omega)\cos 2\pi f t \, dt \right]^2$$

where Ω is a phase factor given by $\Omega = \phi + \Phi(\sigma')$
alternatively we may write

$$P'_{\sigma'}(\omega) = i_a^2(\sigma')\Delta\sigma^2 \left[2\int_0^{T/2} \cos(\omega_o t+\Omega)\cos\omega t \, dt \right]^2$$

$$= i_a^2(\sigma')\Delta\sigma^2 \left[\int_0^{T/2} \cos((\omega_o+\omega)t+\Omega) + \cos((\omega_o-\omega)t+\Omega) \, dt \right]^2$$

$$= i_a^2(\sigma)\Delta\sigma^2 \left[\left[\frac{\sin((\omega+\omega)t+\Omega)}{\omega_o+\omega} + \frac{\sin((\omega-\omega)t+\Omega)}{\omega_o-\omega} \right]_0^{T/2} \right]^2$$

$$= i_a^2(\sigma)\Delta\sigma^2 \left[\left[(\sin((\omega_o+\omega)T/2+\Omega) - \sin\Omega) / (\omega_o+\omega) \right] + \left[(\sin((\omega_o-\omega)T/2+\Omega) - \sin\Omega) / (\omega_o-\omega) \right] \right]^2$$

$$= i_a^2(\sigma)\Delta\sigma^2 \left[\left[(\cos\Omega\sin((\omega_o+\omega)T/2) + \sin\Omega\cos((\omega_o+\omega)T/2) - \sin\Omega) / (\omega_o+\omega) \right] + \left[(\cos\Omega\sin((\omega_o-\omega)T/2) + \sin\Omega\cos((\omega_o-\omega)T/2) - \sin\Omega) / (\omega_o-\omega) \right] \right]^2$$

the complete power spectrum is given by

$$P_{\sigma'}(f) = P'_{\sigma'}(f) \times \text{Ш}(Tf)/T^2$$

where Ш(Tf) is the Dirac comb of harmonic spacing $f_c = 1/T$, so that the total power in the signal is given by

$$P_{\sigma'} = i_a^2 (\partial) \Delta\sigma^2 \sum_{n=0}^{n=\infty} \left[\cos\Omega \frac{\sin\pi(n_c+n) - \sin\Omega(1-\cos(n_c+n))}{2\pi(n_c+n)} + \cos\Omega \frac{\sin\pi(n_c-n) - \sin\Omega(1-\cos\pi(n_c-n))}{2\pi(n_c-n)} \right]^2$$

where n is an intiger which corresponds to the order of the harmonic i.e.

$$n = \omega T/2\pi$$

and

$$n_c = 4a/\lambda'$$

APPENDIX 3 Measurement of Noise Power

Consider the gaussian random variable signal v(t) as depected in Figure 1

Fig. A3.1

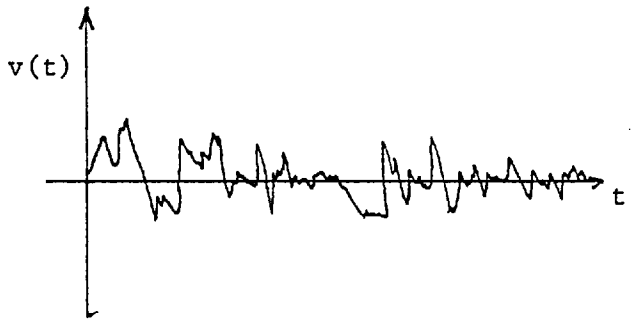

We wish to measure the power in the signal in a small bandwidth ΔB of centre frequency fo, see Figure 2

Fig. A3.2

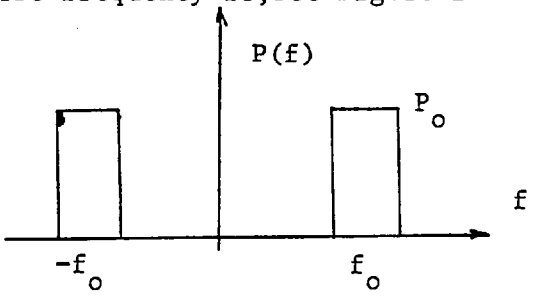

We can define $\phi(t_1) = \langle (v(t)v(t+t_1)) \rangle$

so that

$$\phi(t_1) = \int_{-\infty}^{+\infty} P(f) \exp(i2\pi f t_1)\, df$$

$$P(f) = \int_{-\infty}^{+\infty} \phi(t_1) \exp(-i2\pi f t_1)\, dt_1$$

In order to measure the power we shall use a square law detector so that the output is given by

$$V(t) = v^2(t)$$

It can then be easily shown that

$$\langle (V(t)V(t+t_1)) \rangle = \phi^2(0) + 2\phi(t_1)$$

The first term gives a DC component representing the total signal power in V(t)

since

$$\phi(0) = \int_{-\infty}^{+\infty} P(f)\, df$$

$$\phi^2(0) = \int_{-\infty}^{+\infty} P(f) * P(f)\, df$$

Now the autocorrelation of P(f) is as shown in Figure 3

Fig. A3.3

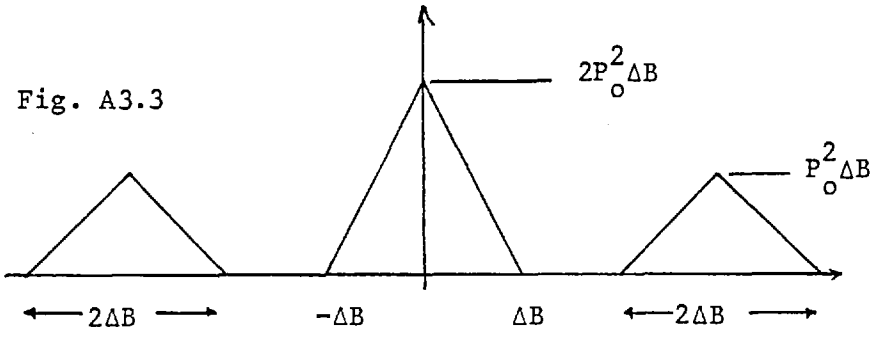

so that the total power in $V(t) = 8Po^2_\Delta B^2$

therefore power in $v(t) = 2Po_\Delta B\sqrt{2}$

Now $FT\{2\phi^2(t)\} = 2(P(f) * P(f))$

this is a fluctuational term the total power of which depends on the post detection integration time.

If we have no post detection integration then we must integrate over the whole of the frequency plane of Figure 3 so that

$$Noise^2 = 16Po^2_\Delta B$$

$$Noise = 4Po_\Delta B$$

So that the signal to noise ratio for the case of no post detection integration is given by

$$\frac{S}{N} = 1/\sqrt{2}$$

If however we have the situation where the integration time is such that $\tau \gg 1/B$ then

$$Noise^2 = 8Po^2_\Delta \frac{B}{\tau}$$

and

$$Noise = 2Po\left(\frac{\Delta B}{\tau}\right)^{\frac{1}{2}}$$

So that in the case where the post detection integration time is τ, then the signal to noise ratio is given by

$$\frac{S}{N} = (\Delta B\tau)^{\frac{1}{2}}$$

APPENDIX 4 Gold Coating of Chopper Mirrors

a) Cleaning Procedure for Glass Plates prior to Gold Evaporation

1) Form a paste of Decon 90 concentrated detergent and fine chalk, on a pad of cotton wool.Use pad to scrub both sides of plate.

2) Wash off paste with plenty of cold tap water.

3) It is useful at this stage to have a wire holder for the plate or plates as shown below

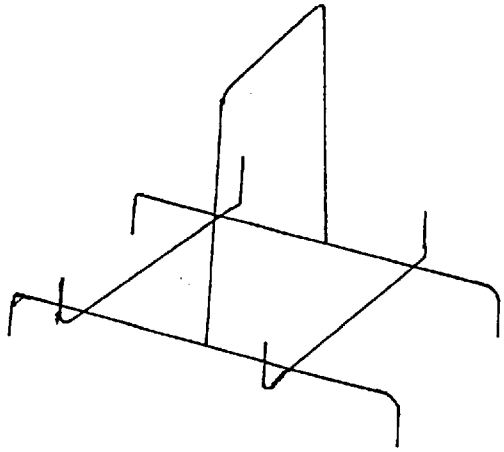

4) Place holder and plate onto beaker and run tap water into beaker for a few minutes.

5) With enough water in beaker to cover the glass plate place the beaker in an ultrasonic bath and leave for several minutes.

6) Wash again by running tap water into beaker.

7) Immerse in Chromic Acid for about ten minutes (not much longer or the glass may be damaged)

Chromic Acid - Mix a saturated solution of Sodium Dichromate in water with concentrated Sulphuric Acid (35cc per litre of Sulphuric Acid)
Warning the mixture is Exothermic.

8) Wash for at least half an hour in tap water.

9) Wash in several changes of doubly distilled water.

10) Boil plate in Doubly distilled water.

11) Remove excess water by placing in vapour bath containing Isopropyle Alchohol .

b) Evaporation of Gold onto Glass

1) Make evaporation baskets from tungsten wire as below

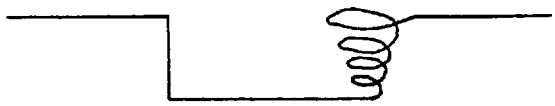

Two baskets are required as a thin layer of chromium should be evaporated onto the glass before the gold.

2) Fit the baskets to separate electrodes in the vacuum unit and place a charge of chromium chips in one and gold wire in the other,

3) Pump down the system without the glass plates in position and melt the gold onto the wire.

4) Open the system and mount the plates above the electrodes.

5) Pump down and measure green light transmission.

6) Evaporate a 10% absorption layer of chromium onto the glass.

7) Evaporate the gold to the required green absorption.

APPENDIX 5

```
LIST
2000  PRINT " SPECKLE INTERFEROMETRY CO LINE ANALYSIS "
2001  PRINT
2010  PRINT " NO OF POINTS PER SCAN ";
2020  INPUT N
2021  PRINT
2022  REM
2030  LET N1=4
2040  LET N2=6
2045  LET N3=7
2050  CALL 1, 0
2060  CALL 1,3
2070  CALL 2,N1, 0,26
2080  CALL 2,N2, 0,25
2090  PRINT "  OBJECT REF ";
2100  INPUT N4
2101  PRINT
2110  FOR S1=1 TO N
2120    LET R(1,S1)= 0
2130  NEXT S1
2140  LET S3= 0
2150  CALL 2,N2, 0,8
2160  CALL 5,Q,X
2170  IF Q= 0 GOTO  2150
2180  CALL 4,N2, 0, 0,D
2190  IF D<>1 GOTO  2150
2200  FOR S1=1 TO N
2210    LET R( 0,S1)=512
2220  NEXT S1
2225  LET S2=S3
2230  LET S3=S2+1
2235  CALL 3,N3,2,17,2
2240  CALL 2,N1, 0,8
2250  CALL 5,Q,X
2260  IF Q= 0 GOTO  2240
2270  FOR S1=1 TO N
2280    CALL 4,N1, 0, 0,M1
2283    FOR Z=1 TO 50
2284    NEXT Z
2285    LET M1=M1-512
2290    LET R( 0,S1)=R( 0,S1)+M1
2300    LET R(1,S1)=((R(1,S1)*S2)+M1)/S3
2305    CALL 2,N1, 0,10
2310    CALL 100,R( 0,1),N, 0
2320    CALL 100,R(1,1),N, 0
2330    CALL 2,N1, 0,8
2340    CALL 5,Q,X
350     IF Q= 0 GOTO  2310
2360  NEXT S1
2370  CALL 2,N2, 0,8
2380  CALL 5,Q,X
2390  IF Q= 0 GOTO  2200
2393  CALL 3,N3,2,17,1
2395  CALL 4,N2, 0, 0,D
400   PRINT " AFTER ";S3;"SCANS POINTS OF POWER SPECTRUM ARE "
2410  FOR S1=1 TO N
2420    PRINT R(1,S1)
2430  NEXT S1
2431  PRINT
2432  PRINT
2433  PRINT
2440  GOTO  2010
2450  STOP
2460  END
```

APPENDIX 6 FORTH data reduction blocks.

```
                              BLOCK NO. 125
 1    ( BLOCK 125 CONTNS CODE TO DO FAST AUTOCORRELATION )
 2    : BEGIN. DTOP @ ;  0 INT DAT 0 INT AUTO 20 ARRAY INF
 3    HEX : JNP-NOT-NEG 4310 , , ;    DECIMAL
 4
 5       ( REGISTER      USAGE                  [  ] MEANS CONTENTS OF
 6          R2            I
 7          R3            J
 8          R4          [DAT]                  POINTER TO START OF DATA BLOCK
 9          R5          [AUTO]                 POINTER TO START OF A-C BLOCK
10          R6-R7       MULTIPLYER PAIR
11          R8          [[DAT]+J]
12          R9          [[DAT]+J+I]
13          R10         [AUTO]+I*2             DOUBLE PRECISION INTEGERS
14
15                    )
16      NEXT-BLOCK              ;S        RICK   14/6/77


                              BLOCK NO. 126
 1    ( BLOCK 126 CONTINUES CODE FOR FAST AUTOCORRELATION )
 2    CODE ASAM  4 DAT 0 LH,          ( [DAT])
 3               5 AUTO 0 LH,         ( [AUTO])
 4               3 942 0 LHI,         ( J-MAX)
 5       BEGIN,
 6               2 162 0 LHI,         ( I-MAX*2)
 7               10 5 RLH,
 8               10 2 RAH,            ( [AUTO]+I-MAX*2)
 9               9 4 RLH,             ( [DAT])
10               9 3 RAH,             ( [DAT]+J)
11               8 0 9 LH,            ( [[DAT]+J])
12               2 80  0 LHI,         ( I-MAX)
13               9 2 RAH,             ( [DAT]+J+I-MAX)
14
15
16    NEXT-BLOCK              ;S              NLV  13/9/77


                              BLOCK NO. 127
 1    ( BLOCK 127 CONTINUES CODE FOR FAST AUTOORRELATION )
 2         BEGIN,
 3                 7 8 RLH,          ( R7=[[DAT]+J])
 4                 6 0 9 MH,         ( * BY [[DAT]+J+I])
 5                 7 0 10 AH,        ( ADD LSW TOTAL TO REG)
 6                 6 -2 10 ACH,      ( ADD MSW TOTAL TO REG)
 7                 7 0 10 STH,       ( STORE DOUBLE PRECISION)
 8                 6 -2 10 STH,      (    BACK IN TOTAL)
 9                 10 4 SIS,         ( DEC [AUTO]+I-MAX)
10                 9 2 SIS,          ( DEC [DAT]+J+I-MAX)
11                 2 2 SIS,          ( DEC I)
12            JNP-NOT-NEG
13                 3 2 SIS,          ( DEC J)
14            JNP-NOT-NEG
15                   NEXT
16     NEXT-BLOCK                              ;S  NLV  13/9/77
```

```
                                BLOCK NO. 128
 1    ( TO CONVERT DOUBLE PRECISION INTEGER TO F.P....+VE NOS ONLY)
 2    CODE DPFLOAT
 3        7 0 S)     LH,          ( LOAD REGS FROM STACK)
 4        6 2 S)     LH,
 5        8 32512 0 LHI,          ( LOAD EXPONENT MASK)
 6        8 6       RNH,
 7    HEX 2337 ,  DECIMAL         ( JMP TO 1  IF ZERO EXPONENT)
 8        6 8 0     SRL,          ( SHIFT RIGHT 8 BITS)
 9        8 18432 0 LHI,
10        6 8       ROH,          ( LOAD 72 INTO EXP.)
11    HEX 2304 ,  DECIMAL         ( SKIP TO 2.)
12        8 17920 0 LHI,          ( 1.)
13        6 8       ROH,          ( LOAD 70 INTO EXP.)
14        7 2 S)    STH,          ( 2.  STORE REGS ON STACK)
15        6 0 S)    STH,
16     NEXT-BLOCK                                  ;S   NLV/JDA 13/9/77


                                BLOCK NO. 129
 1           ( DP-TO-FP CONTINUED )
 2           0 0 S)          LE,        ( F.P.  LOAD TO NORMALISE )
 3           0 0 S)          STE,       ( AND STORE ON STACK AGAIN )
 4                           NEXT
 5
 6
 7
 8
 9
10
11
12
13
14
15
16    NEXT-BLOCK       ;S


                                BLOCK NO. 130
 1    (  CODE TO CHANGE DP INTIGER -VE - +VE )
 2    CODE 2NEGATE HEX
 3         7  0  S)      LH,
 4         6  2  S)      LH,
 5         6  FFFF 0     XHI,
 6         7  FFFF 0     XHI,
 7         8  8          RXH,
 8         7  1          RIS,
 9         6  8          RACH,
10         7  0  S)      STH,
11         6  2  S)      STH,
12    DECIMAL     NEXT
13
14
15
16    NEXT-BLOCK       ;S
```

```
                              BLOCK NO. 131
 1    ( BLOCK 131 CONTAINS WORD TO DISPLAY DATA BLOCK )
 2    6 0 NA CRY    6 1 NA CRX     11 0 NA INTEK
 3    : DISPLY DUP BLOCK CRY ENABLE SA 16 CRY WRITE2 SA
 4         CRX CLEAR SA 1024 0
 5         DO DUP I + @ 512 + CRY WRITE SA 2 +LOOP DROP ;
 6    : D-BLOCK INTER CLEAR SA INTER ENABLE SA
 7         BEGIN DISPLY INTER TLAM SA0 END
 8         DROP ;
 9
10    : D-P  SWOP BLOCK AUTO ! BLOCK DUP 202 0
11          DO AUTO @ I 2 * + DUP @ SWOP 2 +
12         @ SWOP DUP 0< IF SWOP 2NEGATE DPFLOAT FMINUS
13                   ELSE SWOP DPFLOAT THEN
14         ROT F! 4 + DUP 2 +LOOP DROP DROP ;
15
16                  ;S


                              BLOCK NO. 132
 1       ( DATA NORMALIZATION )    0 INT FT
 2    : FMAX BLOCK FT ! 0.0 1024 0
 3           DO FDUP FT @ I + F@ FABS F>
 4                IF
 5                ELSE FDROP FT @ I + F@ FABS
 6                THEN 4 +LOOP ;
 7    : FNORM FMAX FDUP FDUP INF    2 + F!      F.    1024 0
 8           DO FDUP FT @ I + F@ FSWOP F/ FT @ I + F!
 9                4 +LOOP UPDATE FLUSH FDROP ;
10
11
12
13
14
15
16    NEXT-BLOCK                          ;S


                              BLOCK NO. 133
 1        ( FLOATING  POINT TEST WORDS )
 2    : FZERO BLOCK 1024 0
 3           DO DUP I + FLOAT 0.0 FSWOP FIX F! 4 +LOOP
 4                        DROP FLUSH ;
 5    : FTEST-LIST BLOCK 1024 0
 6           DO DUP I + F@ F.  SPACE SPACE 4 +LOOP DROP ;
 7    : FTEST-PRINT 3 =LUOUT FTEST-LIST 5 =LUOUT ;
 8    : FDISPLY DUP BLOCK CRY ENABLE SA 16 CRY WRITE2 SA
 9           CRX CLEAR SA 804 0
10             DO DUP I + F@ 100  F* 512  F+ FIX CRY WRITE SA
11        CRY WAIT-L 4 +LOOP DROP ;
12    : FD-BLOCK INTER CLEAR SA INTER ENABLE SA
13           BEGIN FDISPLY INTER TLAM SA0 END DROP ;
14
15
16    NEXT-BLOCK      ;S          RICK 15/9/77
```

```
                                BLOCK NO. 134
 1     ( WORDS TO DO P-T ON INTIGER DATA )
 2          0 INT PT
 3     : PTBUFF BLOCK PT ! BLOCK AUTO ! ;
 4     : P-T PTBUFF AUTO @ @ 2 / AUTO @ ! AUTO @ 200 + @ 2 /
 5           AUTO @ 200 + ! 202 0 DO
 6             202 0 DO AUTO @ I + @ FLOAT I 2 / J 4 / * FLOAT
 7                      1 8  F* COS F* PT @ J + F@ F+ PT @ J + F!
 8                           2 +LOOP
 9                      4 +LOOP UPDATE
10           AUTO @ @ 2 * AUTO @ ! AUTO @ 200 + @ 2 * AUTO @ 200
11          + !      UPDATE ;
12
13
14
15
16     NEXT-BLOCK                ;S


                                BLOCK NO. 135
 1          ( WORDS TO DO FLOATING POINT P-T )
 2          0 INT PT
 3     : FTBUFF BLOCK PT ! UPDATE BLOCK AUTO ! UPDATE ;
 4     : FP-T FTBUFF AUTO @ F@ 2.  F/ AUTO @ F! AUTO @ 160 + F@
 5           2.  F/ AUTO @ 160 + F! 804 0
 6           DO 164 0
 7                DO AUTO @ I + F@ I 4 / J 4 / * FLOAT 0.0157 F* FDUP
 8           6.284 F/ FIX 1 + FLOAT 6.284 F* F- COSINE F* PT @ J + F@
 9       F+ PT @ J + F!                          4 +LOOP
10                           4 +LOOP
11           AUTO @ F@ 2.  F* AUTO @ F! AUTO @ 160 + F@ 2.  F*
12              AUTO @ 160 + F! ;
13
14
15
16           ;S


                                BLOCK NO. 136
 1
 2     ( BLOCK 136 CONTAINS WORDS TO DO AUTOCORRELATION )
 3                                  0 INT BS       0 INT AUTUMN
 4     : SAM DAT @ AUTO @
 5                          826 0 DO
 6                                  200 0 DO OVER J + DUP I + @
 7           SWOP @ * OVER I + +! 2 +LOOP
 8                                2 +LOOP
 9           DROP DROP UPDATE ;
10     : AUTO-BUFF AUTUMN ! BS    !  DUP INF   ! ;
11     : NEWB BS    @ + BS    @
12                  DO  I BLOCK DAT ' AUTUMN @ BLOCK
13           AUTO ' SAM UPDATE                LOOP ;
14     : ACOR AUTO-BUFF NEWB ;
15
16     NEXT-BLOCK       ;S
```

```
                              BLOCK NO. 137
 1      ( BLOCK 137 CONTAINS WORDS TO TEST AUTOCORRELATION )
 2    : TSAM DAT @ AUTO @
 3                          10 0 DO
 4                          12 0 DO OVER J + DUP I + @ SWOP @ *
 5         OVER I + +! 2 +LOOP
 6                             2 +LOOP
 7        DROP DROP  ;
 8    : TAUTO-BUFF BLOCK AUTO ! BS    ! ;
 9    : TNEW8 BS    @ + BS    @
10                        DO I BLOCK DAT ! ASAM        LOOP
11                                                   UPDATE ;
12    : ZERO BLOCK
13                 1024   0 DO DUP I + 0 SWOP ! 2 +LOOP
14                 UPDATE DROP ;
15
16    NEXT-BLOCK                        ;S 3/6/77   RICK


                              BLOCK NO. 138
 1    ( BLOCKS 138 AND 139 CONTAIN FAST DATA INPUT WORDS )
 2
 3    0 INT SBLOCK 0 INT NBLOCK 0 INT CKS 9 0 NA ADC 11 0 NA INTER
 4    : PRE SBLOCK ! 0 NBLOCK ! ADC ENABLE SA INTER CLEAR SA
 5       INTER ENABLE SA ;
 6    : RBLOCK SBLOCK @ NBLOCK @ + DUP ZERO BLOCK CKS ! ;
 7    : RAD ADC WAIT-L ADC READ SA ADC CLAM SA ;
 8    : INBLOCK NBLOCK @ 1 + NBLOCK ! ;
 9    : INLAM INTER TLAM SAD ;
10    : FLOCKS        NBLOCK @ . SPACE " BLOCKS STORED ON DISC " ;
11    : DATA-IN PRE BEGIN   RBLOCK  ADC CLAM SA
12                942 0 DO RAD 511 - CKS @ I + ! 2 +LOOP
13              UPDATE INBLOCK  INLAM END
14              INTER CLEAR SA FLOCKS ;
15
16    NEXT-BLOCK                          ;S 3/6/77 RICK


                              BLOCK NO. 139
 1    ( BLOCK 139 CONTAINS WORD TO TEST FAST DATA INPUT )
 2       8 2 NA SETPC 3 0 NA STAPC
 3    : T-RUN     SETPC WRITE SA 66 STAPC WRITE2 SA 150 DATA-IN ;
 4    : T-LIST BLOCK
 5                      1024 0 DO DUP I + @ . SPACE 2 +LOOP CR ;
 6
 7    : T-PRINT 3 =LUOUT T-LIST 5 =LUOUT ;
 8
 9
10
11
12
13
14
15
16    NEXT-BLOCK                                ;S 3/6/77/  RICK
```

```
                                BLOCK NO. 140
 1      ( SOME MORE TEST WORDS )
 2    : NUM-TEST  20 0 DO DUP BLOCK I + 2 I + 2 / SWOP !
 3        2 +LOOP UPDATE ;
 4    : TENS BLOCK 824 0 DO DUP I + -10 SWOP ! 2 +LOOP
 5        DROP UPDATE ;
 6    : S-TEST BLOCK 41 0 DO 20 I * 20 + I 20 *
 7        DO DUP I + 10 SWOP ! 2 +LOOP
 8         2 +LOOP DROP UPDATE ;
 9    0 INT AREA
10    : AREAS DUP 1 + DUP FZERO BLOCK AREA ! BLOCK PT !
11        SWOP DO PT @ I 4 * + F@ AREA @ F@ F+
12        AREA @ F! LOOP  AREA @ F@    INF 6 + F!
13           " AREA IS " SPACE AREA @ F@ F. ;
14
15
16                                  ;S


                                BLOCK NO. 141
 1          (  ST-LN FIT VOCABULARY )
 2    0 INT MSUM          0 INT GEN
 3    : GENSLOPE BLOCK GEN !
 4                 804 0 DO I 4 / 10 - FLOAT GEN @ I + F! 4 +LOOP
 5              UPDATE ;
 6    : XSUM
 7          201 161 DO MSUM @ F@ I FLOAT F+ MSUM @ F! LOOP ;
 8    : YSUM
 9
10          201 161 DO MSUM @ 4 + F@ PT @ I 4 * + F@ F+ MSUM @
11            4 + F! LOOP ;
12    : XYSUM
13
14          201 161 DO MSUM @ 8 + F@ PT @ I 4 * + F@ I FLOAT F* F+
15           MSUM @ 8 + F! LOOP ;
16    NEXT-BLOCK          ;S


                                BLOCK NO. 142
 1      ( ST-LINE FIT CONT )
 2    : X2SUM
 3
 4          201 161 DO MSUM @ 12 + F@ I FLOAT I FLOAT F* F+
 5               MSUM @ 12 + F! LOOP ;
 6    : INCEPT MSUM @ 4 + F@ MSUM @ 12 + F@ F*
 7             MSUM @ F@ MSUM @ 8 + F@ F*        F-
 8             40.  MSUM @ 12 + F@ F* MSUM @ F@ MSUM @ F@ F* F-
 9           F/  MSUM @ 16 + F! ;
10    : SLOPE 40.  MSUM @ 8 + F@ F* MSUM @ F@ MSUM @ 4 + F@ F* F-
11           40.  MSUM @ 12 + F@ F* MSUM @ F@ MSUM @ F@ F* F- F/
12            MSUM @ 20 + F! ;
13
14
15
16    NEXT-BLOCK       ;S
```

BLOCK NO. 143

```
1         ( ST-LN CONT )
2     : RSLOPE 804 0 DO PT @ I + F@ I 4 / FLOAT MSUM @ 20 +
3             F@ F* MSUM @ 16 + F@ F+ F- PT @ I + F! 4 +LOOP ;
4     : ST-FIT DUP 2 + BLOCK MSUM ! UPDATE BLOCK PT ! UPDATE
5         XSUM YSUM XYSUM X2SUM INCEPT SLOPE RSLOPE ;
6     : MDISPLY DUP BLOCK CRY ENABLE SA 16 CRY WRITE2 SA
7           CRX CLEAR SA 804 0 DO DUP I + F@ 100. F* 512. F+ FIX
8           CRY WRITE SA 8 +LOOP DROP ;
9     : DMARK DUP BLOCK CRY ENABLE SA 16 CRY WRITE2 SA
10    CRX CLEAR SA 20 0 DO 9 0 DO DUP J 10 * I + 4 * + F@ 100. F*
11      512. F+ FIX CRY WRITE SA LOOP 492 CRY WRITE SA LOOP DROP ;
12    : MD-BLOCK INTER CLEAR SA INTER ENABLE SA
13          BEGIN  DMARK INTER TLAM SA0 END DROP ;
14
15
16    NEXT-BLOCK            ;S
```

BLOCK NO. 144

```
1         ( POWER TRANSFORM OPERATION )
2     : POWER DUP ZERO ACOR AUTUMN @ DUP DUP 1 + DUP FZERO
3         " I AM NOW WORKING ON THE PT "  CR
4          D-P DUP 1 + DUP 1 + DUP FZERO FP-T 2 + DUP
5         " NORM IS " FNORM DUP CR MD-BLOCK 0 200 ROT AREAS ;
6     : SPACES 0 DO SPACE LOOP ;
7
8
9     : INFO 3 =LUOUT " RUN REF " 10 SPACES .  CR SPACE CR
10          INF @ " NUMBER OF BLOCKS "  SPACE .  CR
11          INF 2 + F@ " NORM IS " 10 SPACES F.  CR
12          INF 6 + F@ " AREA IS " 10 SPACES F.  CR
13          INF 6 + F@ INF @ FLOAT F/ FSWOP F/ INF 2 + F@ F*
14          INF 10 + F! INF 10 + F@ " POWER IS " 9 SPACES F.
15          CR SPACE CR SPACE CR       5 =LUOUT ;
16                                          ;S
```